Herbert Hackl, BSc

A Combined Ion- and Capacitance Probe for Ionosphere Research

MASTERARBEIT

zur Erlangung des akademischen Grades

Master of Science

Masterstudium Elektrotechnik

eingereicht an der

Technischen Universität Graz

Betreuer

Ass.Prof. Dipl.-Ing. Dr.techn. Gunter Winkler

Institut für Elektronik

Zweitbetreuer
Ao.Univ.-Prof.i.R. Dipl.-Ing. Dr.techn. Martin Friedrich
Institut für Kommunikationsnetze und Satellitenkommunikation

Graz, Mai 2014

EIDESSTATTLICHE ERKLÄRUNG

AFFIDAVIT

Ich erkläre an Eides statt, dass ich die vorliegende Arbeit selbstständig verfasst, andere als die angegebenen Quellen/Hilfsmittel nicht benutzt, und die den benutzten Quellen wörtlich und inhaltlich entnommenen Stellen als solche kenntlich gemacht habe. Das in TUGRAZonline hochgeladene Textdokument ist mit der vorliegenden Masterarbeit identisch.

I declare that I have authored this thesis independently, that I have not used other than the declared sources/resources, and that I have explicitly indicated all material which has been quoted either literally or by content from the sources used. The text document uploaded to TUGRAZonline is identical to the present master‘s thesis.

Datum / Date

Unterschrift / Signature

Acknowledgments

I am very grateful to Prof. Martin Friedrich for his continuous encouragement and help during the work on this thesis. He provided me with a great number of his own writings and experiences, helping me to gain insight into the theory and instruments of ionospheric research.

Likewise I thank Prof. Gunter Winkler for showing me several electronic 'tricks', equipping me with some of his personal precious hardware and finally for spending long hours in the laboratory with me, preventing me from going insane.

The practical work presented in this document has been carried out at the Institute of Electronics, Graz University of Technology. I am indebted to Mr. Eduard Dorner and his team for supplying me with everything I needed and to Prof. Peter Söser for spontaneous advice.

Most importantly I thank my wife for being a true companion during a challenging 1.5 years, and for her unfailing patience and support. Finally, kudos to my son who brimmed over with enthusiasm for my papers and screens.

Abstract

The number densities of free electrons are one of many outputs of any atmospheric model. The agreement between model and observation of this particular parameter is but one of many checks to assess the credibility of theoretical atmospheric models.

Ground based instruments are not well suited for ionospheric measurement below 100 km. Since the availability of sounding rockets in the late 1940's methods were developed to measure plasma parameters *in situ* by instrumentation as part of the rocket payload.

The inclusion of dust or ice particles in the ion chemistry governing the production-and-loss balance of free electrons in the mesosphere is a hot topic which requires measurements with new and dedicated instruments, some of which are still poorly understood.

Fixed-frequency capacitance probes have been flown successfully many times in the past. In ten flights with TU Graz participation since 1991 the outer grid of an ion probe was used as a fixed frequency capacitance probe forming a combined ion and capacitance probe.

The objective of this MSc Thesis was to produce an updated version of such a combined ion and capacitance probe. The previous circuits were modernized with the aim to make them smaller, faster, more accurate and sensitive by using modern components.
Two versions of each of the probes will be flown on the forthcoming MaxiDusty sounding rocket payload (Summer 2015) aiming at definitive answers as to which of them provides the better sensitivity and resolution. The capacitance probes will operate with extremely different frequencies (about 220 kHz and 8 MHz), whereas the two corresponding ion probes will operate with different bias voltages of -2.5 V and -8.3 V. Based on the resulting experiences one may choose the version to be used in later flights.
The ion probe provides a small output current which can be directly measured using a logarithmic current amplifier capable of measuring currents as low as 1 pA. The capacitance probe changes its capacitance primarily as a function of the ambient electron density. The probe's capacitance is included as the frequency determining part of an LC-oscillator (Clapp type) resulting in minute measurable changes in frequency. This frequency is the input to the digital counter electronics which converts it to a digital 20 bit output.

Contents

List of Figures

List of Tables

List of Symbols

Constants

ϵ_0 ... permittivity of free space = $8.854\,19 \cdot 10^{-12}\,\mathrm{m}^{-3}\,\mathrm{kg}^{-1}\,\mathrm{s}^4\,\mathrm{A}^2$
k ... Boltzmann constant = $1.380\,65 \cdot 10^{-23}\,\mathrm{J/K}$
m_e ... electron mass = $9.109\,38 \cdot 10^{-31}\,\mathrm{kg}$
e ... elementary charge (charge of an electron) = $1.602\,18 \cdot 10^{-19}\,\mathrm{C}$
C ... capacitance in F
f ... frequency in Hz
G ... conductance = 1/R
L ... inductance in H
n ... an integer number. multiple used
T ... temperature in degrees K ($273.15\,\mathrm{K} = 0\,^\circ\mathrm{C}$)
X ... reactance = 1/Z

Chapter 3: Ion Probe

a ... a variable term containing v_R and v_T
I_0 ... thermal current to a stationary sphere in A
I_C ... collector current to a bipolar transistor in A
I_{ref} ... reference current to the logarithmic amplifier in A
I_{cal} ... calibration current provided by resistor in A
m_i ... ion mass in kg
N^+ ... ion number density in m^{-3}
r_0 ... outer radius of the spherical probe in m
V_+ ... positive supply voltage (+12 V)
V_{BE} ... emitter base voltage of a bipolar transistor in V
V_{cm} ... common mode voltage (to line driver) = $2.5\,\mathrm{V}$
V_T ... thermal voltage in V
v_T ... thermal velocity of ions in m/s
v_R ... rocket velocity in m/s

Chapter 4: Cap Probe

$\vec{B}$ ... magnetic field
C_0 ... free-space capacitance of the probe = $2.5\,\mathrm{pF}$
ΔC ... change in the probe's capacitance in pF
d ... distance of the probe's center and an earthed plane (calibration) in mm
f_c ... counting frequency = $250\,\mathrm{MHz}$
f_N ... plasma frequency in Hz
g_m ... transconductance of a FET

List of Symbols

λ_D ... Debye length in m
ν ... collision frequency in s^{-1}
N ... digital counter value
N_e ... electron number density in m^{-3}
ω_r ... angular resonance frequency in s^{-1}
P_s ... digital prescaler value
r_0 ... outer radius of the spherical probe in m
S ... (adopted) ion sheath thickness in m
T_e ... electron temperature in degrees K
V_F ... forward voltage of a diode in V
V_{pp} ... peak-to-peak amplitude in V
Z ... probe's impedance in Ω

Chapter 5: Digital

b ... binary prescaler variable = 0 - 11
d ... decimal prescaler variable = 0 - 9
f ... Cap Probe electronics output frequency in Hz
f_c ... counting frequency = $250\,\text{MHz}$
f_{Gate} ... telemetry sampling frequency = $361\,\text{Hz}$
f_{min} ... lowest expected signal frequency in Hz
N ... digital counter value
P_s ... digital prescaler value
T_{Gate} ... telemetry sampling period in s
T_{Signal} ... signal period in s
t_{pLH} ... signal propagation time through optocoupler for rising input edge
t_{pHL} ... signal propagation time through optocoupler for falling input edge

Acronyms and Abbreviations

approx.	... approximately
CapProbe	... Capacitance Probe (Ch. 4)
cf.	... compare (latin: confer)
Digital1/2	... Digital counter electronics, part 1 or 2 (Ch. 5)
e.g.	... for example (latin: exempli gratia)
ESD	... Electro Static Discharge
$GNDA$	... Ion Probe bias voltage (LV or HV)
HF	... high frequency (approx. 9 MHz) capacitance probe
HV	... high voltage (-8.3 V) biased ion probe
IC	... Integrated Circuit
i.e.	... that is (latin: id est)
LF	... low frequency (approx. 200 kHz) capacitance probe
LogAmp	... logarithmic (current) amplifier
LSB	... Least Significant Bit.
LV	... low voltage (-2.5 V) biased ion probe
MSB	... Most Significant Bit.
OPA	... Operational Amplifier
PCB	... Printed Circuit Board
PCM	... (PCM encoder) Pulse-Code Modulation
PIP	... Positive Ion Probe (Ch. 3)
RF	... radio frequency
TTL logic	... digital logic family accepting inputs from 0 V to 5 V

1. Foreword by assoc. prof. (ret.) Dr. Martin Friedrich

An Introduction to Ionosphere Research

Both pressure and density of the atmosphere decrease exponentially with altitude. This is, however, not the only difference to the situation close to the ground. Above, say, 60 km the overhead air column is dramatically reduced, so much so that it allows appreciable fluxes of ionizing radiation to reach the upper atmosphere. The Sun is the major source of this radiation (UV to X-rays). Although the air's major constituents up to the so-called turbopause (somewhere above 100 km) are essentially the same as on the ground, a tiny fraction of its composition is ionized - at most 1% at the peak electron density (*F*-region peak near 400 km). In the region of the Institute's [1] main interest (the mesosphere, or - in ionospheric parlance - the *D*-region) the degree of ionization is between $10^{-11}\,\mathrm{m}^{-3}$ to $10^{-7}\,\mathrm{m}^{-3}$. Original interest in the number density of free electrons was because of their impact on radio wave propagation. The peak electron density (in the *F*-region) determines up to what frequency waves are reflected and thus allows radio communication beyond the horizon. The electron densities of the *D*-region, on the other hand, are responsible for absorption of traversing radio waves. Both the absorption and the minimal electron density required for reflection, are inversely proportional to the square of the signal frequency.

Modern communication largely makes use of relay satellites in geostationary orbits. The frequencies used are all in the GHz range, on the one hand to allow more data transfer, and on the other to facilitate narrow beam antennas targeting specific areas on the ground and radiating only to specific satellites. These high frequencies penetrate the ionosphere essentially unaffected, and outages are due to atmospheric conditions (*e.g.*, heavy rain), but only rarely are they the consequence of exceptional ionospheric conditions. Understandably interest of applied science in detailed studies of the ionosphere has largely vanished, and today ionospheric physics is but one area of atmospheric science. Atmospheric science can be treated both theoretically and empirically. Ultimately theoretical models of the behavior of the air's constituents should agree with measurements of the corresponding parameters, or - rephrased - convergence of theoretical and empirical models is the scientific goal.

Ionization initially produces both free electrons and positive ions. The simplest reverse reaction is provided by recombination of the electrons with the positive ions again leading to neutrals. A somewhat more complex ion chemistry shows that (1) the initially produced ions can form large cluster ions with much higher recombination rates, and (2) that electrons may attach either to neutrals but also to dust particles (see Fig. 1.1). The inclusion of dust or ice particles in the ion chemistry governing the production-and-loss balance of free

[1] Institute of Communication Networks and Satellite Communications, TU Graz

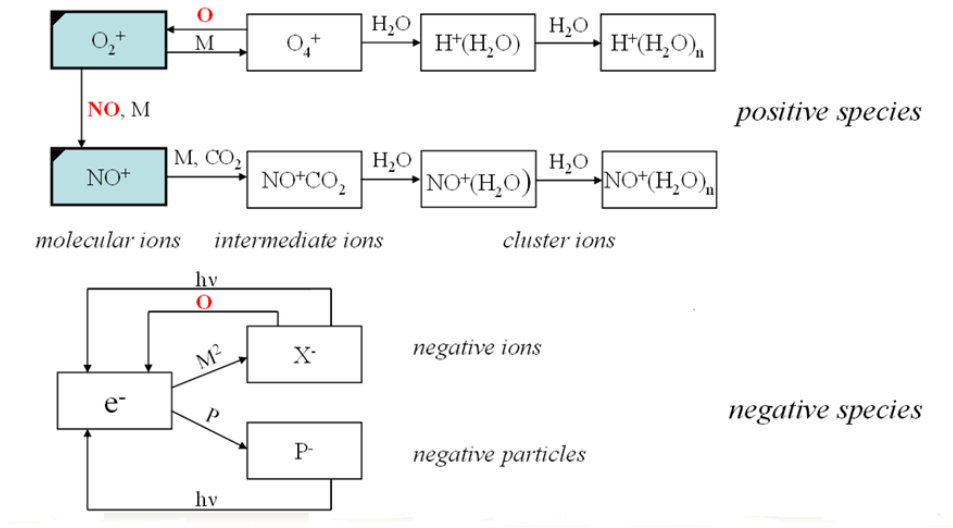

Figure 1.1.: Simplified scheme of ionization and reverse reactions. The earmarked (blue) ions are the ones initially produced [Friedrich *et al.*, 2012].

electrons in the mesosphere is a hot topic requiring measurements with new and dedicated instruments, some of which are still poorly understood and may require verification of the their results by redundant instrumentation.

Instrumentation to measure plasma densities

The oldest method to derive electron densities makes use of the frequency dependent reflection of the ionosphere. The so-called ionosonde is a pulsed radar which varies its frequency. The delay of the echo yields the altitude of the reflection, whereas from the frequency one can deduce the electron density. Ionosondes have been around since the 1930's and still constitute the backbone of many studies, among them the long-term variation of the ionosphere's behavior. Other ground based instruments able to provide electron densities are, *e.g.*, incoherent scatter radars such as EISCAT, a large installation located near Tromsø in northern Norway. Both these instruments are not well suited for measurements below 100 km (the mesosphere or *D*-region), and in addition incoherent scatter radars require regular adjustment of their "system constant" to normalize the results.
Since the availability of sounding rockets in the late 1940's methods were developed to measure plasma parameters *in situ* by instrumentation as part of the rocket payload. In the following are some of the most common ones listed with their pros and cons.

(1) Langmuir probe - a metallic probe (needle or sphere) is biased positively and thus attracts an electron current from the ambient ionospheric plasma. The current is

$$I = I_0\sqrt{1 + \frac{qV}{kT}} \tag{1.1}$$

and thus depends on the probe potential relative to that of the ambient plasma [Smith, 1969] . The instrument is simple and high time and density resolution can easily be achieved. However, the electron current drawn from the plasma has to be neutralized by an equal current provided by the much less mobile ions. According to calculations by Szuszczewicz (1972) the area for the return current (essentially the payload surface) must be at least $10\,000$ times larger than that of the probe, otherwise the payload will charge negatively, the potential of the probe *vs*. the plasma is less positive and the collected current will be reduced. An example of the problem is shown in Fig. 1.2.

(2) Impedance probe - A magneto-plasma constitutes a complex frequency-dependent impedance. By sweeping the frequency of a signal applied to a probe, various features can be observed. This rather more complex instrument can potentially yield electron densities without the need for normalization. However it takes the time of one frequency sweep to obtain one electron density values, which reduces the height resolution.

(2a) Tracking impedance probe - The most pronounced resonance of the sweeping impedance probe is tracked, thus in fact eliminating the need to sweep (better time/height resolution). The drawback is that track can be lost in a low electron density environment.

(2b) Fixed frequency (capacitance) probe - A conductor immersed in a plasma changes its capacitance with the ambient electron density. Since this instrument is neither sweeping nor tracking a particular resonance frequency, it potentially provides safe operation and good time resolution.

(3) Radio wave propagation - An HF radio wave is transmitted to the sounding rocket with linear polarization. The magneto-plasma between transmitter and receiver changes the signal from linear to elliptic polarization. Both the rotation of the ellipse's major axis (Faraday rotation) and the axis ratio can be used to derive electron density [*e.g.*, Bennet *et al.*, 1972]. This *semi-in situ* method is immune to payload charging and aerodynamic effects, but one has to rely on ionospheric stability for the duration of the measurement (approx. 2 minutes). Another shortcoming is the poor height resolution (0.5 to 1 km) which is tied to the rocket spin.

(4) Gridded sphere (Gerdien) ion probe - An aerodynamically transparent sphere at payload (plasma) potential has an inner collector biased negatively. The current to that device is predominantly determined by the relative velocity between the probe and the plasma and only to a minor extent due to the ions' thermal velocity [Folkestad, 1970]. Due to the much heavier mass of the ions compared to that of electrons, a change in the payload potential has little influence on the collection efficiency.

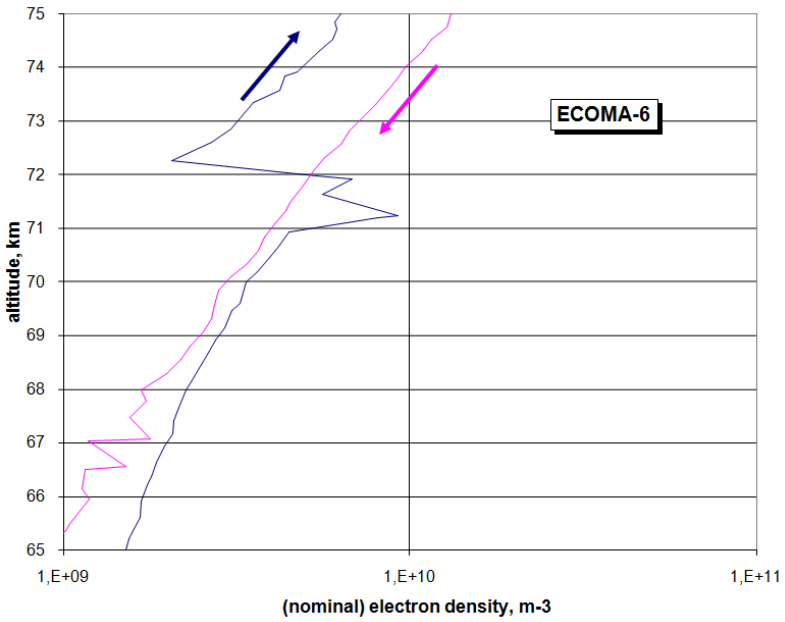

Figure 1.2.: Langmuir probe: Current decrease by 1/3 in the instant of payload separation due to reduced surface for return current (blue line, potential more negative) whereas on downleg (pink line) no discontinuity is observed [Friedrich and Torkar, 2009].

In situ probes sample the plasma in the vicinity of the fast flying rocket which is therefore necessarily disturbed, whereas at satellite altitudes the air is thin enough that free molecular flow prevails. This means that molecules that directly hit the spacecraft are the only ones affected, but do not change the air or plasma flow otherwise. In addition, the payload potential impacts on all probes with different degrees. A recent version of the Langmuir type uses four needles with different biases; the observed currents are at a known relation to each other and one is thus in the position to eliminated the influence of the payload charging [Bekkeng *et al.*, 2013].

Objective

The objective of the present MSc Thesis is to produce an updated version of a combined ion and capacitance probe to be flown on the forthcoming MaxiDusty sounding rocket payload. Two versions of each of the probes will be flown aiming at definitive answers as to which of them provides the better sensitivity and resolution. The recent flights aboard the accurately attitude controlled CHAMPS payloads revealed some unexpected features [Friedrich *et al.*, 2013] which motivated the revival of the idea of combined plasma probes.

References

Bekkeng, T.A., A. Barjatya, U.-P. Hoppe, A. Pedersen, J. I. Moen, M. Friedrich, and M. Rapp: Payload Charging Events in the Mesosphere and Their Impact on Langmuir Type Electric Probes, *Ann. Geophys.* **31**, pp. 187-196, 2013.

Bennett, F.D.G., J.E. Hall, and P.H.G. Dickinson: *D*-Region Electron Densities and Collision Frequencies from Faraday Rotation and Differential Absorption, *J. atmos. terr. Phys.* **34**, pp. 1321-1335, 1972.

Folkestad, K.: Ionospheric Studies by *in situ* Measurements in Sounding Rockets, Internal NDRE Report **59** (and PhD Thesis University of Oslo), 1970.

Smith, L.G.: Langmuir Probes in the Ionosphere, in: *Small Rocket Techniques*, N. Holland, pp. 1-15, 1969.

Szuszczewicz, E.P.: Area Influences and Floating Potentials in Langmuir Probe Measurements, *J. Appl. Phys.* **43 (3)**, pp. 874-880, 1972.

Friedrich, M., and K. Torkar: Trying to understand probes, PowerPoint presentation, Beijing, 2009.

Friedrich, M., K. Torkar, S. Robertson, and Shannon Dickson: Bonus Results from Ion Probes, *ESA-SP* **721**, pp. 75-80, 2013.

Friedrich, M., M. Rapp, T. Blix, U.-P. Hoppe, K. Torkar, S. Robertson, Shannon Dickson, and Kristina Lynch: Electron loss and meteoric dust in the mesosphere, *Ann. Geophys.* **30**, pp. 1495-1501, 2012.

assoc. prof. (ret.) Dr. Martin Friedrich

2. Introduction

2.1. The MaxiDusty project

The MaxiDusty sounding rocket is a project technically conducted by Andøya Rocket Range (Andenes, Norway). Andøya Rocket Range (ARR) is responsible for all sounding rocket and scientific balloon operations performed from Norwegian territory [http://www.rocketrange.no]. The participants are the Universities of Tromsø (project scientist prof. O. Havnes), Boulder, Graz, Oslo and Stockholm providing 11 different experiments (some of them in part providing redundant data) on a 35 cm diameter payload. The rocket's apogee will be about 120 km. The flight of MaxiDusty-1 is currently scheduled for Summer 2015. The project aim is the study of meteoric dust and atomic oxygen which have been identified as new factors for understanding the mesosphere.

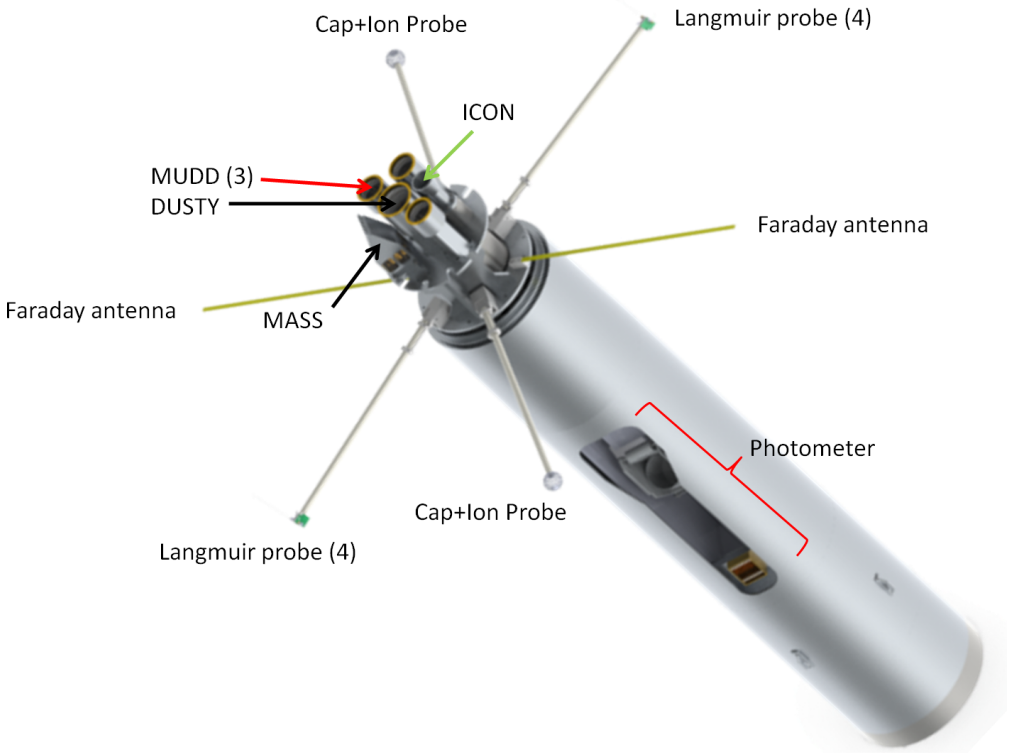

Figure 2.1.: Probes on MaxiDusty payload [Havnes, 2012]

The prime experiments are three dust probes of different design (DUSTY, ICON, MUDD) by the University of Tromsø and a mass spectrometer by the University of Boulder (MASS) dedicated to investigate charged dust. (MASS instruments were already flown very successfully in 2007 and 2011.) The combination of these instruments is expected to be capable

to differentiate between dust and ice particles while providing best height resolution and several readout instruments to assess their validity.
A multi-needle Langmuir probe by the University of Oslo will provide electron densities expected to come closest to the absolute values from radio wave propagation data.
A Faraday experiment using four sounding frequencies is provided by TU Graz. It yields the absolute electron densities unaffected by aerodynamics or electrical charging of the payload and therefore indispensable for calibration purposes [Friedrich, 2013].
Finally the scope of this thesis are two combined ion- and capacitance probes, namely a combination of a gridded sphere ion probe with a fixed frequency capacitance probe. The probes will measure the density of positive ions with different masses, indicating the presence of heavy positive particles (*i.e.* dust or ice). The probes are mounted on two laterally deployed booms opposite to each other.

2.2. Overview

Fixed-frequency capacitance probes have been flown successfully many times in the past [Jacobsen, 1972]. In ten flights with TU Graz participation since 1991 the outer grid of the ion probe was used as a fixed frequency capacitance probe. At the time, this dual use of one probe to measure two parameters was a new idea. In the MaxiDusty flight the two capacitance probes will operate with extremely different frequencies (about 220 kHz and 8 MHz). Based on the resulting experiences one will choose the frequency to be used in later flights [Friedrich, 2013].

The contribution of this work to the MaxiDusty project are the electronics processing the signals from the two combined ion- and capacitance probes (termed Ion Probe and Cap Probe). The probe's outputs are analog signals, *i.e.* the Ion Probe provides a small current which can be directly measured and the Cap Probe changes its capacitance primarily as a function of the ambient electron density. The Cap Probe's capacitance is included as the frequency determining part of an LC-oscillator resulting in a measurable change in frequency. This frequency is the input to the digital counter electronics (Digital) which converts it to a digital 20 bit output.
Two small Analog Boxes house two PCBs each, containing the ion current measurement circuit and the oscillator circuit. Those boxes are mounted close to the probe's booms to minimize the cable length and therefore its influence on the measurements. A larger Main Box contains altogether three PCBs: one digital processing circuit for each of the two Cap Probe frequency outputs and in addition the power supply unit for the whole system (termed DC/DC). Additionally all supply components are placed in the Main Box to maintain a low noise environment an the Analog Boxes.
The digital electronics in the Main Box also process the input control signals from the rocket's telemetry. Power and control signals are transmitted by five lines to the Analog Boxes.

Each boom hinge is equipped with a microswitch to indicate the deployment of the boom during flight.

2.2.1. Scope of the work

The probes as treated in this work have been operated for decades, as have the electronics. The scope was to modernize the old circuits, making them smaller, faster and more accurate by using modern components and minimizing leakages and stray capacitances. The outputs had to be adjusted to the interface specification of MaxiDusty.

1. Ion Probe electronics: Development of a current measurement circuits for input currents in the range of $1 \cdot 10^{-12}$ A to $1 \cdot 10^{-7}$ A. Status quo was the circuit of Fig. 3.3 used since 1994 .
2. Cap Probe electronics: Development of an oscillator circuit capable of measuring the small capacitance deviations of the capacitance probe with high capacitance resolution while providing an operation frequency as low as 200 kHz or as high as 9 MHz. Status quo was the circuit of Fig. B.4 in the Appendix.
3. Digital electronics: Development of a digital frequency counter with high frequency resolution which converts the Cap Probe's output frequency into a 20 bit value. The circuit additionally processes the control signals from the rockets telemetry. Status quo was the circuit of Fig. C.5 in the Appendix.
4. Power supply: Development of a power supply unit which converts the rockets +28 V battery voltage to the supply levels used by the own electronics *and* isolates the battery power from local ground.
5. Design of the PCB layouts for the four circuits listed above.
6. Construction of the PCB housing boxes Analog Box and Main Box.
7. Assembly, test and calibration of the system as illustrated in Fig. 2.2.

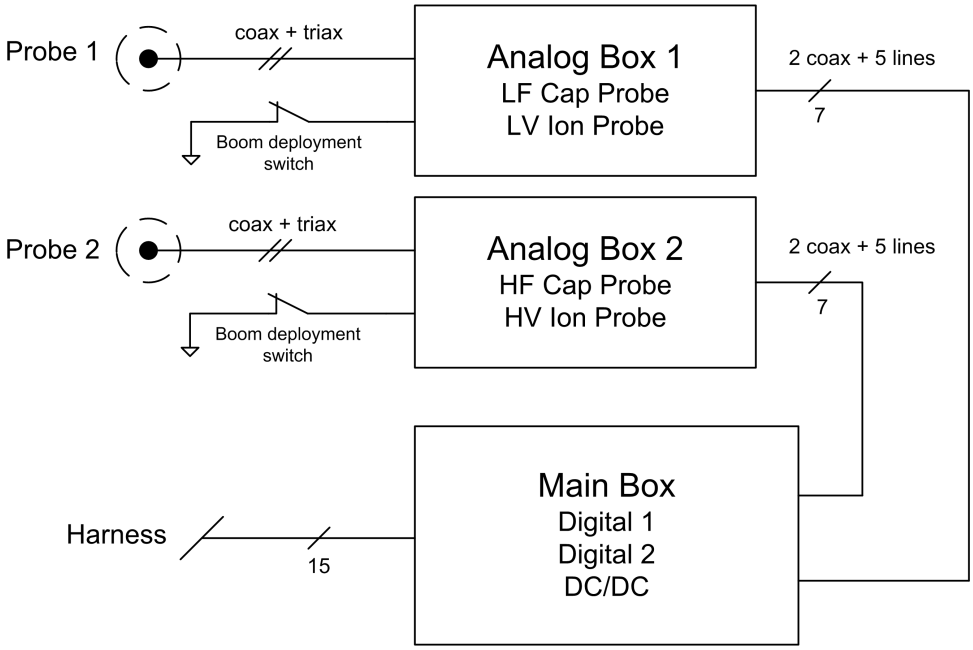

Figure 2.2.: The combined probes are each connected to the Analog Boxes with a coaxial cable for the Cap Probe and a triaxial cable for the Ion Probe. The Analog Boxes contain the analog electronics processing the signals of the two probes: current and capacitance. The output is transmitted via two coaxial cables to the Main Box. The digital electronics in the Main Box converts the frequency information of the Cap Probe electronics into a serial output stream.

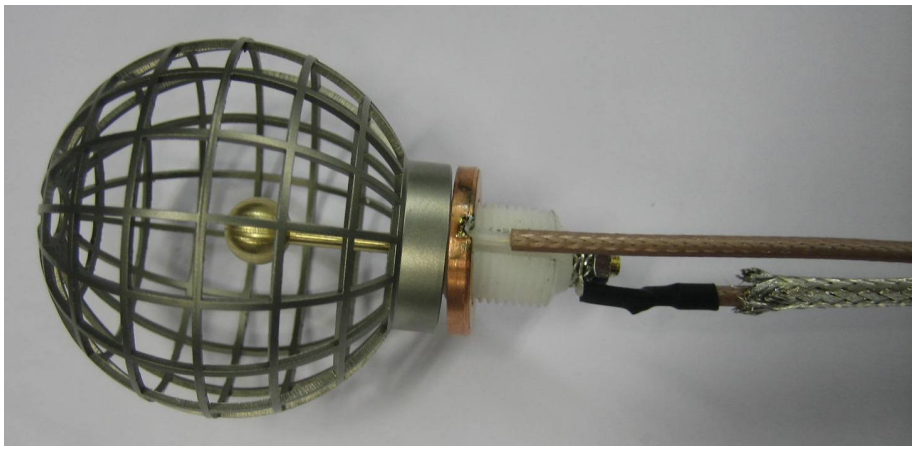

Figure 2.3.: Photo of the combined ion and capacitance probe. The combined probe is connected with two cables: The core of the coaxial cable connects to the outer grid, which functions as capacitance probe. The probe's signal is bypassed to the coax shield to minimize the stray capacitance of the cable. The core of the triaxial cable connects to the small solid sphere inside the grid, *i.e.* the ion probe's inner collector. The inner shield of the triax is at the core's potential to reduce leakage currents and parasitic capacitance. The outer shield is at ground potential and shields the RF signal of the CapProbe's coax.

3. Positive Ion Probe (PIP) electronics

3.1. Theory of operation

Electrostatic probes to measure the number density of ions in the ionosphere have been used by the rocket community for decades.
For charge neutrality the number density of negatively charged particles, *i.e.* electrons and negative ions, must be balanced by positive ions. During the day negative ions can be ignored, because their number densities are expected to be negligibly low, but at night they outnumber electrons below about 80 km. If negative ions can be ignored the positive ion density can be used as a proxy for electron density [Friedrich, 2014].

The basic idea is that a gridded sphere sweeping through stationary plasma, collects an ion current because the path of any positively charged 'thing' (ion, aerosol) once inside the gridded sphere will be sufficiently deflected to end at the negatively biased inner collector.

The current collected by a stationary gridded sphere is

$$I = I_0 \left[\frac{1}{2} e^{-a^2} + \sqrt{\pi} \left(\frac{a}{2} + \frac{1}{4a} \right) erf(a) \right] \tag{3.1}$$

where I_0 is the thermal current to a stationary gridded sphere

$$I_0 = \pi r_0^2 e N^+ v_T \tag{3.2}$$

N^+ is the ion density to be measured.
a contains the rocket velocity v_R and the thermal velocity of the ions v_T

$$a = \frac{2 v_R}{v_T \sqrt{\pi}} \tag{3.3}$$

$$v_T = \sqrt{\frac{8kT}{\pi m_i}} \tag{3.4}$$

where m_i is the ions mass [Folkestad, 1970].

The ion current is primarily determined by the (relative) velocity, the probe's effective cross section and the grid's transparency. [Friedrich, Torkar, Robertson, et al., 2013]. The current to a stationary probe I is due to the ion's thermal velocity v_T, but the main contribution is due to the velocity of the probe relative to the plasma [Folkestad, 1970]. Fig. 3.1 illustrates this relationship. For usual sounding rockets a linear relation between the known velocity of the rocket v_R and the collected current holds and an exact knowledge of v_T is therefore not critical [Friedrich, 2014].

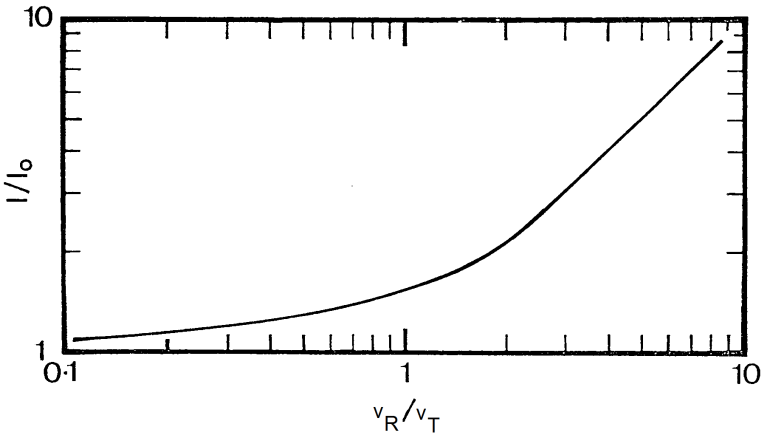

Figure 3.1.: Ratio of the actually observed ion current to a stationary probe I while the rocket moves with a velocity v_R to the thermal ion current I_0 caused by the thermal ion velocity v_T [Folkestad, 1970]

The most common position of PIPs is on a boom deployed laterally. The length of the boom ideally positions the probe outside the shock cone which develops by the forward instrumentation (Fig. 3.2), thus the probe is expected to sample the undisturbed ionosphere [Friedrich, Torkar, Robertson, et al., 2013].

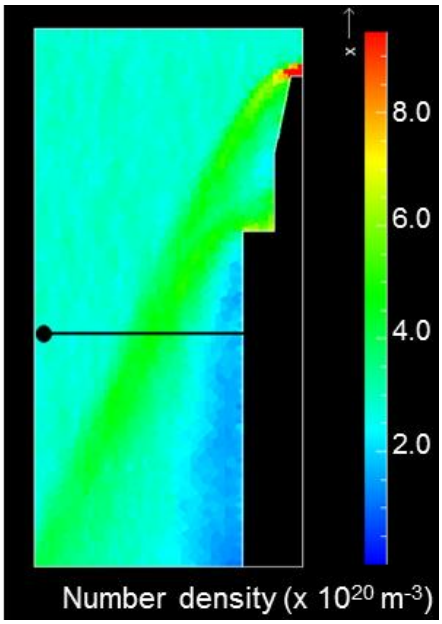

Figure 3.2.: Simulation of the neutral number density at 80 km (rocket velocity about 1 km/s) showing the shock cone developed by the forward instrumentation. The boom ideally positions the probe outside the shock cone [Robertson et al., 2014].

3.1.1. Why use two PIPs with different bias voltages?

There are two reasons:

First, even with a very long boom - particularly with rocket axis aligned with the velocity vector - the current measured by a deployed PIP will generally be modulated by the payload's spin due to the probe's motion in and out of the shock cone. The usual approach is to consider the highest value in a spin period to represent the undisturbed ion density. This means, that the height resolution of one probe is reduced to only one value per spin period [Friedrich, 2014]. By using two probes opposite to each other one can double the height resolution.

Second, by using different bias voltages one can collect ions with different maximum masses m_i (as described in more detail by [Friedrich, Torkar, Robertson, et al., 2013]):
A low-voltage (LV) PIP will collect only 'light' positive ions. A high-voltage (HV) PIP will also collect 'heavy' ions, notably including positively charged ice or dust particles. In the Maxi Dusty project, the region of main interest is 70 km to 90 km, *i.e.* where charged meteoric dust and ice particles are expected.
Past experiments show, that the measurement results regarding ion density do not agree with the modeled values if the amount of dust particles in the altitude region is high [Friedrich, Torkar, Robertson, et al., 2013]. Using one LV probe which collects only 'pure' ions and one HV probe which also collects charged particles, is expected to reveal new findings of how to incorporate dust and ice for modelling the ion density.
The used biased voltage must not be too low otherwise ions may not be captured at all ('mass discrimination'). Nor may it be arbitrary large because this may cause secondary emissions.

In this treatise, *i.e.* for the MaxiDusty project, the two bias voltages are LV = -2.5 V and HV = -8.3 V. The available range for those bias voltages is not only limited by physical reasons but moreover by the input and output voltage ranges of the OPAs used in the processing circuit.

3.2. The 'old' Ion Probe circuit

Fig. 3.3 shows the schematic of the Ion Probe circuit used since 1994.
This configuration cannot be used to measure ion currents lower than 10 pA because it is based in the logarithmic current amplifier ICL8048 of Intersil. Today this product is out of production, an alternative is *e.g.* LOG112 of Texas Instruments but the replacement would not bring any improvement.
The probe's bias voltage was adjusted with R_6 and R_7. An additional bias was realized by

placing batteries in series to the probe. Unfortunately that way it is not possible to exactly determine the bias voltage or, more importantly to actively guard the shield of the coaxial cable connecting the probe to the circuit.
The reference current is fixed and independent of the bias voltage since it is derived from another voltage reference.
The input/output characteristics were evaluated by calibrating the circuit with a decade resistor as described in Ch. 3.5.

3.3. Ion Probe circuit

The objective of this work was to design an improved circuit which should be capable of measuring currents in the range of 10^{-12} A to 10^{-7} A (= 1 pA to 100 nA) while offering a probe bias voltage $GNDA$ of LV = -2.5 V or HV = -8.3 V, ideally using a single, easily adjustable design.
Since the previously used logarithmic current amplifier ICL8048 and the replacement LOG112 cannot amplify currents lower than 10 pA, the only alternative at hand was to re-build an amplifier with discrete ICs, using an ultra-low input bias current OPA as input stage.

Contrary to the CapProbe electronics (Ch. 4) which produces a digital output to the rocket's telemetry, the PIP electronics output is analog. The interface recommendations [Andøya Rocket Range, 11 August 2009] of MaxiDusty specify that the analog output is differential and its range must not exceed 0 V to 5 V.

The Faraday receivers, also part of at the MaxiDusty project use a supply voltage of +12 V which is provided by the DC/DC section in the Main Box of this work (see Ch. 6). Since this supply level was already available, the supply voltage for the PIP electronics (and thus the CapProbe electronics) was chosen $\pm$12 V. This resulted in a few limitations (a higher supply would be better) which will be discussed in the following sections.

3.3.1. Measuring pA currents

Measuring currents as low as 1 pA results in problems which had not to be considered in past designs. The most important for this work are summarized in the following discussions. The interested reader may refer to [Grohe, 2011] or [Keithley Instruments, 2004].

First of all the input bias current of the projected amplifier must not be greater than the current to be measured (ideally at any temperature). Unfortunately the integrated circuit ICL8048 or LOG112 could not be used any more because the input bias current of those devices is much higher than 1 pA. Their output voltage tends to $\pm V_S$ if an input current lower than 10 pA is applied. That creates problems because the output result is not

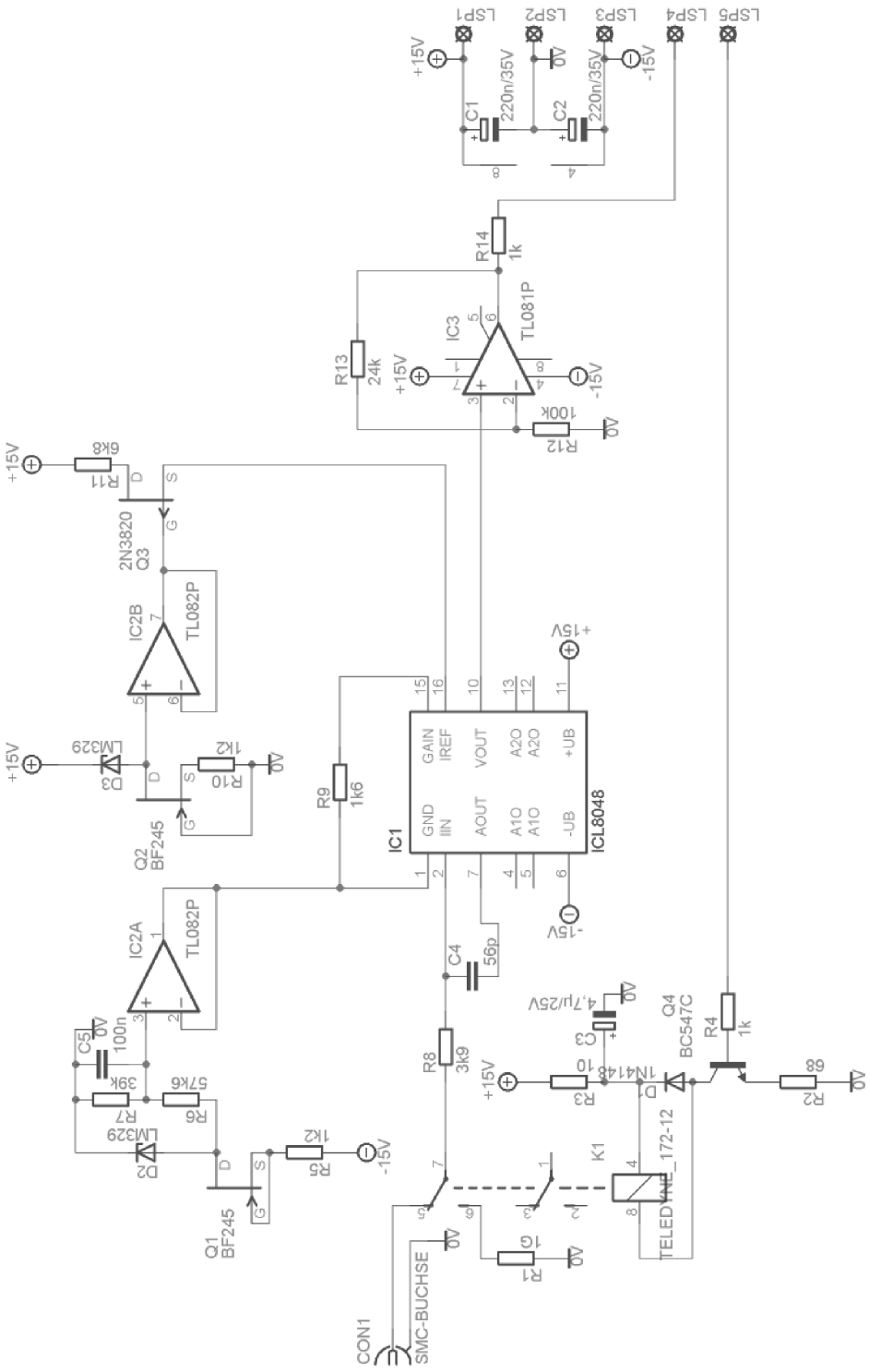

Figure 3.3.: Schematic of the Ion Probe circuit used since 1994. The logarithmic current amplifier ICL8048 processes the probe current, its output voltage is scaled by IC3. The probe's bias voltage is adjusted with R6 and R7. The reference current is fixed and independent of the bias voltage since it is derived from another voltage reference.

only not useful, but it exceeds the specified output limits of 0 V to 5 V. A result like this has to be avoided.
'Ultra-low (input) bias current' OPAs offer input bias currents I_B at subpicoamp levels, like the LMP7721 ($I_{B,max}$ = 20 fA at 25 °C, V_S = 5 V) or the OPA129U ($I_{B,max}$ = 250 fA at 25 °C, $V_S = \pm$12 V) both by Texas Instruments . For this work the OPA129U had to be chosen due to its higher common-mode input range.
The bias (and offset) current typically doubles every 10 °C. Hence I_B of the OPA129U is approx. 1 pA at 55 °C, the upper limit of the expected operating temperature. Obviously the temperature dependence of I_B takes great effect on the measurement result. It must therefore be compensated.

When measuring currents in the pA-range, it is highly recommended to use a triaxial cable. The inside shield of the triax is used as a driven guard preventing the leakage resistance of the cable from degrading the low current measurement. By driving the inside shield to the same potential as the core, here the probe's bias, the difference in potential between cable core and guard is ideally zero, so the leakage current is eliminated [Keithley Instruments, 2004].
Furthermore, the guarded inside shield speeds up the measurement by eliminating the core-to-shield capacitance. The probe-cable-system can be understood to be a first order system where R is the extremely high source resistance of the Ion Probe and C is the core-to-shield capacitance, forming a RC time constant. It limits the rise time of the ion current input. Changes in the current will be recorded delayed or not at all. With no difference in potential between cable core and guard the capacitance between those layers is nearly eliminated which minimizes the RC time constant. However, the Ion Probe circuit still reacts very slowly for currents below 10 pA due to the dielectric absorption of the coaxial cable and the input capacitance of the circuit. In Ch. 3.6 the time response of the Ion Probe is described on the basis of oscilloscope screenshots.
The outside shield of the triax is at payload potential (ground). It prevents the RF signal on the close-by Cap Probe coax from affecting the Ion Probe cable.

There are some more considerations regarding the component selection and layout discussed in the respective chapters.

3.3.2. Schematic

3.3.2.1. Logarithmic current amplifier (LogAmp)

The circuit of the logarithmic current amplifier (LogAmp) is basically the same as the integrated circuit of the ICL8048 or LOG112. The used schematic is inspired by [Texas Instruments Inc., 2013a]. A more detailed description concerning the theory and applications of LogAmps is provided in [Texas Instruments Inc., 2013b].

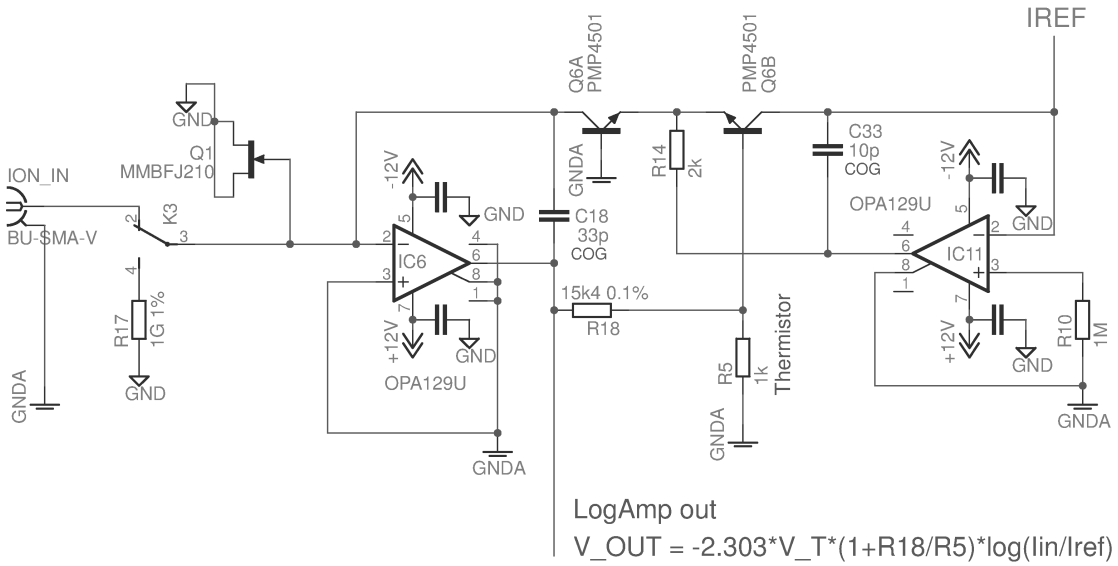

Figure 3.4.: Simplified detail of the Ion Probe schematic: self-build logarithmic current amplifier (LogAmp).

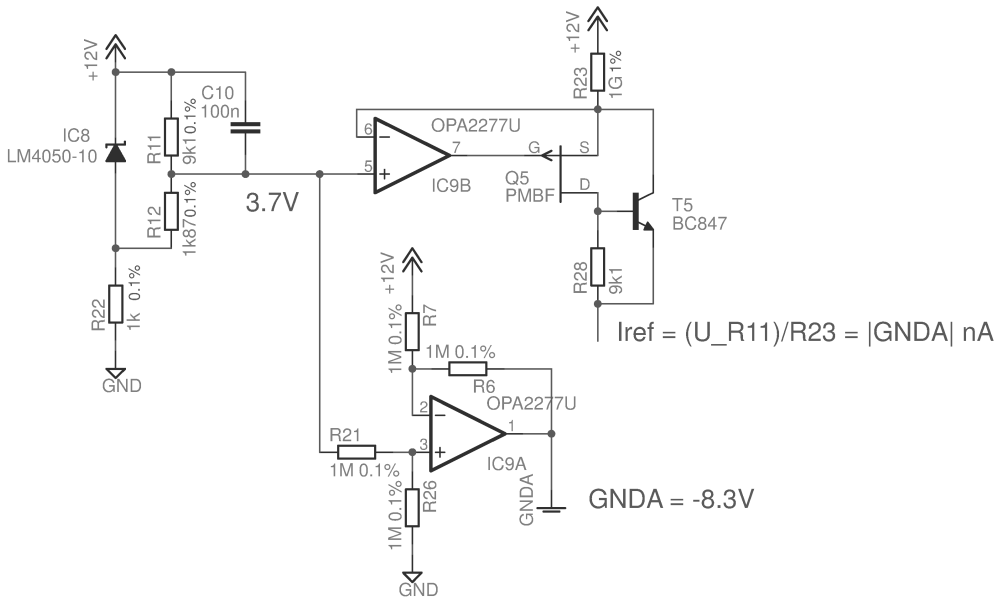

Figure 3.5.: Simplified detail of the HV Ion Probe schematic: generation of bias voltage $GNDA$ and reference current I_{ref} as function of $GNDA$.

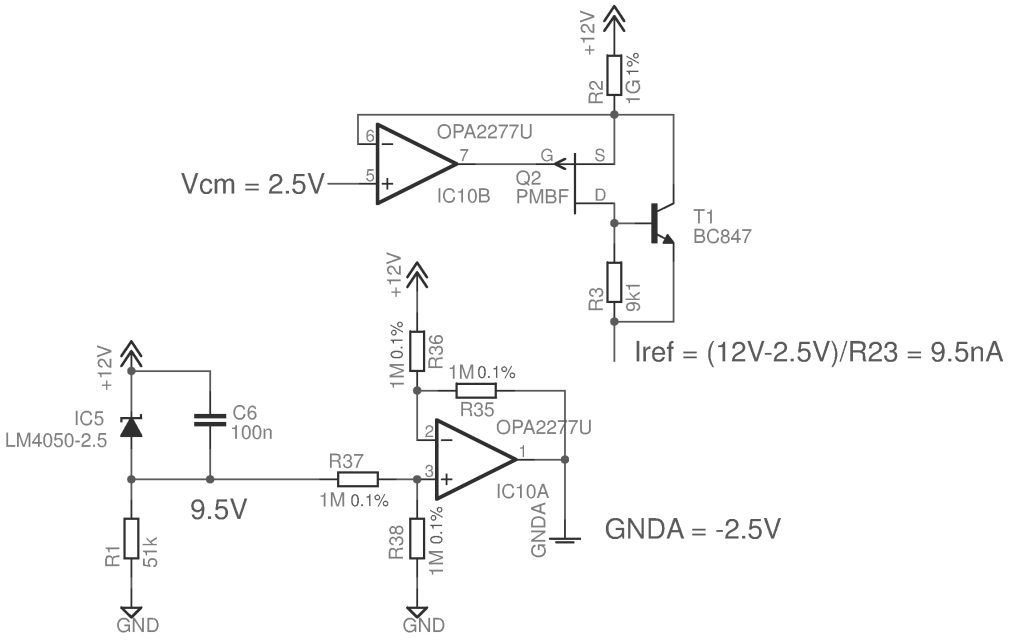

Figure 3.6.: Simplified detail of the LV Ion Probe schematic: generation of bias voltage $GNDA$ and fixed reference current I_{ref}

The bipolar transistors Q6A and Q6B are in the respective feedback path of the OPAs IC6 and IC11. This forces the collector current of Q6A to be exactly the input current, *i.e.* the ion current, and the collector current of Q6B to be equal to the current through R_{14}. Since the collector current of Q6B remains constant, its emitter base voltage also remains constant. Therefore, only the V_{BE} of Q6A varies with a change of input current. The output voltage is a function of the difference in emitter base voltages V_{BE} of Q6A and Q6B:

$$V_{out} = \frac{R_{18} + R_5}{R_5}(V_{BE,6B} - V_{BE,6A}) \tag{3.5}$$

Q6A and Q6B are matched transistors in a single package. The emitter base differential is:

$$\Delta V_{BE} = \frac{kT}{e} \cdot log_e \frac{I_{C,6A}}{I_{C,6B}} = V_T \cdot 2.303 \cdot log_{10} \frac{I_{C,6A}}{I_{C,6B}} \tag{3.6}$$

where

$$V_T = \frac{kT}{e} = 25.61 \text{ mV at } 25\,^{\circ}\text{C}$$

is the thermal voltage.
Combining these two equations gives:

$$V_{out} = -V_T \frac{R_{18} + R_5}{R_5} \cdot 2.303 \cdot log_{10} \frac{I_{in}}{I_{ref}} \tag{3.7}$$

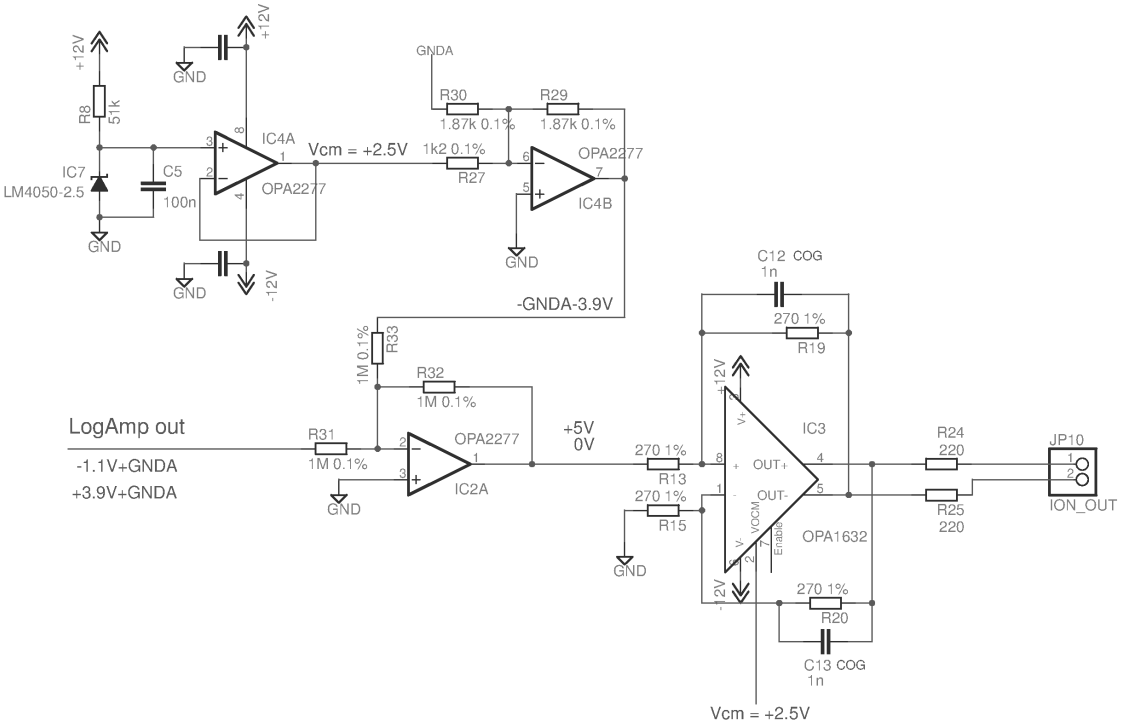

Figure 3.7.: Simplified detail of the Ion Probe schematic: output voltage (range) adaptation and the differential line driver.

Due to the logarithmic relationship between collector current and V_{BE} of a bipolar transistor, the output voltage V_{out} is proportional to the logarithm of the input current. The divider, R_{18} and R_5, sets the gain while the reference current I_{ref} sets the zero.
The coefficient of the log term is directly proportional to absolute temperature through V_T. This can be easily compensated by making R_5 also directly proportional to temperature. For this purpose R_5 is realized as linear PTC thermistor with a temperature coefficient of +4110 ppm/K.
The amplifier's (ideally temperature stable) gain is set by the resistances R_{18} = 15.4 kΩ and R_5 = 1 kΩ. The equation for the ideal output voltage results in

$$V_{out} = -0.967\,\mathrm{V} \cdot log_{10}\frac{I_{in}}{I_{ref}} \tag{3.8}$$

IC6 additionally has the function of biasing the probe. The bias voltage $GNDA$ is applied to its non-inverting input. Its input common-mode range is the ultimate limit for the probe's bias voltage. With a supply of $\pm 12\ V$ the OPA129's common-mode input limit is 9 V [datasheet of OPA129]. The HV bias used of -8.3 V is chosen close to this limit. A higher supply voltage would allow even higher bias voltages.
For proper operation all the signals of the LogAmp circuit are referred to $GNDA$, hence its output voltage V_{out} is.
As mentioned above, the zero of V_{out} is set by I_{ref}, namely were $I_{in} = I_{ref}$. Since the reference current is derived from a 1 GΩ-resistor (see Ch. 3.3.2.3) it is always in the (upper) nA range, hence it is the zero of V_{out}.
The circuit's speed and accuracy is determined by the values of C_{18} and C_{33}. For the actual application the speed was more critical, thus the capacitors are as small as possible. C_{18} = 33 pF is the minimum possible value. $C_{18} > C_{33}$ has to be fulfilled.

One may note that there is no possibility to compensate the offset voltage of the input stage amplifier IC6. This is because the offset voltage of an OPA is temperature dependent, hence a simple compensation would only work for a particular temperature. Additionally a compensation with a potentiometer adds that much noise that the compensation becomes useless. Besides, an offset compensation does not seem to be necessary, as the measurement results in Ch. 3.4 show.

3.3.2.2. Input bias current compensation

Fig. 3.9 illustrates the LogAmp's output without input bias current compensation. The red lines mark the -1.1 V and +3.9 V output limits according to the 5 V output range (see. Ch. 3.3.2.4). Note that a higher output voltage V_{out} means a lower input current I_{in}. The measured current is always lower than the ideal value and rapidly decreasing with temperature. Apparently the OPA IC6 (see schematic, Fig. 3.4) has an input bias current directed out of its input, decreasing the effective input current. Since the bias current is

increasing with temperature the measured current is decreasing. The major problem arising is that V_{out} by far exceeds the upper range limit. Such a measurement result cannot be processed by the rocket's telemetry. Thus, ensuring that the measurement result is inside the output voltage range is even more important than to be near the ideal values. The bias current needs compensation, at least in a way that the results are inside the limits.

The major source for an OPA's input bias current is the leakage of its ESD (electro static discharge) protection structures. Since they are basically diodes, they have a leakage profile which follows that of a diode over temperature [Grohe, 2011]. It is possible to use a reversed biased diode, or a diode-connected transistor for lower leakage, to add a 'leakage' current to the input node in the reverse direction of the OPA's leakage current. That way the additional 'leakage' ideally has the same temperature dependence as the bias current of the OPA and is therefore capable of compensating the bias current over the whole temperature range.
The reverse current of a transistor depends on its reverse voltage. It would be possible to use an adjustable reverse voltage to compensate the bias current exactly but this needs great effort. In the actual circuit Drain and Source are connected to ground and the reverse voltage is determined by the probe's bias voltage. Hence it is not the same for the LV and HV circuit.
Unfortunately both the OPA's input bias current and the diode-connected transistor's reverse current are component-dependent and very difficult to determine. Measurements without compensation showed that the bias current of the (used) OPA129 (IC6) was about 0.5 pA (25 °C) directed out of the OPA's input. The used JFET transistor MMBFJ210 (Q1) was measured to have a reverse current certainly greater than the bias current at any reverse voltage and was therefore suitable for this application.
Fig. 3.8 shows the same measurement as referenced above but now with bias current compensation through Q1. Apparently the reverse current of Q1 is greater than the OPA's input bias current since the measured current is now always below the ideal value (higher output voltage). The introduced current neglects the opposite directed bias current and adds to the original input current, hence the measured current increases. Over temperature the transistor's reverse current is always higher than the bias current, the measured current increases with temperature, but the output value is much more stable and predictable than without compensation. Most important, the output is always inside its limits.

3.3.2.3. Generation of probe bias voltage $GNDA$ and LogAmp reference current I_{ref}

Fig. 3.5 shows the proposed schematic for generating the probe bias voltage $GNDA$ and the LogAmp reference current I_{ref} using only one voltage reference. By this approach I_{ref} is a function of $GNDA$ which has the advantage that the in-flight calibration value is independent of the bias voltage. Furthermore during calibration with a decade resistor (see Ch. 3.5) the dependence of the bias voltage is also eliminated. On the other hand the

measured ion current I_{in} thereby also depends on the bias (see Eq. (3.8) and Eq. (3.14)). The probe's bias can be adjusted with the divider R_{12}, R_{11} as it was in the past design. The resistors have only 0.1% tolerance and ± 100 ppm/K to ensure the accuracy of the set voltage. The equation for the voltage on the non-inverting input node of IC9B, here 3.7 V, is

$$V_{IC9B,+} = V_+ - V_{R11} = V_+ - V_{IC8}\frac{R_{11}}{R_{11}+R_{12}} \tag{3.9}$$

where V_{IC8} is the voltage of the voltage reference IC, here 10 V, and V_+ is the positive supply voltage, here 12 V. Note that $V_{IC9B,+}$ is a function of the supply voltage!
The subtractor IC9A generates the negative bias voltage:

$$GNDA = V_{IC9B,+} - V_+ = V_+ - V_{IC8}\frac{R_{11}}{R_{11}+R_{12}} - V_+ = -V_{IC8}\frac{R_{11}}{R_{11}+R_{12}} \tag{3.10}$$

Note that $GNDA$ is finally independent of the supply voltage and therefore insensitive to supply noise or ripples. The reference current, provided by a temperature stable current source (Q5, T5, R_{28}), is also independent of the supply:

$$I_{ref} = \frac{V_+ - V_{IC9B,+}}{R_{23}} = \frac{V_{R11}}{R_{23}} = \frac{\mid GNDA \mid}{R_{23}} \tag{3.11}$$

The 'built-in' independence of the supply is an improvement compared to the 'old' Ion Probe circuit of Fig. 3.3. There two FET current sources (and two voltage references) were used to achieve insensitivity of the supply voltage. The actual circuit offers same functionality while requiring fewer components. Additionally the power consumption is reduced by using only one voltage reference.
As already mentioned the in-flight calibration current is a function of the bias:
$I_{cal} = \mid GNDA \mid /1\,\mathrm{G\Omega}$. By making I_{ref} also a function of $GNDA$ the dependence on $GNDA$ is eliminated according to Eq. (3.8) since $R_{17} = R_{23}$:

$$V_{out,Cal} = -0.967\,\mathrm{V} \cdot log_{10}\frac{I_{Cal}}{I_{ref}} = -0.967\,\mathrm{V} \cdot log_{10}\frac{R_{17}}{R_{23}} = 0\,\mathrm{V}$$

The in-flight calibration value is ideally always equal 0 V.

Unfortunately the output range of the reference current source is limited by the performance of the JFET Q5. The smallest current (requiring the highest Gate voltage) which can be generated with the used PMBFJ174 is approx. 5.8 nA. Using a 2N3820 type (for instance) would enable to provide currents not lower than 3.5 nA. Accordingly, this design does not seem to be applicable for arbitrary low reference currents. A reference current of only 2.5 nA as would result for the LV circuit ($GNDA$ = -2.5 V) cannot be generated by using the circuit of Fig. 3.5.
An alternative is to use the V_{cm}= 2.5 V reference to generate a fixed reference current I_{ref} = 9.5 nA as depicted in Fig. 3.6. For the LV circuit $GNDA$ = -2.5 V can be directly generated by using a 2.5 V reference where R_{11} is open and R_{12} is shortened.
With fixed I_{ref} the calibration values are no longer independent of the bias. But now the

zero of V_{out} is fixed, namely where I_{in} = 9.5 nA. This makes the adaption of the output range easier, since the limits are constant for arbitrary bias (compare Ch. 3.3.2.4). However, in the actual configuration $I_{ref,LV}$ was chosen near $I_{ref,HV}$ so that the output limits also stay the same.

In conclusion, the schematics of Fig. 3.5 and Fig. 3.6 are equivalent, but one provides constant calibration values and the other a constant zero. By using the V_{cm}-reference already needed for the differential line driver both circuit variations require the same number of components and therefore the same PCB area.

3.3.2.4. Adaption of the LogAmp's output voltage

Since the output voltage of the LogAmp is referred to the probe's bias $GNDA$ and its zero depends on I_{ref} and can therefore not be adequately adjusted, V_{out} needs to be adapted 'manually' to values between 0 V and 5 V which are accepted by the telemetry. Fig. 3.7 shows the simplified detail of the Ion Probe schematic responsible for the output voltage adaption.

Inserting the projected limits for the ion current of $1 \cdot 10^{-7}$ A to $1 \cdot 10^{-12}$ A and the values of the reference current I_{ref} for LV or HV circuit into Eq. (3.8) yields the expected limits of the LogAmp's output voltage V_{out}:

LV circuit (I_{ref} = 9.5 nA): $V_{out} = -0.983\ V$ to $3.827\ V$

HV circuit (I_{ref} = 8.3 nA): $V_{out} = -1.040\ V$ to $3.770\ V$

The rocket's telemetry accepts voltages in a range of 5 V. Hence the output range limits for the LogAmp were extended to -1.1 V and +3.9 V. Note that the LogAmp's output is referred to the bias voltage $GNDA$. Therefore its output range limits are :

$$V_{out,min} = -1.1\ V + GNDA \qquad V_{out,max} = +3.9\ V + GNDA$$

These limits apply for both circuit options, LV and HV. The actual output value depends on the probe's bias voltage $GNDA$. This issue is eliminated by subtracting $GNDA$. Additionally the upper limit of +3.9 V is subtracted (adjustable by R_{27}, R_{29}). Thereby the lower output limit is assigned a final output value of 5 V and the upper limit is assigned 0 V. Since the LogAmp's output is also inverted by the adder IC2A, finally a higher ion current results in a higher output voltage as illustrated in Figs. 3.13 and 3.12.

$$-((-1.1\ V + GNDA) + (-GNDA - 3.9V)) = +5\ V$$
$$-((+3.9\ V + GNDA) + (-GNDA - 3.9V)) = 0\ V$$

The differential line driver IC3 converts the single-ended signal into a differential one and applies a common-mode voltage of +2.5 V.

3.3.3. Component selection

The circuit in Figs. 3.5 and 3.6 use an OPA subtractor circuit (IC9A) to generate $GNDA$ out of $V_{IC9B,+}$. Since the subtractor's output is sensitive to the real resistor values, it is expedient to discuss their maximum acceptable resistance tolerance. Thus, one could use the well-tried voltage-reference-configuration (D2, R_6 ,R_7, IC2A) of the old circuit (Fig. 3.3) instead which is also independent of the supply since V_{R7} is referred to ground. A worst case estimation considering the resistor tolerances and the output voltage tolerance of IC2A shows that the maximum output error of the two circuit variations is about the same (± 23 mV) for 0.1% resistors but that the output error of the subtractor drastically increases when using 1% resistors. Hence all performance-critical resistors have an accuracy of 0.1%. The resistors connected to IC9A and IC2A must not be lower than 1 MΩ so as not to stress the reference voltage or the LogAmp's output, respectively.

The used OPA2277U provides ultra low temperature drift and ultra low offset. This is crucial for the stability of $GNDA$ and I_{ref} over temperature and therefore the LogAmp's temperature stability.
Note that IC9A and IC9B of Fig. 3.5 are in the same package, hence will have similar offset and drift aiding the matching of I_{ref} to $GNDA$.
The output voltage swing of IC9 can limit I_{ref} and $GNDA$.

As already discussed the input bias current of the LogAmp's input amplifier IC6 is crucial for the overall low-current performance and its common-mode input range limits the bias voltage.
Note that the common-mode input range of IC2A and IC4B is no criterion since the adder circuit's common-mode voltage is equal 0 V.

The differential line driver IC3 should be chosen for low offsets since they directly influence the final output value.
The OPA1632 used has a maximum offset voltage of ± 3 mV, an input bias current of 6 μA and an input offset current of ± 500 nA. Including these errors yields an ion current measurement error of 1.4 %.
The driver does not need to be fast since the Ion Probe signal only changes slowly.

The high-value resistors R_{17} and R_{23} should ideally be hermetically sealed and through hole mounted to reduce leakage currents [Grohe, 2011]. The larger the dimensions of the resistor are, the smaller is the expected leakage.
However, in the actual work the dimension of the resistors (hence their value) was limited by the dimension of the PCB housing, *i.e.* the Analog Box (see. Ch. 7). The used resistor is HB11G0FZRE (TE Connectivity), its resistance is 1 GΩ. Resistors with higher values simply do not fit into the housing box.
Unfortunately the value of the calibration resistor R_{17} is too low. As depicted in Fig. 3.8 or

Fig. 3.10 a current in the nA range as provided by $R_{17} = 1\,\mathrm{G}\Omega$ is not temperature dependent. Hence the in-flight calibration (see Ch. 3.6) cannot monitor the circuit's temperature drift.

To provide an ideal noise-free environment all the power supply components (most notably the DC/DC converters) are located on another PCB in the Main Box. An extensive supply filter (see the complete schematic in the Appendix) was added to the Ion Probe PCB to maintain a clean supply even after the long cable between Analog Box and Main Box .

3.3.4. Layout

In the article [Grohe, 2011] many low-current design techniques are explained. They are summarized in the following. As far as possible they were considered in the actual layout. The overall objective is to keep leakage currents low.

The smallest packages used are SOIC as packages with tighter lead packages tend to have higher leakages. This is mainly because of the tight lead spacing and closer proximity to the supply lines and other pins.
Guard traces should surround all the input traces and sensitive feedback components to minimize capacitive coupling. The output does not need to be guarded, but it should be shielded from the input.
The input surface area should be minimized to reduce the stray input capacitance and to make the input easier to guard. Since I-R drop is not a big issue at low-current levels, the narrowest trace width is preferred.
The PCBs solder mask can be removed in the input area to reduce the effects of surface charges.

Fortunately the analog PCBs are housed in a very tight aluminum box so electrostatic interference from the outside, airflow or dust is negligible.

3.4. Measurement results

Figs. 3.8 and 3.10 show the measured LogAmp output voltages over input current for different temperatures. Obviously the results deviate from the ideal output values, especially at high temperatures (see Ch. 3.3.2.2). However, the curves can be mathematically described: Tables 3.4 and 3.4 give the coefficients of a polynomial of degree 5 that fits the measured data points for currents less than $1 \cdot 10^{-10}$ A ($V_{out,diff} < 1.9$ V, approx.). Using Eq. (3.13) the ion current corresponding to a measured voltage and a given temperature can be derived. Naturally, during flight only the differential output voltage is measured. Eq. (3.12)

	35 °C	45 °C	50 °C	60 °C
p_1	4.7832e-013	4.5022e-011	1.4693e-011	6.7573e-010
p_2	3.666e-011	-5.0454e-010	-1.2402e-010	-7.6526e-009
p_3	-4.6922e-010	2.1366e-009	2.4934e-010	3.4329e-008
p_4	2.1241e-009	-4.0895e-009	5.3258e-010	-7.6085e-008
p_5	-4.2431e-009	3.0921e-009	-2.4946e-009	8.3032e-008
p_6	3.1996e-009	-2.3084e-010	2.4335e-009	-3.5488e-008

Table 3.1.: HV Ion Probe: coefficients of the fitted polynomial $I_{ion}(V_{LogAmp})$ of Eq. (3.13).

describes how to calculate the LogAmp's output voltage which can be inserted to Eq. (3.13). For currents above $1 \cdot 10^{-10}$ A, *i.e.* for output voltages $V_{out,diff}$ above 1.9 V, and for room temperature the ideal relationship according to Eq. (3.14) applies.

$$V_{LogAmp} = -(V_{out,diff} - 3.9\,\mathrm{V}) \tag{3.12}$$

$$I_{ion,fit} = p_1 V_{LogAmp}^5 + p_2 V_{LogAmp}^4 + \cdots + p_5 V_{LogAmp} + p_6 \tag{3.13}$$

for $V_{out,diff} < 1.9\,\mathrm{V}$ or 25 °C

$$I_{ion,ideal} = 10^{\wedge}\left(\frac{V_{LogAmp}}{-0.967\,\mathrm{V}}\right) \cdot I_{ref} \tag{3.14}$$

for $V_{out,diff} > 1.9\,\mathrm{V}$
where
$I_{ref,HV} = 8.3\,\mathrm{nA}$
$I_{ref,LV} = 9.5\,\mathrm{nA}$

3.5. Calibration with decade resistor

It needs at least an adjustable pA-source and an extremely high-impedance volt meter to determine the LogAmp's input/output characteristic of Figs. 3.8 to 3.10. Naturally such high level equipment is not always at hand. A well-tried alternative is to connect a high-ohmic decade resistor between ground and the current input. The negative bias voltage leads to a current $I = GNDA/R_{decade}$ directed to the circuit's input. Since this calibration current is

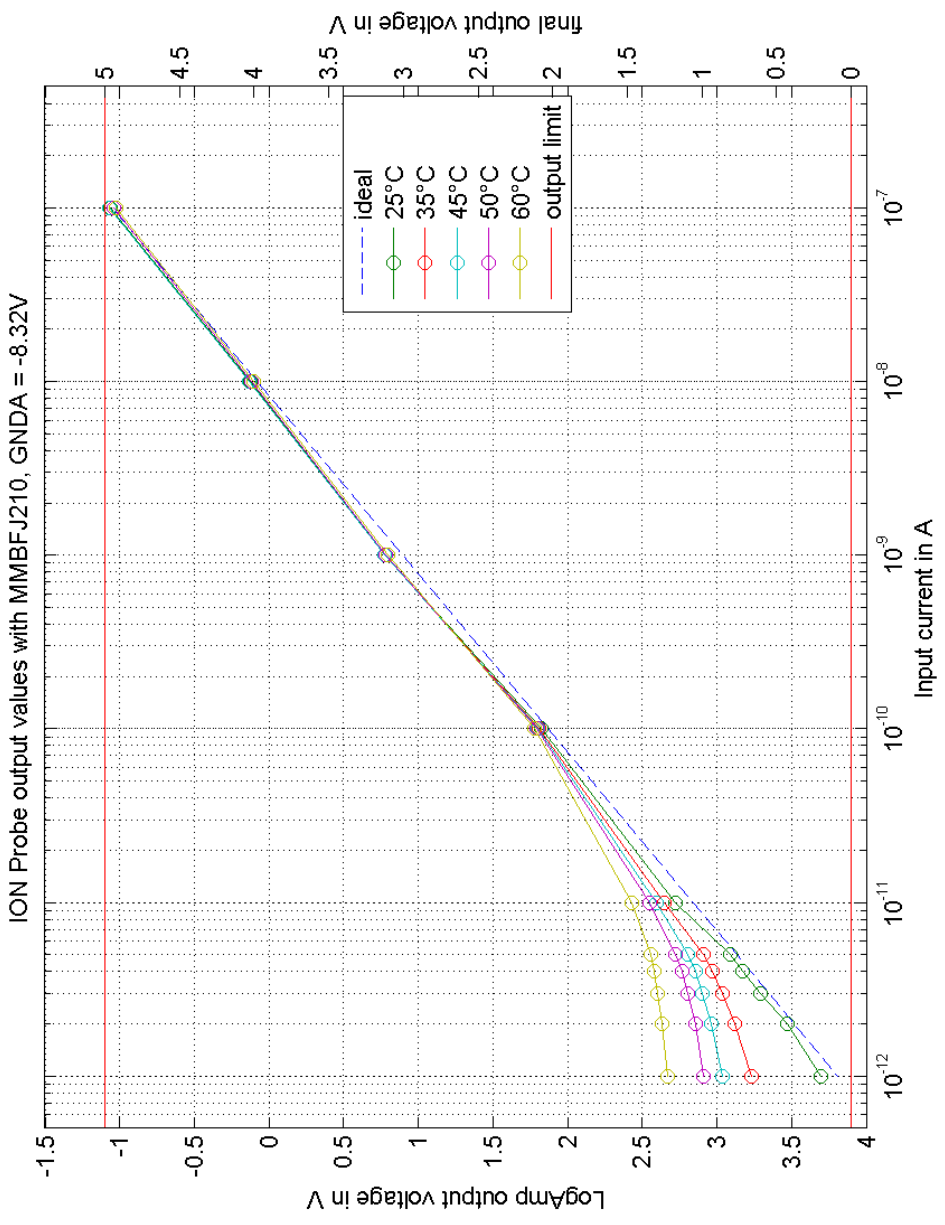

Figure 3.8.: LogAmp output voltage (and adapted output voltage) over input current and temperature for HV Ion Probe with bias current compensation. The red limit lines mark the 5 V output range. The characteristic is ideally -0.962 V/decade.

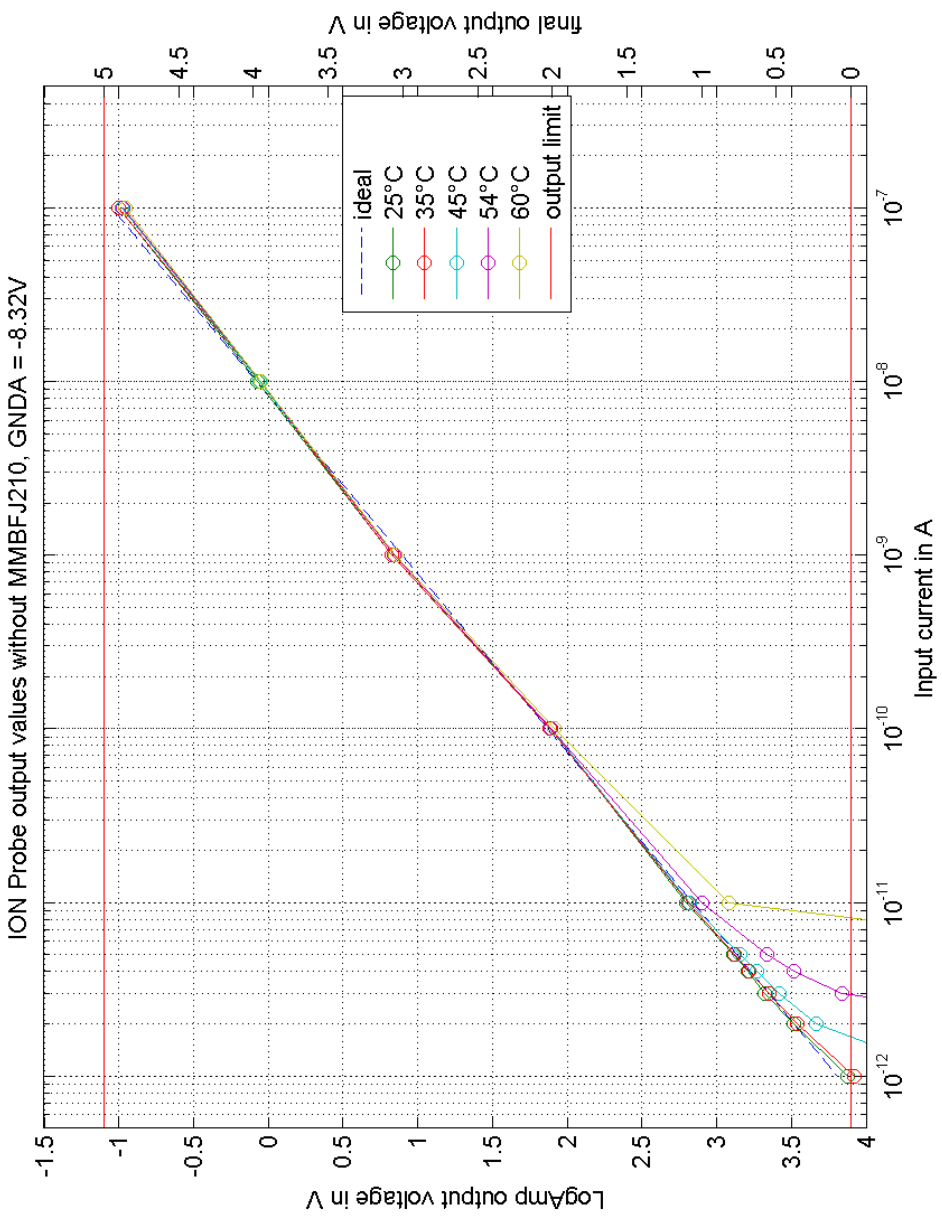

Figure 3.9.: LogAmp output voltage (and adapted output voltage) over input current and temperature for HV Ion Probe without bias current compensation. At temperatures above 25 °C the output voltages corresponding to currents lower than 10 pA exceed the +3.9 V limit.

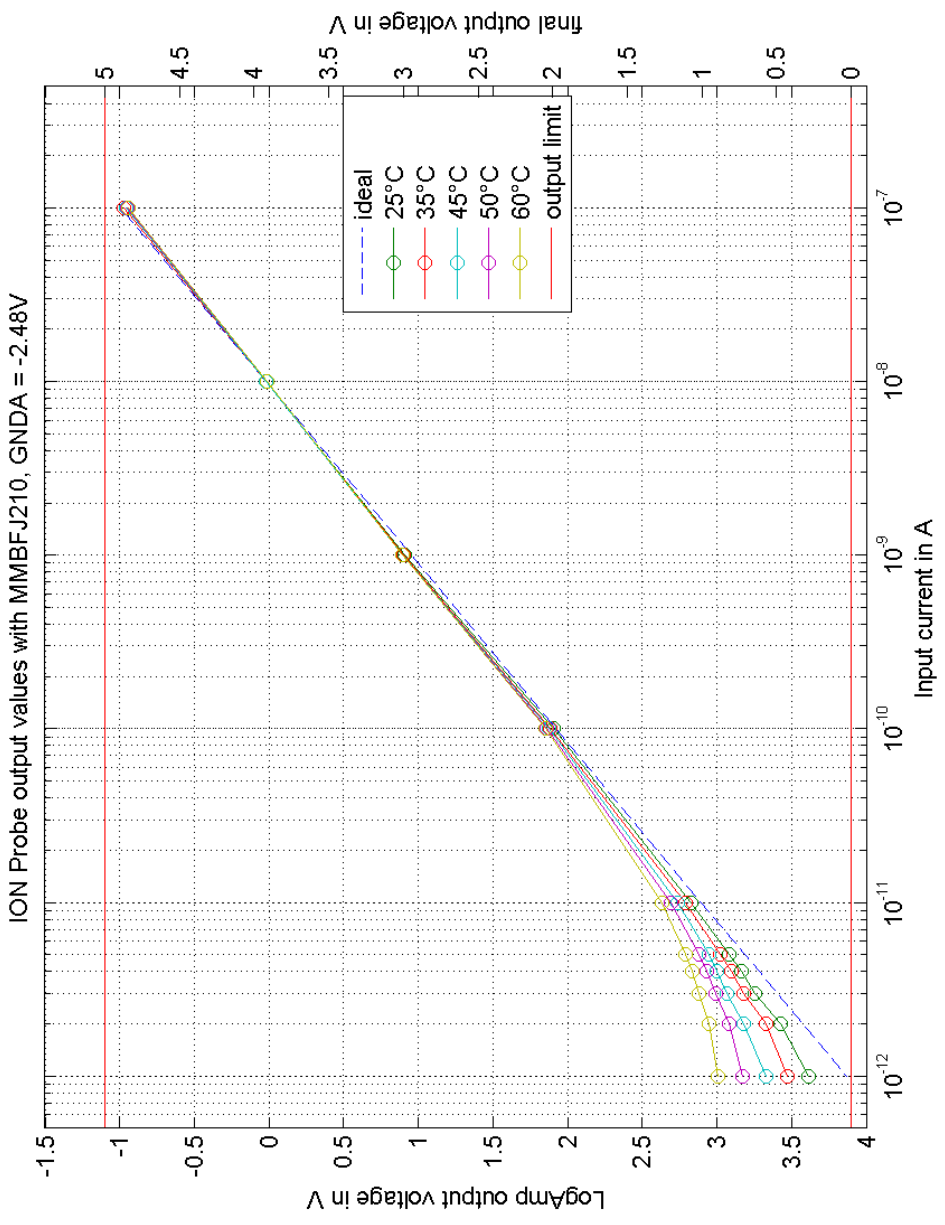

Figure 3.10.: LogAmp output voltage (and adapted output voltage) over input current and temperature for LV Ion Probe with bias current compensation. The red limit lines mark the 5 V output range. The characteristic is ideally -0.962 V/decade.

	35 °C	45 °C	50 °C	60 °C
p_1	4.7832e-013	4.5022e-011	1.4693e-011	6.7573e-010
p_2	3.666e-011	-5.0454e-010	-1.2402e-010	-7.6526e-009
p_3	-4.6922e-010	2.1366e-009	2.4934e-010	3.4329e-008
p_4	2.1241e-009	-4.0895e-009	5.3258e-010	-7.6085e-008
p_5	-4.2431e-009	3.0921e-009	-2.4946e-009	8.3032e-008
p_6	3.1996e-009	-2.3084e-010	2.4335e-009	-3.5488e-008

Table 3.2.: LV Ion Probe: coefficients of the fitted polynomial $I_{ion}(V_{LogAmp})$ of Eq. (3.13).

Figure 3.11.: Calibrating the Ion Probe electronics with a decade resistor. An adapter is needed to connect the coaxial SMC plug to the electronics' triaxial connector.

a function of the bias voltage one needs to know $GNDA$ (and R_{decade}, naturally) exactly to be able to evaluate the accuracy of the measurement. The circuit presented in Fig. 3.5 resolves this problem by eliminating the dependence of $GNDA$, see Ch. 3.3.2.3.
Although this method is not suitable for evaluating the accuracy of the circuit, especially the LogAmp's, it is an easy and quick way to ensure the functionality of the complete circuit. Figs. 3.12 and 3.13 illustrate the calibration results using a decade resistor with $1 \cdot 10^{12}\,\Omega$ to $1 \cdot 10^{7}\,\Omega$. The output voltages of the LogAmp are compared to the final differential output of the line driver. The signal is inverted by the output stage (Fig. 3.7). Obviously, the output stage introduces no notably error. The differential output limits are marked with red lines. Note that a resistance of $1 \cdot 10^{7}\,\Omega$ provides a current higher than the processible limit of $1 \cdot 10^{-7}$ A.

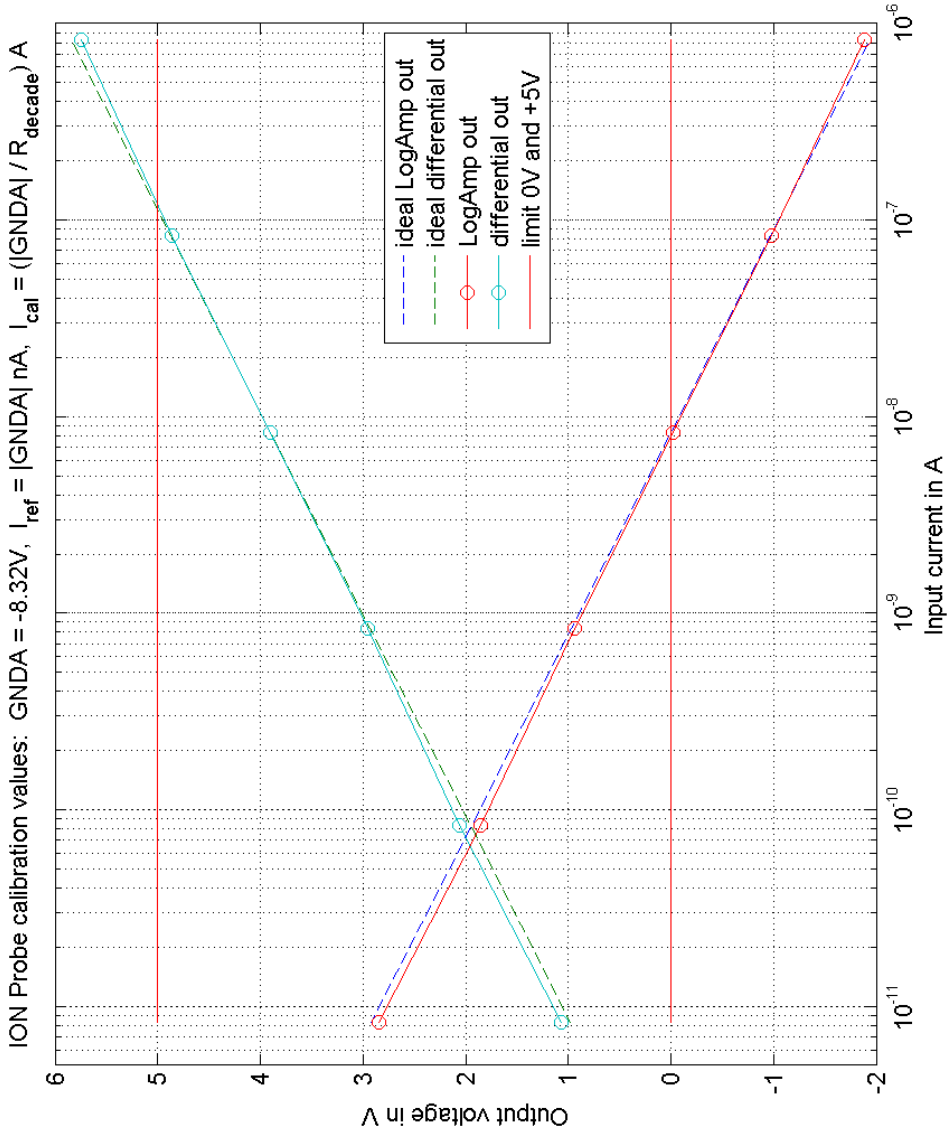

Figure 3.12.: HV Calibration curve: Output voltage over calibration current set with decade resistor to $I_{Cal} = |\ GNDA\ |\ R_{decade}$ A = 2.48/R_{decade} A. The differential output voltages for currents greater $1 \cdot 10^{-7}$ A exceed the 5 V limit.

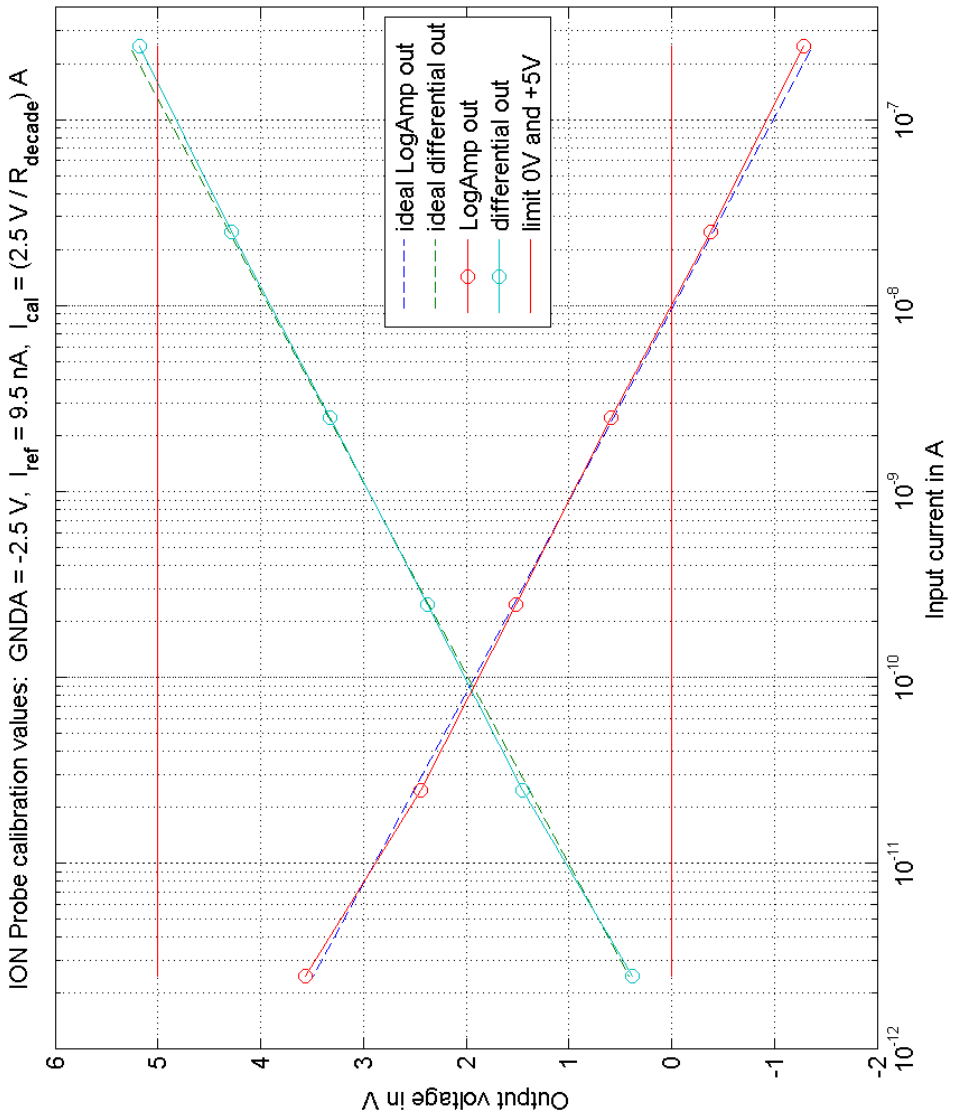

Figure 3.13.: IV Calibration curve: Output voltage over calibration current set with decade resistor to $I_{Cal} = 2.5/R_{decade}$ A. The differential output voltages for currents greater $1 \cdot 10^{-7}$ A exceed the 5 V limit.

3.6. In-flight calibration

Every 11 s or 22 s (see Ch. 5) during flight the measurement is calibrated to check stability and monitor the temperature drift. Therefore the input of the measurement circuit is switched with a relay from the Ion Probe to an internal 1 GΩ calibration resistor. A mechanical relay is used because of its extremely high insulation resistance (measured value $>$ 1 TΩ), since this insulation resistance is in parallel to the Ion Probe introducing leakage currents if it is not high enough.
During the in-flight calibration the bias voltage is applied to the calibration resistor R_{17} providing a calibration current $I_{cal} = GNDA/R_{17}$ into the measurement input (since the bias is negative). Notably this calibration current is a function of the bias voltage! The circuit of Fig. 3.5, introduced in Ch. 3.3.2.3 eliminates this issue by making the LogAmp reference current I_{ref} also a function of the bias. By this the calibration output is always ideally 0 V.

Using a monoflop (see complete schematic in the Appendix) the duration of the calibration signal is extended to about 110 ms. Thereby is secured that the Ion Probe can settle to its calibration value and that the calibration value is sampled several times. Thus, the analog signal is only sampled with 361 Hz (= every 2.77 ms) by the rockets telemetry.

During the measurement phase, *i.e.* when the boom is deployed, the calibration signal comes every 22 s. But for the worst case scenario, *i.e.* the smallest possible measurement value of 1 pA, the Ion Probe output signal needs about 14 s to rise back to the original value (Fig. 3.16). Hence, the Ion Probe submits only 6 s long valid measurement values before the next calibration impulse interrupts the measurement. However, if the current measured before calibration was 10 pA the signal needs only 5 s to settle back after calibration (Fig. 3.15). That is about three times faster (!) and results in a valid measurement phase of already 17 s.
Concluding, it would be good to have an idea of ion currents are expected during flight, thus the trustable measurement time before the next calibration impulse can be estimated.

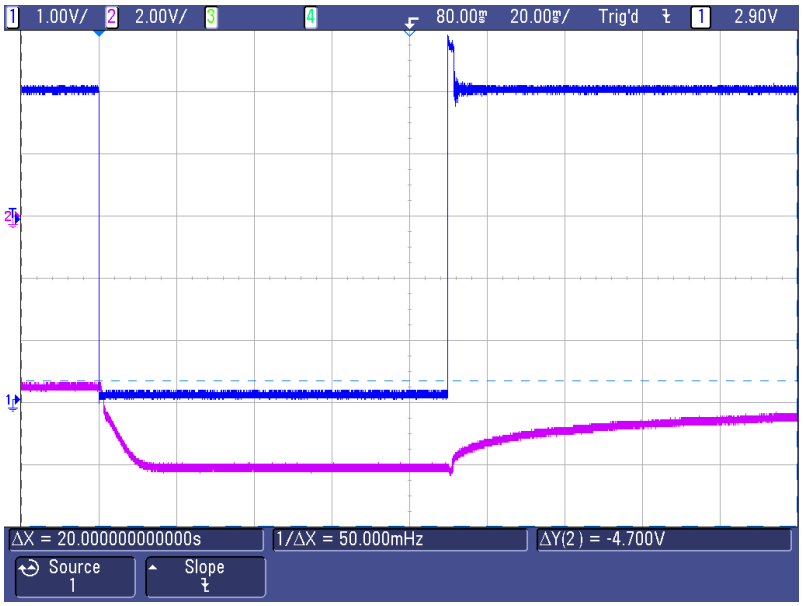

Figure 3.14.: Oscilloscope-screenshot: The calibration impulse from the digital electronics is about 110 ms long. Worst case fall time: The Ion Probe output needs about 20 ms to fall from its lowest value corresponding to 1 pA to the calibration value (nA)

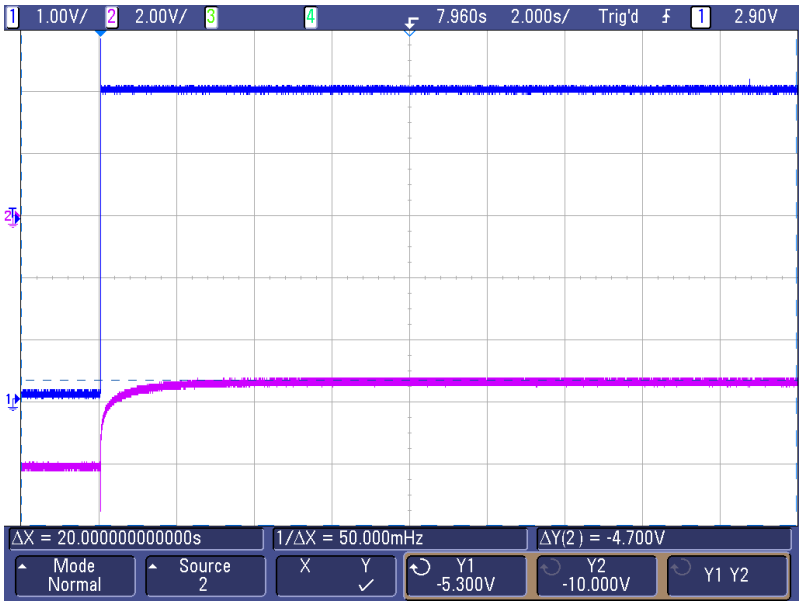

Figure 3.15.: Oscilloscope-screenshot: The Ion Probe output needs about 5 s to rise from the calibration value back to a measurement value corresponding to 10 pA.

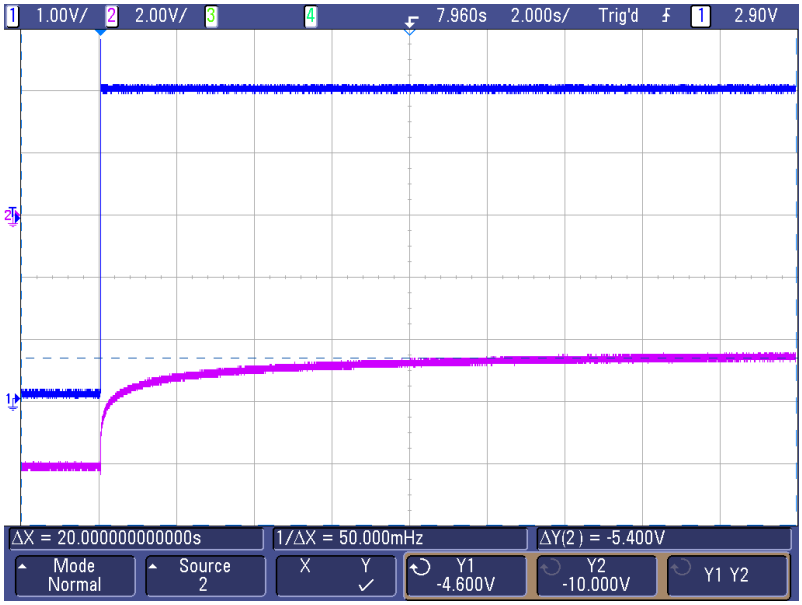

Figure 3.16.: Oscilloscope-screenshot: Worst case rise time: The Ion Probe output needs already 14 s to rise from the calibration value back to its smallest measurement value corresponding to 1 pA. That is nearly three times longer than for 10 pA.

4. Capacitance Probe (Cap Probe)

4.1. Theory of operation

A conducting probe in a plasma has an impedance Z which depends on the frequency, the electron density N_e, the collision frequency ν, the electron temperature T_e and the magnetic field $\vec{B}$ [Friedrich, 1979]. It is a well-tried approach to use sounding rockets equipped with spherical, gridded fixed frequency impedance probes (Cap Probe) to measure the deviation of N_e (but not the absolute value!) at altitudes above 70 km.
The physical theory regarding this kind of probes was studied by [Jacobsen, 1972] in detail. For this work it suffices to know that the change of impedance can actually be expressed as a change of capacitance between the probe and infinity corresponding to

$$\Delta C = C_0 \frac{r_0}{S} \tag{4.1}$$

where

ΔC	...	adds to the free-space capacitance of the probe C_0
r_0	...	radius of the probe in m
S	...	(adopted) ion sheath thickness = $n \cdot \lambda_D$
λ_D	...	Debye length in m

Due to the different thermal velocities of electrons and ions, a conductor in a plasma will acquire a negative potential. Its vicinity will therefore be devoid of electrons but be populated by positive ions. The so-called ion sheath has a thickness S which is expected to be a multiple n of the Debye length λ_D [Friedrich, 1979]

$$\lambda_D = \sqrt{\frac{\epsilon_0 k T_e}{e^2 N_e}} \tag{4.2}$$

The adopted sheath thickness was chosen to be $5 \cdot \lambda_D$ after [Tarstrup and Heikkila, 1972]. Inserting $S = n \cdot \lambda_D$ and Eq. (4.2) into Eq. (4.1) yields

$$\Delta C = C_0 \frac{r_0}{n} \sqrt{\frac{e^2 N_e}{\epsilon_0 k T_e}} \tag{4.3}$$

T_e for most purposes can be assumed to be known from ionospheric models. For the altitudes interesting for the Maxi Dusty flight it is between 100 K and 300 K, whereas N_e is expected to vary over orders of magnitude. The systematic errors introduced are acceptable and less than the uncertainties due to the wake near the fast moving sounding rocket [Friedrich, 1979].
C_0 is the free-space capacitance of a sphere, namely the probe itself:

$$C_0 = 4\pi\epsilon_0 r_0 \tag{4.4}$$

The used probe has a radius r_0=22.5 mm. Using the above equation C_0 is

$$C_0 = 2.5\,\mathrm{pF}$$

	ΔC	
N_e	T_e = 100 K	T_e = 300 K
10^7 m^{-3}	0.051	0.0298
10^{12} m^{-3}	16.3	9.41

Table 4.1.: Limiting values for ΔC in pF using Eq. (4.3). The highest deviation is expected to be +16.3 pF.

The simplest way to measure the change of the probe's capacitance ΔC is to include it as part of a free running LC-oscillator [Friedrich, 1979]. The oscillator will then run with an easy to measure frequency depending on ΔC respecting

$$f = \frac{1}{2\pi\sqrt{L(C + C_0 + C_p + \Delta C)}} \tag{4.5}$$

where

C ... value of the build-in capacitor (in schematic: C_2)
C_0 ... free-space capacitance of a sphere according to Eq. (4.4)
C_p ... sum of all (parallel) parasitic capacitances

C_p can be determined by calibrating the assembled Cap Probe, see Ch. 4.4.
Note that the frequency f decreases with increasing ΔC, *i.e.* increasing N_e. But since T_e is height-dependent ΔC will vary with height even if N_e remains constant! The largest deviation of ΔC is +16.3 pF as Table 4.1 summarizes. The frequency is lowest at this point. Its minimal expected value has to be considered when setting the prescaler of the digital electronics, see Ch. 5.4.

Experimental investigations indicate that the RF-voltage on the probe must be kept as low as possible to obtain reasonable experimental results. A too high probe voltage causes non-linear phenomena occurring in the plasma in the vicinity of the probe [Jacobsen, 1972]. Furthermore it may interfere with other instruments. Hence, the amplitude is limited to $2V_F$ by a pair of antiparallel diodes D1 across the inductance in order to avoid non-linearities by large fields in the vicinity of the probe [Friedrich, Boh, et al., 1994].

4.1.1. Choosing the operation frequency f_0

Maxi Dusty will be flown under daytime conditions (Summer at 69° N). The most interesting altitudes are from about 80 km to 100 km. Experiments of the last 50 years yield that

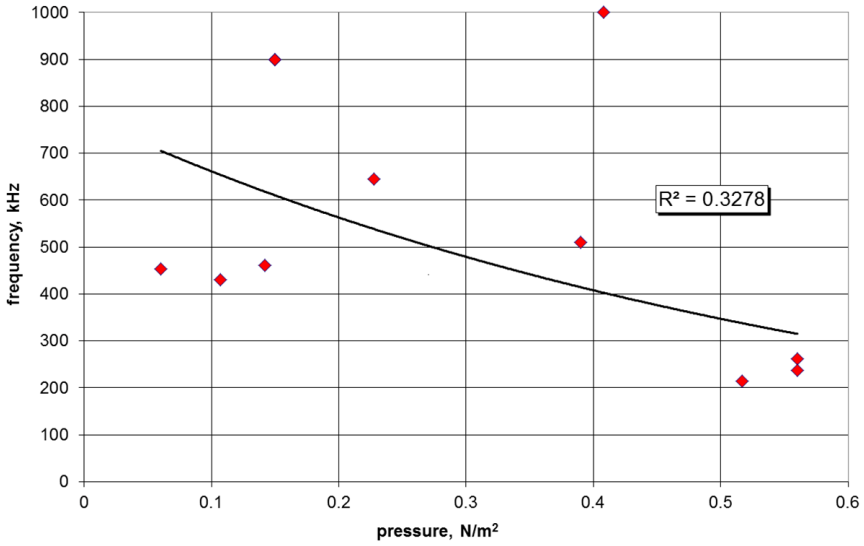

Figure 4.1.: Atmospheric pressure at the beginning of usable measurements as a function of probe frequency. The pressure range in the figure approximately corresponds to an altitude range of 83 to 93 km [Friedrich, 2013].

the electron density N_e at that altitude may be between 10^7 m^{-3} and 10^{12} m^{-3} [Friedrich, 2012].
The operation of the capacitance probe is impaired by the (electron-neutral) collision frequency, itself proportional to the atmospheric pressure. Jacobsen (1972) studied the impact of the collision frequency, but the outcome is somewhat inconclusive pertaining to the operating frequency of the probe. In Fig. 4.1 the pressure below which the capacitance probe began to operate properly as a function of the probes‘ frequency using the experience of ten past rocket flights is illustrated. It appears that lower frequencies should be better suited for operation at low altitudes (high pressure), although much higher frequencies (above the plasma frequency) should theoretically be less influenced by the ambient pressure [Friedrich, 2013]. Therefore two extreme frequencies are employed to test the validity of the assertion.

The capacitance probe is part of the frequency sensitive network of a free running oscillator. The probes are termed high or low frequency probes, depending on whether the operating frequency is below or above the expected plasma frequency $f_{N_{max}}$. The operation frequency should always either be below the lowest or above the highest plasma frequency expected to occur during flight [Jacobsen, 1972]. For the Maxi Dusty project one low frequency (LF) and one high frequency (HF) probe is used.
The plasma frequency can be calculated as

$$f_N = \frac{1}{2\pi}\sqrt{\frac{N_e e^2}{m_e \epsilon_0}} = 8.978 \text{ Hz} \cdot \sqrt{N_e} \tag{4.6}$$

Setting the expected limits of N_e into equation (4.6) yields

$$f_{N_{min}} = 28.39 \text{ kHz and } f_{N_{max}} = 8.978 \text{ MHz.}$$

Jacobsen (1972) predicts that a probe with $f_0 \simeq 200$ kHz is suitable for measurements of electron densities not lower than 10^9 m^{-3}. Probe experiments designed to measure lower electron densities should have a still lower operation frequency. However previous experiments like [Friedrich and Torkar, 1995] show that it is possible to measure $N_e \simeq 10^7$ m^{-3} with $f_0 \simeq 200$ kHz.
Finally, it is difficult to ensure a stable oscillation with center frequencies much lower than 200 kHz. Hence the oscillator for the low frequency probe was designed to work with about 190 kHz. The operation frequency for the high frequency probe was aimed to be about 9 MHz.
The final values for f_0 first appear in the calibration data (see Ch. 4.4).

4.2. Clapp oscillator

4.2.1. Theory of operation

The Clapp oscillator is similar to a Colpitts oscillator, but with an L-C series circuit replacing the inductor and C_1, C_3 being many times larger than those usually employed in a Colpitts oscillator. The oscillator was developed to have an "unusual frequency stability" [Clapp, 1948] but in the application at hand it is used because its frequency can be made very sensitive to changes of C_2 which is replaced with the capacitance probe itself.

The general requirements for the build-up of an oscillation are a loop gain >1 and a positive feedback, *i.e.* a phase shift between output and input of $0°$ or $n \cdot 360°$ [Tietze et al., 2012].
As amplifying element transistors in all basic bias circuits may be used. For the actual oscillator it is a FET in common-source configuration. The circuits requires a feedback from drain to gate with an additional $180°$ phase shift since the common-source amplifier circuit itself shifts the signal phase by $180°$.
The phase shift in the feedback is effectuated by a L-C resonator realized as π-network.

Fig. 4.2 summarizes the principle of operation. Fig. 4.3 shows a more detailed view of the oscillator circuit.

The oscillation frequency is determined by $X_1 + X_2 + X_3 = 0$ where X_2 is the reactance of the L_{eff}-C_2 series circuit. $X_2 = -(X_1 + X_3)$ may require a very small inductance which might be hard to realize. Hence a capacitor C_4 can be set in series to L_2 which yields an

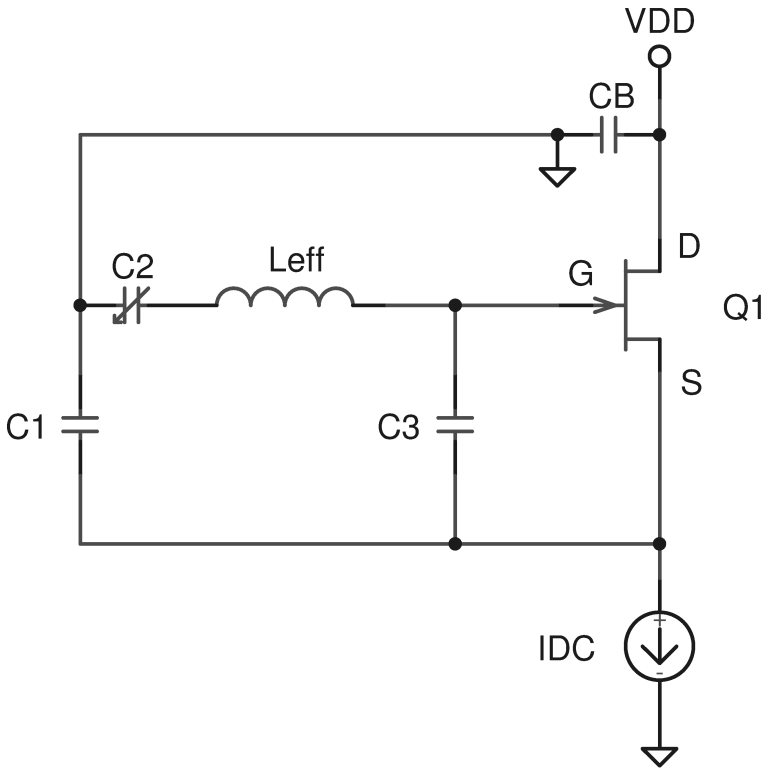

Figure 4.2.: Clapp-oscillator: principle of operation: The common-source FET amplifier and the L-C resonator as π-network produce each $180°$ of phase shift. The AC feedback loop from D to G is closed over the bias capacitor C_B.

effective inductance of

$$L_{eff} = L_2(1 - \frac{1}{\omega_r^2 L_2 C_4}) < L_2 \tag{4.7}$$

as long as

$$\omega L_2 > \frac{1}{\omega C_4} \tag{4.8}$$

complies [Zinke and Brunswig, 1999]. Using L_{eff} of equation (4.7) the series resonance of the π-network is [Böhmer, 2004]

$$\omega_s = \frac{1}{\sqrt{L_{eff} C_2}} \tag{4.9}$$

The parallel resonance with C_1 and C_3 which is decisive for the oscillation can be found by using the condition

$$\omega L_{eff} - \frac{1}{\omega C_2} = \frac{1}{\omega C_1} + \frac{1}{\omega C_3} \rightarrow \omega_p = \frac{1}{\sqrt{L_{eff} C_2}} \cdot \sqrt{1 + \frac{C_2}{C_1} + \frac{C_2}{C_3}} > \omega_s \tag{4.10}$$

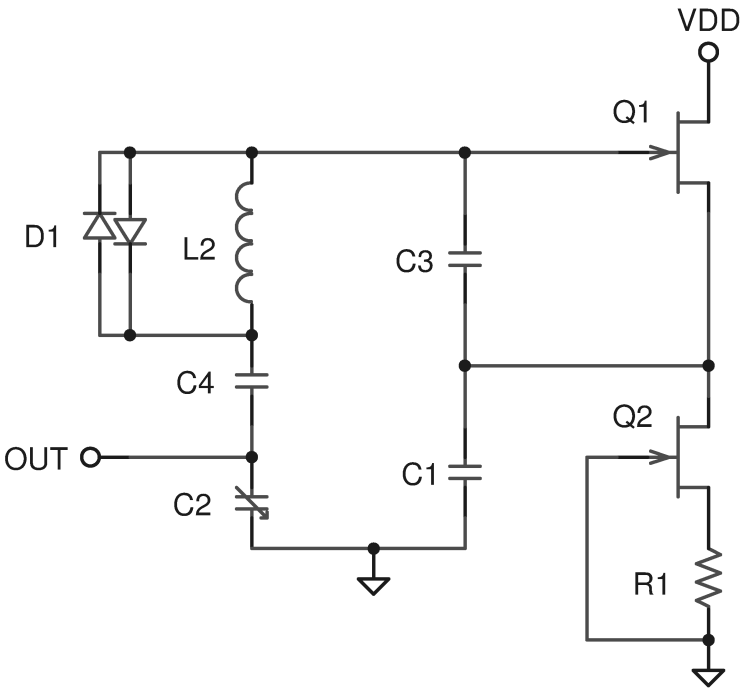

Figure 4.3.: Clapp-oscillator: more detailed schematic: L2 and C4 form L_{eff} according to equation (4.7). The series diodes D1 limit the oscillation's V_{pp} to $2V_F$. The current source Q2 sets the operation point of Q1.

Apparently if $C_2 \ll C_1, C_3$ the oscillation frequency is practically ω_s and independent of C_1 and C_3 and of all parallel parasitic capacitances like those operating point dependent capacitances of the transistor Q1 [Böhmer, 2004].

$$f_0 = \frac{1}{2\pi\sqrt{L_{eff}C_2}} \qquad \text{if} \qquad C_2 \ll C_1, C_3 \tag{4.11}$$

The maximum load conductance G for oscillation can be calculated according to

$$G = g_m \frac{C_1}{C_3}. \tag{4.12}$$

with g_m being the transconductance of the FET [Zinke and Brunswig, 1999].
In practice the load conductance G is not known and difficult to determine and g_m is a parameter of the employed FET. The oscillation has to be attained by altering the ratio C_1/C_3 [Zinke and Brunswig, 1999].

The optimal ratio C_1/C_3 is somewhere between 1:1 to 3:1. Typical values for the capacitances range from about 47 pF to 1000 pF [Neubig and Briese, 1997].
The larger C_1 and C_3 are, the lower is the influence of the FET but the lower is the output

amplitude.
Reducing C_1 increases the output amplitude which supports the build-up of an oscillation but also increases the tendency toward overtone oscillation. If C_1 is much larger than C_3 the oscillation will decay.

Clapp (1948) himself stated that an ideal configuration is $C_1 = C_3 = n \cdot C_2$ with the reactances being $X_1 = X_3 = 1/40$ of X_L or X_2.
The frequency swing is caused by varying C_2, the center frequency is set by the series tuning capacitor C_4.

Furthermore, [Jacobsen, 1972] investigated that the oscillator's sensitivity to changes of C_2 increases with increasing L-C ratio.

4.2.2. Dimensions of the actual oscillator

Fig. 4.4 shows a detail of the interesting schematic of the Cap Probe circuit.
The primary goal was to dimension the oscillator in a way that its oscillation is stable for both the HF and the LF frequency while the inductor L_2 and the reference capacitor C_{10} should be the only components needed to be exchanged.
The operation frequency of the oscillator can be evaluated using Eq. (4.5) where the sum of capacitances may be roughly estimated to 20 pF for a first approach. Since inductors are not easily available at any value, one has to choose an inductance value that results in a frequency close to the desired LF or HF operation frequency. The selected values were 33 mH and 14.7 μH, respectively.

$$f_{33mH} = 196\,\mathrm{kHz}\ \ (LF) \qquad\qquad f_{14.7\mu H} = 9.3\,\mathrm{MHz}\ \ (HF)$$

The actual operation frequency cannot be determined with certainty before calibration (see Ch. 4.4) because the Cap Probe electronics are very sensitive so that the housing of the PCB and the cabling to the probe have great influence on it.

Theoretically C_4 can be used to fine-tune the center frequency. f_0 decreases with increasing C_4 since L_{eff} increases according to Eq. (4.7) with C_4. But the impact of C_4 is only recognizable if it is very small. The minimal allowed value of the tuning capacitance can be estimated for a desired center frequency and a given L_2 by rearranging Eq. (4.8). It is about 22 pF for both probes. However, experiments showed that the RF-amplitude increases with C_4 too. For the application at hand f_0 did not need to be fine-tuned, but the amplitude was desired to be maximized. Therefore C_4 was given a high value of 1.5 nF

The oscillator needs at least a minimum capacitance C_2 = 4.7 pF parallel to the probe for stable oscillation. C_2 should be chosen as low as possible to not reduce the sensitivity for

the probe's capacitance changes (see Eq. (4.5)).

Following the suggestions of [Neubig and Briese, 1997] is a good start when dimensioning C_1 and C_3. But in the end this has to be done purely empirical, as indicated by [Zinke and Brunswig, 1999]. As already mentioned C_1 and C_3 have to be as large as possible to ensure that f is mainly depending on the probe's capacitance. Unfortunately the oscillation will not be stable if C_1, C_3 exceed 82 pF. Chosing a ratio different from 1:1 would also bring no improvement. Hence, $C_1 = C_3 = 82$ pF.

4.3. Capacitance Probe circuit

Fig. 4.4 and Fig. 4.5 show simplified details of the circuit. The complete schematic is given in Fig. B.1 of the Appendix.

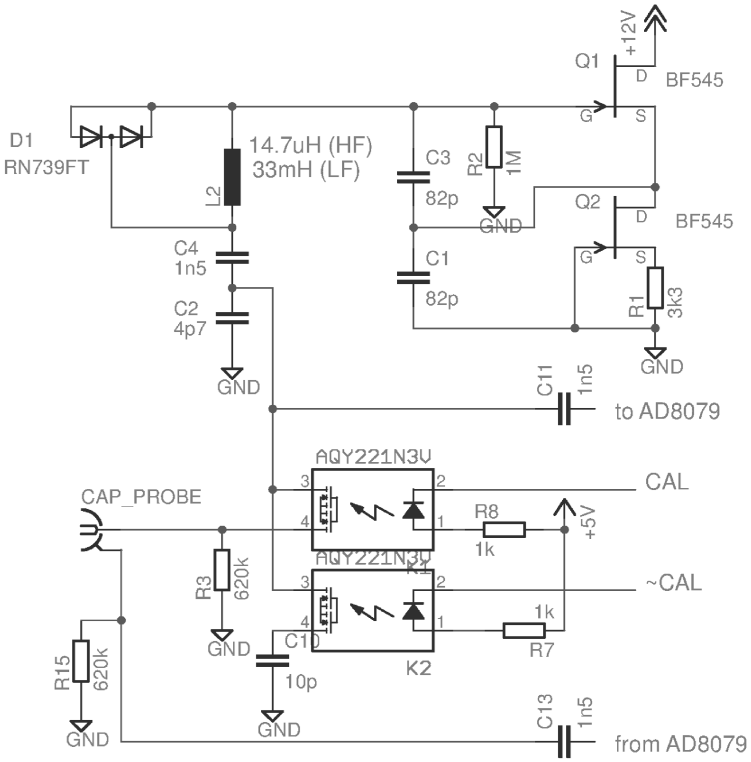

Figure 4.4.: Simplified detail of the schematic showing the oscillator and the relay which switch between probe and reference capacitor C_{10}

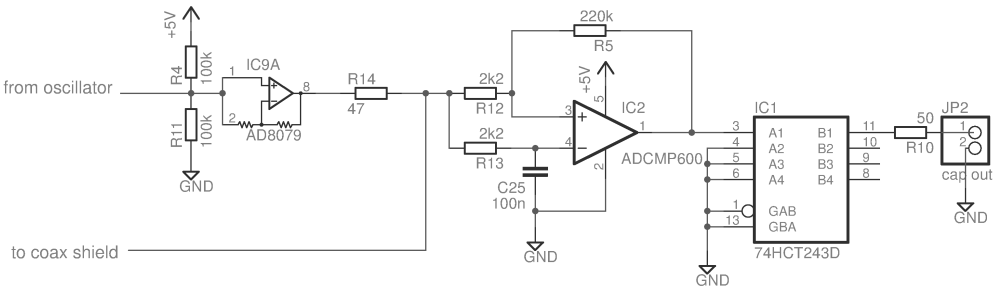

Figure 4.5.: Simplified detail of the schematic showing the circuit subsequent to the oscillator: analog buffer AD8079, comparator ADCMP600 and line transceiver 74HCT243

As stated in Ch. 4.1, form the physical point of view the amplitude of the RF-voltage should be kept as low as possible. The used pin diode RN739F has a low capacitance of typical 0.4 pF. Unfortunately V_F decreases as temperature increases (see [datasheet of RN739F]) which leads to a decreasing limit amplitude. It has to be considered that the amplitude of the oscillator itself changes with the value of C_2. The output's amplitude has to be large enough to be processed by the subsequent circuit (AD8079 and the following) at any temperature and frequency. To ensure this D1 has a comparatively high forward voltage of V_F=600 mV at room temperature and the capacitors of the oscillator were dimensioned in a way that the amplitude becomes as high as possible (see Ch. 4.2). This approach is, however, against the introducing considerations of maintaining a low RF-amplitude.
However, there is evidence that the amplitude is finally limited by the oscillator circuit, not by the diode, since measurements of the peak-to-peak amplitude V_{pp} of the final arrangement show that

$$V_{pp,HF} \simeq 600\,\text{mV} \qquad V_{pp,LF} \simeq 131\,\text{mV}$$

Note that the amplitude depends on the value C_2, *i.e.* the probe's capacitance, and is therefore frequency (and temperature) dependent.
The operation point of the transistor Q1 needs to be in the middle of its linear operation region to ensure stable oscillation. Q2 and R1 form a current source which sets the operation point of Q1.

The coaxial cable connecting the probe to the PCB is about 1 m long. If not compensated it would add a parasitic capacitance of about 100 pF in parallel to the probe, obviously decreasing the oscillator's sensitivity. Hence, the oscillator's output signal buffered (with ideally no phase shift or deviation in amplitude) by the analog buffer AD8079 and fed back to the shield of the coax cable. Doing so there is no difference in potential between the cables core and shield and consequently no capacitance.
Since the AD8079 is only powered with a single supply of +12 V it cannot process the partly negative AC voltage of the oscillator. The voltage divider R4 and R11 set the DC

voltage at the input of the buffer to about 2.5 V.
The comparator ADCMP600 converts the low amplitude sine wave signal to a square wave signal of 0 V or 5 V which can be processed by the subsequent TTL logic. The coaxial cable between analog and digital electronics is driven by the digital line transceiver 74HCT243.

For proper operation as an ion probe the probe's grid is connected by 620 kΩ to payload ground to ensure it does not charge up relative to payload potential [Friedrich, Boh, et al., 1994].

Every 11 s or 22 s (see Ch. 5) the measurement is calibrated by switching to an as-good-as temperature stable reference capacitor C_{10}. This in-flight calibration is expected to show the temperature dependency of the overall circuit. Fig. 4.6 shows an example data published in [Friedrich and Torkar, 1995] which demonstrates the change of the calibration values over flight time and, accordingly, temperature.
The value of C_{10} is chosen in a way that the calibration frequency is in the same range as the probe's operation frequency. $C_{10} = 10$ pF for the LF probe and $C_{10} = 33$ pF for the HF probe.

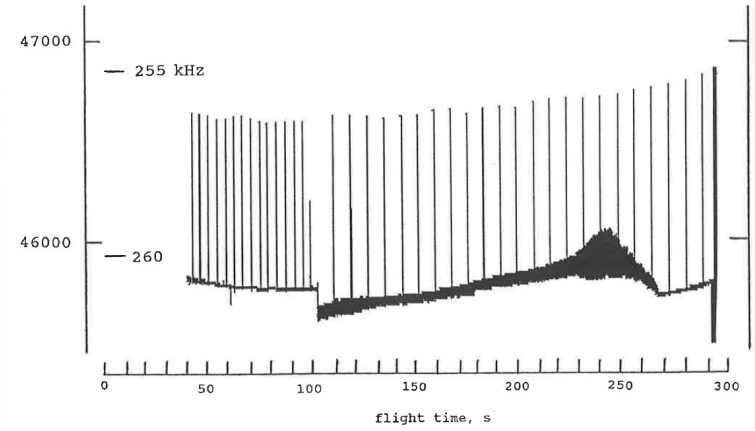

Figure 4.6.: Example data from [Friedrich and Torkar, 1995] showing results of the in-flight calibration. The change in the calibration values is supposed to be due to the temperatures gradient. This gradient can now be corrected for when processing the measurement data. Note that the calibration rate changes after the boom is deployed (at 100 s flight time).

4.3.1. Component selection

Generally, to improve the sensitivity of the circuit the parasitic capacitance has to be kept as low as possible. Where interchangeable, components were selected to have lowest stray capacitance. For instance the relays for the in-flight calibration are of photoMOS type with a low output of 1 pF (typ.).

The ambient temperature is expected to change during flight from approx. $10\,°C$ to not more than $50\,°C$. The oscillator frequency should ideally be temperature independent. Hence, all capacitors which contribute to the frequency were carried out with COG/NPO dielectric.

4.3.2. Layout

As mentioned above, a critical design factor is to minimize parasitic capacitances:
No ground plane was used to achieve low stray capacitance between the layers.
Where possible, lines (and thus components) are far away from each other to keep coupling capacitance between lines low.

4.4. Calibration

In order to convert the recorded probe frequency to electron density, it is necessary to know the exact relation between a change in the probe's capacitance and the frequency.

Therefore the circuit is calibrated by varying the distance d (in small increments) of the probe's center and a conducting earthed plane (a metal plate, large compared to the probe's diameter). This induces a change of the probe's capacitance ΔC which can be observed by measuring the oscillator's output frequency. The capacitance between a sphere and an earthed plane in dependence of d, $C(d)$, can be calculated. Unfortunately there is no closed form for small values of d. However, [Küpfmüller, 1968] gives a series representation which may be summarized as

$$
\begin{aligned}
&C(d) = C_0 \cdot \sum_{n=0} a[n] \\
&\text{where} \\
&a[n] = a[n-1] \cdot c[n-1] \\
&a[0] = 1 \\
&b[n] = r_0 \cdot c[n-1] \\
&b[0] = 0 \\
&c[n] = \frac{r_0}{2d - b[n]} \\
&c[0] = \frac{r_0}{2d}
\end{aligned}
\tag{4.13}
$$

d in mm	C in pF
1	6.3136
2	5.5244
3	5.0854
4	4.7875
5	4.5655
10	3.9391
15	3.6257
20	3.4304
25	3.2952
30	3.1954
50	2.9653
70	2.8508
100	2.7568
150	2.6782

Table 4.2.: C between a sphere and a conducting plane as a function of d according to Eq. (4.13). At clearances greater 150 mm the capacitance of the calibration setup itself would take major effect on the measurement.

where $r_0 = 22.5$ mm is the outer radius of the probe and $C_0 = 2.5$ pF its free space capacitance according to Eq. (4.4).
The first four terms of the expression are stated below. One needs at least 50 terms to get close to the exact value.

$$\begin{aligned} C(d) &= C_0 \cdot \left(a[0] + a[0] \cdot c[0] + a[1] \frac{r_0}{2d - b[1]} + a[2] \cdot c[2] + \ldots \right) \\ &= C_0 \cdot \left(1 + \frac{r_0}{2d} + a[1] \frac{r_0}{2d - r_0 \cdot c[0]} + a[2] \frac{r_0}{2d - b[2]} + \ldots \right) \\ &= \ldots \\ &= C_0 \cdot \left(1 + \frac{r_0}{2d} + \frac{r_0^2}{(2d)^2 - r_0^2} + \frac{r_0^3}{2d((2d)^2 - 2r_0^2)} + \ldots \right) \end{aligned} \tag{4.14}$$

The clearance $d - r_0$ from the probes outer radius to the metal plate and the corresponding values of $\Delta C = C(d) - C_0$ are plotted on the x-axes of the calibration diagrams in Fig. 4.8 and 4.9. The lower y-axis gives the measured frequency corresponding to the set clearance; the upper y-axis $1/f^2$ of the same frequency. According to the equation for the oscillator's frequency, *e.g.* Eq. (4.11), the calculated capacitance $C(d)$, or ΔC respectively, is linearly proportional to $1/f^2$. The red trend line illustrates this linear correlation.
By getting the equation for the trend line, *e.g.* using Matlab, one gets the effective correlation between the oscillator's frequency and the probe's capacitance:

$$\text{HF probe:} \qquad C_{probe} = 8270.5337 \cdot f^{-2} - 1.288 \cdot 10^{-10} + C_0 \qquad \text{f in Hz; C, } C_0 \text{ in pF} \tag{4.15}$$

$$\text{LF probe:} \qquad C_{probe} = 47.2958 \cdot f^{-2} - 9.3177 \cdot 10^{-10} + C_0 \qquad \text{f in Hz; C, } C_0 \text{ in pF} \quad (4.16)$$

By picking two points of the trend line one can also calculate the effective capacitance $C + C_p$ and the effective inductance L of the circuit. The values of L and C which are determined this way are those of an equivalent circuit as described by Eq. (4.5) rather than representing the physical values of the actual circuit.

HF probe:	$C + C_p = 126.2957\,\text{pF}$	$L = 3.0627\,\mu\text{H}$
LF probe:	$C + C_p = 929.2681\,\text{pF}$	$L = 535.572\,\mu\text{H}$

The frequency where ΔC tends to zero, *i.e.* where the overall probe capacitance is equal to C_0, is termed the effective operation frequency f_0. It is depicted from the calibration diagrams and compared to the originally aimed values (see Ch. 4.1.1)

HF probe:	$f_0 = 8.01\,\text{MHz}$	(aim: f_0 = 9 MHz)
LF probe:	$f_0 = 225.3\,\text{kHz}$	(aim: f_0 = 190 kHz)

Note that the HF frequency is now below the assumed maximal plasma frequency $f_{N_{max}}$=8.978 MHz estimated in Ch. 4.1.1.

Note that it is necessary to keep a warm-up phase of at least 10 minutes before recording data, so that the circuit can settle to a constant operation temperature.

4.5. Probe resolution

The frequency deviation which can be observed with the digital counting electronics (see Ch. 5) depends on the prescaler value P_s, the counting frequency f_c and on the oscillator frequency itself. The minimal observable deviation is with the minimal expected frequency f_{min} (determined through calibration, Ch. 4.4):

$$\Delta f = \frac{1}{N} f_{min} = \frac{f_{min}^2}{f_c \cdot P_s} \qquad (4.17)$$

Inserting the actual prescaler values from Ch. 5.4 into Eq. (4.17) yields

$$\Delta f_{HF} = 12.37 \text{ Hz} \qquad \text{and} \qquad \Delta f_{LF} = 0.48 \text{ Hz}$$

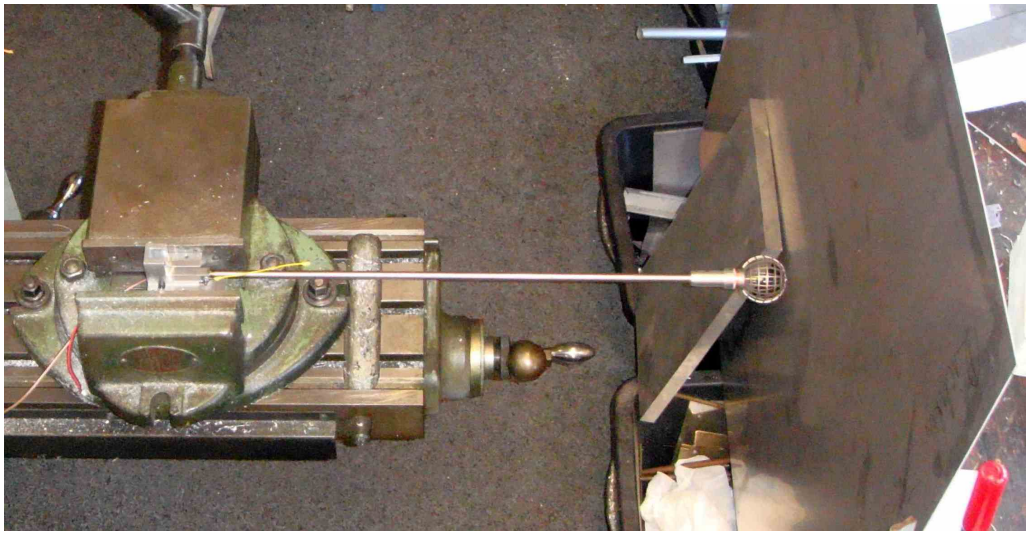

Figure 4.7.: Photo of the calibration setup: The boom with the probe is mounted on the precision slide of a milling machine. The probe is moved away from a metal plate large compared to the probe's diameter.

As can be derived from Figs. 4.8 and 4.9 the change of the oscillator's output frequency with the probe's capacitance is approximately

$$\text{HF probe:} \quad \frac{\Delta f}{\Delta C} = 30 \text{ kHz/pF} \quad \text{or} \quad \frac{\Delta C}{\Delta f} = 33.3 \cdot 10^{-6} \text{ pF/kHz}$$

$$\text{LF probe:} \quad \frac{\Delta f}{\Delta C} = 115 \text{ kHz/pF} \quad \text{or} \quad \frac{\Delta C}{\Delta f} = 0.0087 \text{ pF/kHz}$$

Combined with the digitally minimal observable frequency deviation from above, the minimal measurable change of the probe's capacitance, *i.e.* the capacitance resolution ΔC_{res}, is

$$\text{HF probe:} \quad \Delta C_{res} = 0.412 \cdot 10^{-3} \text{ pF}$$

$$\text{LF probe:} \quad \Delta C_{res} = 4.176 \cdot 10^{-3} \text{ pF}$$

Summarizing, the capacitance resolution of the HF probe is about ten times better than that of the LF probe!

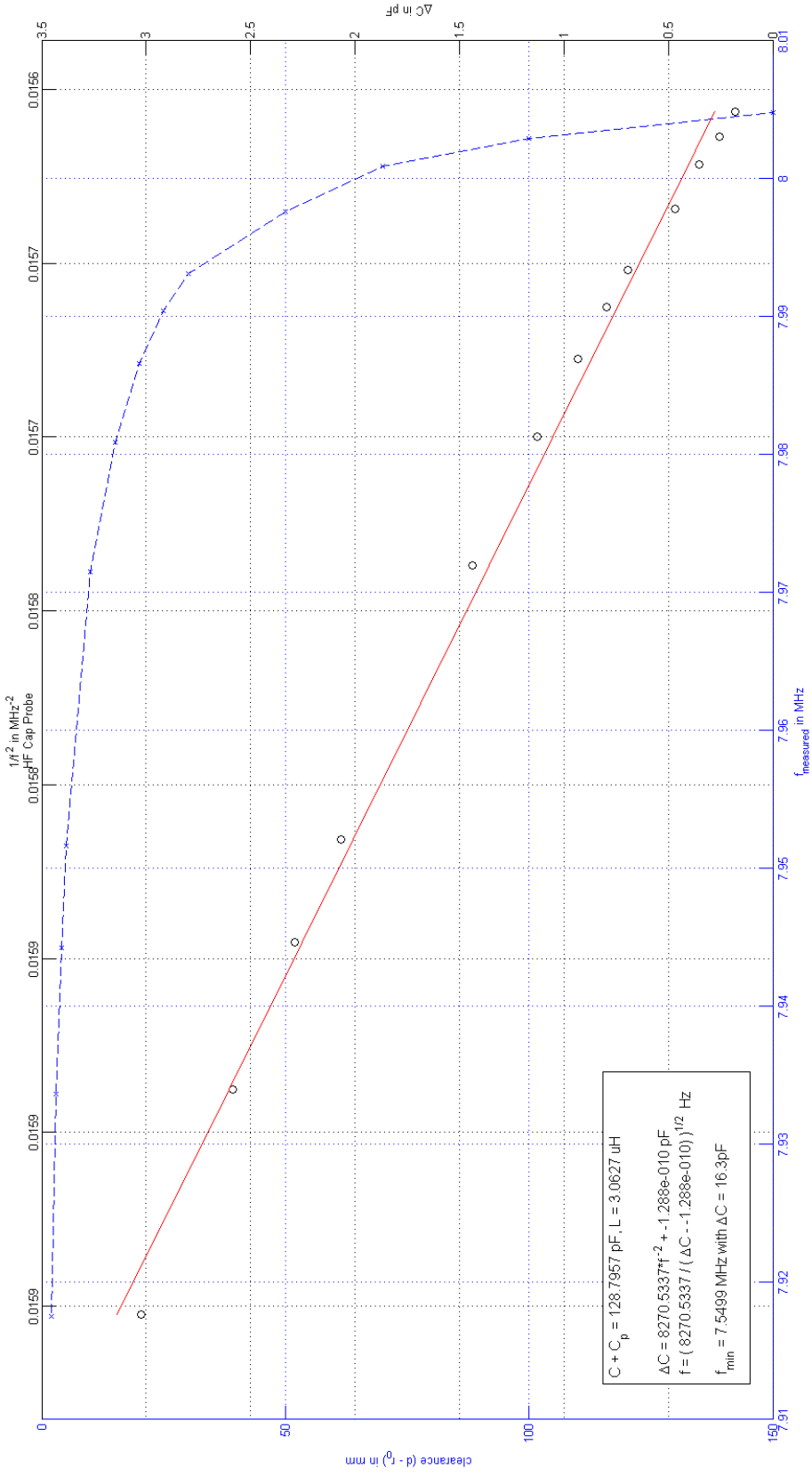

Figure 4.8.: Calibration diagram for HF probe. The minimal expected frequency with ΔC = 16.3 pF is 7.55 MHz; Δf is approx. 30 kHz/pF; f_0 is approx. 8.01 MHz

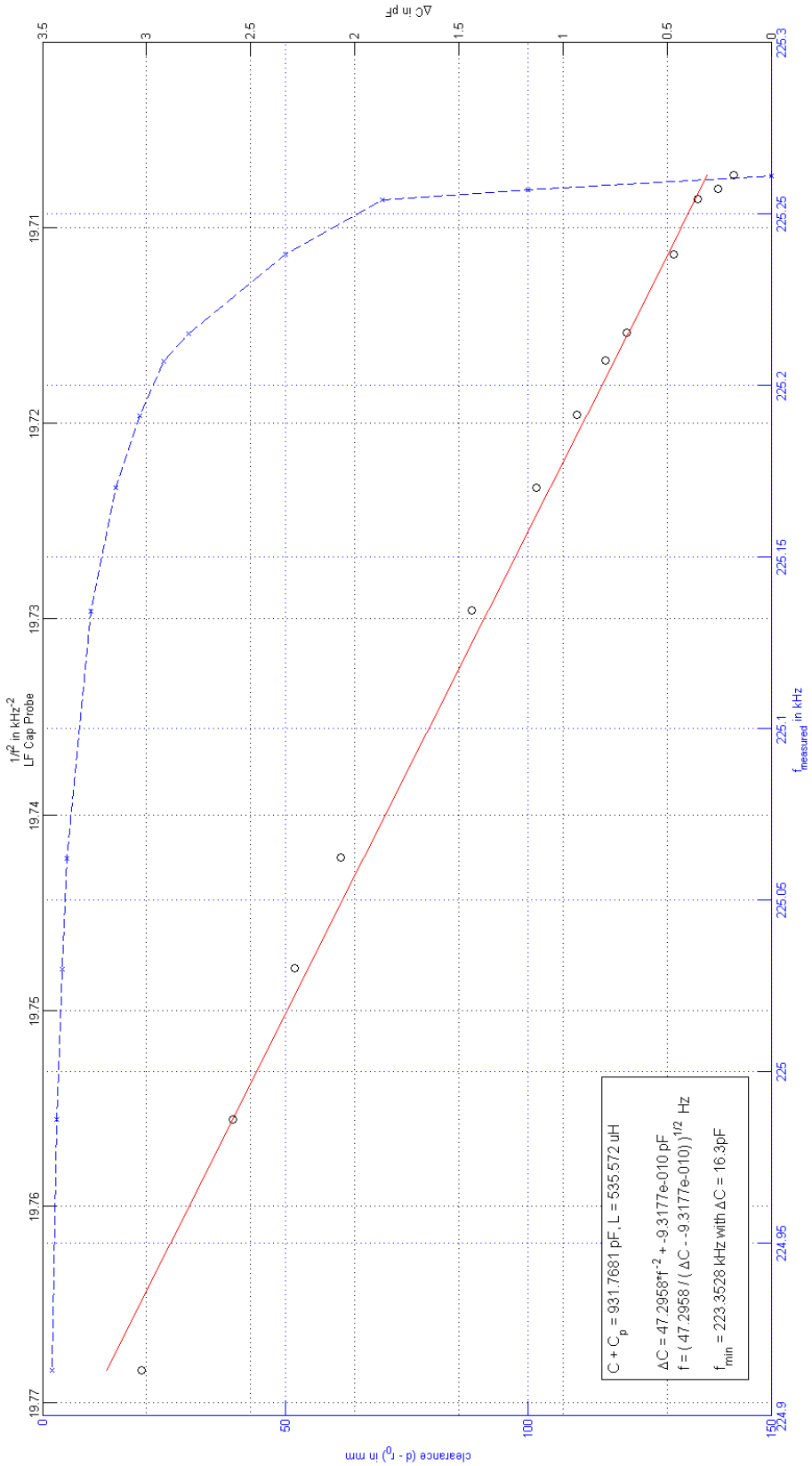

Figure 4.9.: Calibration diagram for LF probe. The minimal expected frequency with $\Delta C = 16.3$ pF is 223.35 kHz; Δf is approx. 115 Hz/pF; f_0 is approx. 225.3 kHz

5. Digital counter electronics (Digital)

5.1. Functional overview

The counter electronics receive the frequency signal of the Cap Probe electronics. Its function is to convert the frequency information into a 20 bit digital value N.
The changes in the oscillator's frequency are minute (a few percent), hence the frequency must be read with high resolution. For this purpose the RF is scaled down by a factor P_s (prescaler) to a half-period a little shorter than the time between telemetry readouts. That period is then measured by gating it with a very high frequency of 250 MHz and counting the resulting pulses [Friedrich, Boh, et al., 1994]. The number of pulses N thus counted relates to the Cap Probe frequency f as:

$$N = \frac{f_c \cdot P_s}{f} \tag{5.1}$$

The counter frequency $f_c = 250\,\text{MHz}$ was chosen much higher than in previous works (so far $f_{c,max}$ was $100\,\text{MHz}$) because it determines the achievable resolution. With the current values of f_c and the sampling frequency f_{Gate} a resolution of 1/N = $1.44 \cdot 10^{-6}$ is realized:

$$\frac{1}{N} = \frac{f_{Gate}}{f_c} = \frac{361\,\text{Hz}}{250\,\text{MHz}} = 1.44 \cdot 10^{-6}$$

The output functionality of the digital counter electronics can be summarized as follows:

- The output is MSB first.
- The output consists of two digital data streams of each 16 bits.
- One stream, termed MSB stream or simply MSB, contains the 15 most significant bits, the other contains 15 least significant bits, termed LSB stream or simply LSB. The first bit of each stream is a flag to identify them.
- That makes 30 bits of valid data. But the first 10 bits of the LSB stream are redundant, only its 5 least significant bits add to the counter value. The result is a 20 bit counter value (see Fig: 5.15).
- Since the probe's frequency is expected to change only marginally, the MSB stream is seldom sent, namely only every 32 LSB streams: ...- 1 MSB - 32 LSB - 1 MSB - 32 LSB - ...

5.1.1. Calibration signal

The counter electronics produce a calibration signal (CAL) which is forwarded to the analog electronics (PIP and Cap Probe). The calibration of the analog electronics is meant to monitor the influence of the environment on the circuit itself. During the rocket's upleg the ambient temperature is expected to increase due to the air friction in the lower atmosphere.

A calibration signal is produced every 11.3 s. The measurement phase begins after the boom is deployed at typically 70 s time of flight or at about 70 km. Then the measurement results are more important than the calibration values, so the time between calibrations is doubled to 22.6 s. A 'boom deployment switch' located in the boom mechanics informs about the deployment of the boom.
The calibration signal stays high for the duration of 4 GATE signals (at 361 Hz) are received. During calibration the usual procedure of 32 LSB - 1 MSB - 32 LSB is interrupted and replaced with 2 MSB - 1 LSB - 1 MSB - 1 LSB (see Fig. 5.13). It is likely that the data of the first MSB is not usable because of the acquisition time of the analogue circuit (The LF Cap Probe oscillator needs about $22\,\mu$s to settle to a constant frequency).

5.2. MaxiDusty interface specifications

The descriptions in this chapter are according to the MaxiDusty interface recommendations issued by the Andøya Rocket Range [Andøya Rocket Range, 11 August 2009].

The Hotel Payload PCM encoder (PCM encoder for short) is the interface between all instruments on the MaxiDusty payload and its telemetry. The PCM encoder consists of five different modules that act together as an entire service module that takes care of digital and analog data acquisition, power management and timed events sequencing [Andøya Rocket Range, 11 August 2009].

The PCM Encoder provides differential digital interface signals to the digital counter electronics and samples the digital output data:

SCLK — Output from encoder. System clock with 3.33 MHz and 50% duty cycle.

GATE — Output from encoder. Used to control the readout of data from the counter electronics. The GATE signal occurs with 772 Hz, and stays high for 16 clock cycles allowing the readout of a 16 bit serial data stream. There is only a single GATE signal available for both digital counting electronics (termed Digital1 and Digital2), so the GATE is split to GATE1 and GATE2 with each 361 Hz (2.77 ms) synchronizing the alternating output of the data from Digital1 and Digital2.

MAJOR Frame — Output from encoder. The MAJOR Frame pulse occurs at 45 Hz (22.2 ms) and stays high for 1 clock cycle. It is used for the timing of the MSB output and the generation of the calibration signal.

DATA — Input to encoder. 16 bit serial data stream (MSB first) from the instrument. Sampled in the encoder a short time before the next positive edge of SCLK.

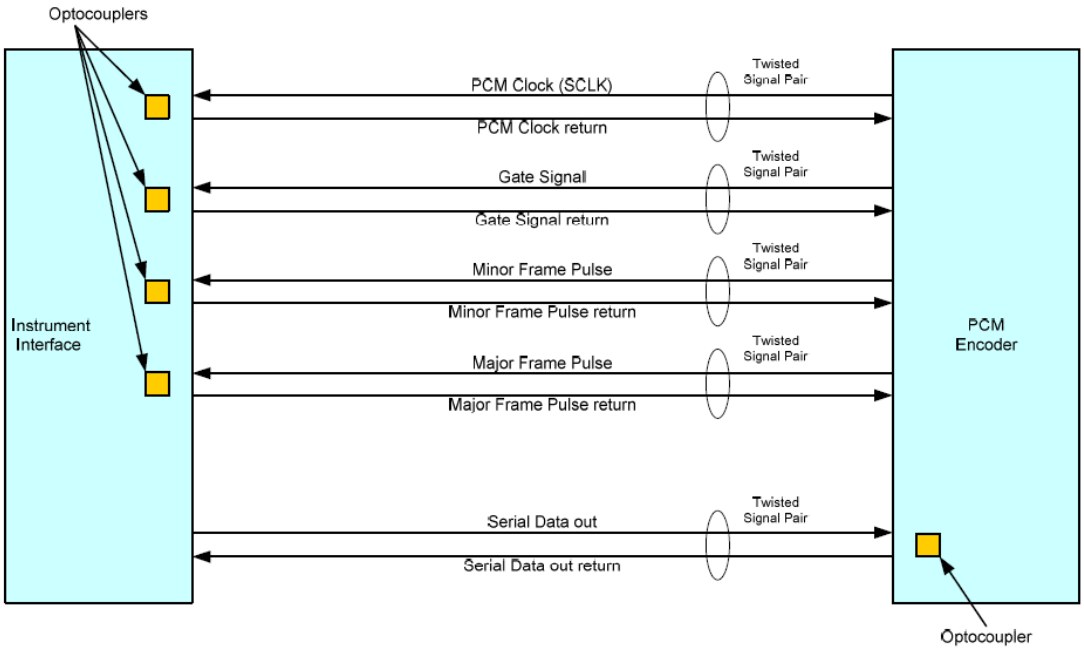

Figure 5.1.: PCM encoder vs. Instrument connection. Figure from [Andøya Rocket Range, 11 August 2009]

It is important to notice that:

- MAJOR and GATE change at the falling edge of SCLK.
- Data must be transmitted from the instrument of the rising edge of SCLK.
- All signals from and to the encoder are differential. The use of optocouplers is recommended to perform the differential to single-ended coversion and to brake possible ground loops (Fig. 5.1). The optocoupler HCPL0630 and the line transceiver 74HCT243 are recommended (amongst others).
- The output impedance of the interface driver stage should be matched to the cable impedance, which is approximately $100\,\Omega$.
- The PCM encoder uses TTL logic levels. Its output signals are between 0 V and 5 V. Analog or digital inputs must not exceed 0 V and 5 V.

Actually, the shared interface components (optocouplers, GATE splitting and output merging, see Fig. 5.3) are not located on the counter electronics PCB but on the common power supply PCB described in Ch. 6.

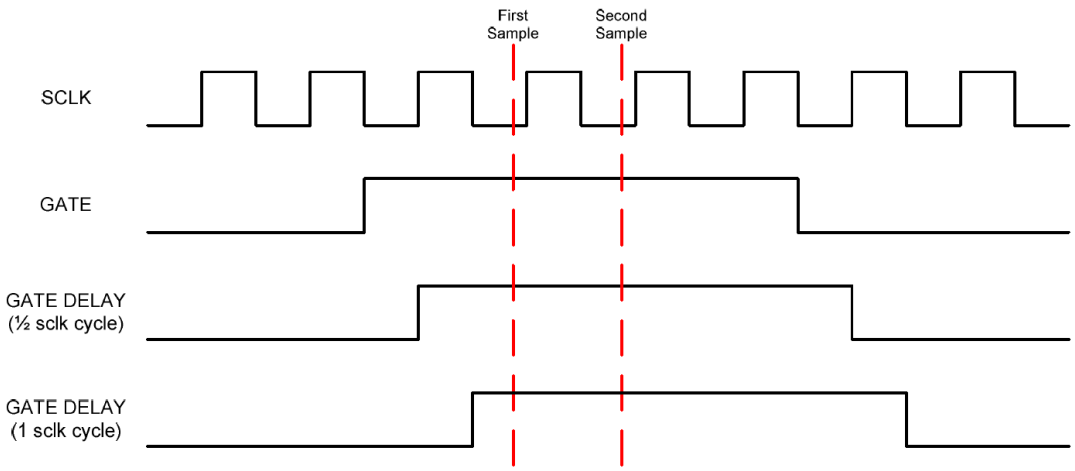

Figure 5.2.: Sampling of instrument data (4 bit example). There is almost a 1.5-clock cycle delay from the GATE goes active (high) and until the PCM encoder samples the first data bit. The data output has to be delayed so as not to lose the first bit (MSB). Figure from [Andøya Rocket Range, 11 August 2009]

5.3. Detailed description of operation

5.3.1. Schematic

Fig. 5.3 shows a detail of the schematic responsible for the splitting of the GATE signal, merging of the outputs from Digital 1/2 and delaying the output data by 1 clock cycle.
Two counting electronics are assembled in the Main Box but there comes only one GATE signal from the encoder and only one digital output to the encoder is provided. Hence the data from Digital 1 and Digital 2 have to be transmitted in alternation . Therefore the GATE signal is split into GATE1 and GATE2, one for each Digital part. The output of IC3 toggles when GATE occurs. It is AND-gated with the delayed GATE (gating with the original signal would produce a glitch) to produce alternating GATE signals.
While GATE1 is active the output of Digital1 is bypassed by the multiplexer U3, otherwise the output of Digital2.
The D-flip-flop IC7A, clocked by SCLK, introduces the required delay of the output data by 1 clock cycle (*cf.* Fig. 5.2). It also produces a differential output required to drive the PCM encoder.

Fig. 5.4 shows the detail of the schematic processing the telemetries MAJOR Frame pulse. By counting the occurrence of this only occasional signal, the selection of LSB or MSB output stream is determined and the Calibration signal (CAL) is generated, which is transmitted to the analog electronics.
The MAJOR Frame pulse (45 Hz) comes after every eighth GATE1/2 signal (361 Hz). By

counting 4 MAJOR pulses an MSB stream is submitted every 32^{nd} LSB stream.
Counting the occurrence of $2^7 = 128$ or $2^8 = 256$ MSB streams (with 45 Hz/4) triggers a calibration signal every 11.38 or 22.76 s.

Fig. 5.5 shows the components responsible for the down-scaling of the input frequency and the generation of the counter input.
By serially combining the outputs of the binary and decimal counters U1 and U2 a prescale factor of $P_s = 2^b(2d - 1)$ can be set (see Ch. 5.4).
The decimal counter U4 controls the counter circuit itself: It resets the prescaler and holds U4.Q1 high for the duration of the prescaled input half-period. Afterwards the shift registers (Fig. 5.6) are loaded and then the counter is reset. After the occurrence of a GATE signal the counting process starts anew.
The ultra-high speed open Drain NAND gate IC2 (NC7SZ38) is the first bottleneck of the digital counter electronics. Its input signals are at 3.3 V level (determined by the output level of the 250 MHz oscillator QG1) but the output has to reach 5 V to conform to the input levels of the high speed D-flip-flop IC3. (The flip-flop could be powered with 3.3 V but at the cost of speed.) The RC-element formed by the pull-up resistor R1 and the input capacitance of the following component limits the fall time of the gate's output. That is very critical since a half-period of the 250 MHz clock is only 2 ns long, allowing a fall/rise time of not more than 1 ns to maintain a clean signal!
The other bottleneck is the D-flip-flop IC3 74LVC1G74 which has to process a 250 MHz input signal (Fig. 5.6). According to its datasheet it can handle a maximal clock frequency of 200 MHz but it makes 250 MHz too. Since this device has no reset (such fast flip-flops with reset pin were not available), the reset is done manually by pulling its clock input and D output down.
The four least significant bits are evaluated using D-flip-flops since they are much faster than the subsequent 12 bit counters U11 and U12. (Note that this configuration would be able to generate a 28 bit counter value.) The 20 bit counter value (with 10 redundant bits) is loaded to four serial shift registers, two each storing 16 bit data for the LSB or the MSB stream. The signals LSB_CLK_INH and MSB_CLK_INH (see Fig. 5.4) manage the selection of the stream to be gated to the output through U17 and IC15A while GATE is active.

Since the 250 MHz oscillator consumes a lot of power it is only assembled on one PCB. Its signal is passed to the other PCB by using a vertical coaxial SMB connector (see Ch. 7).

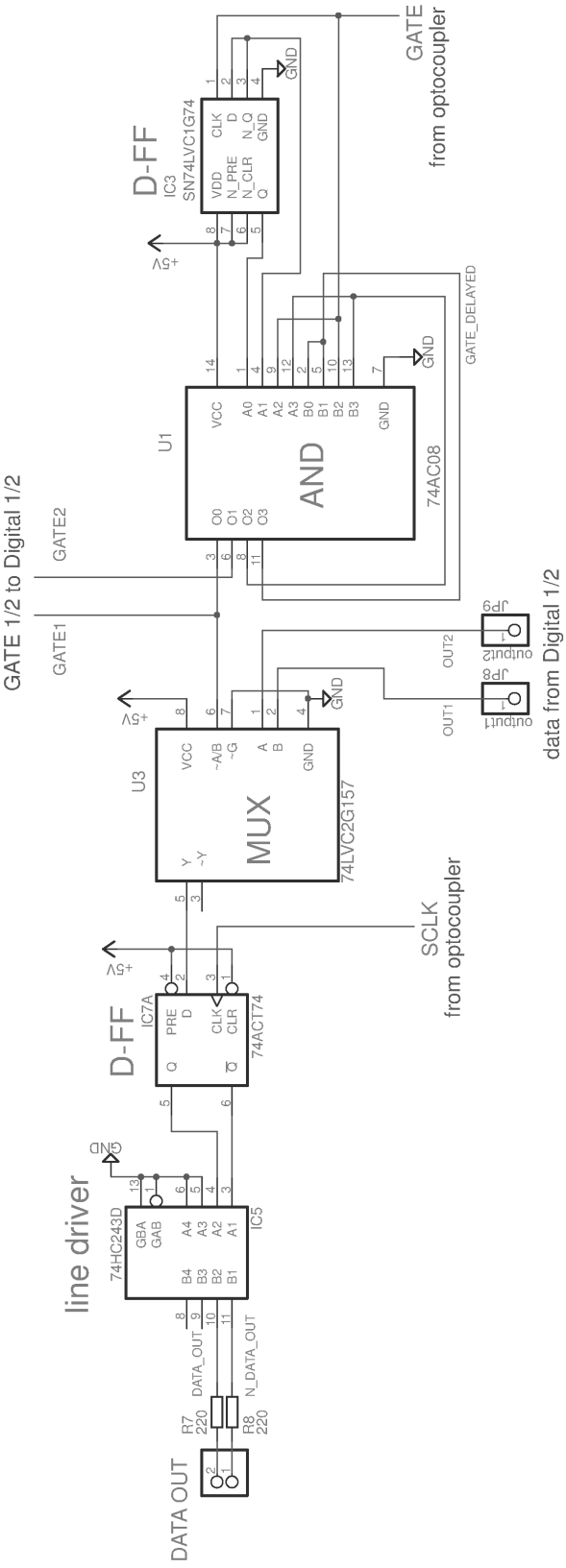

Figure 5.3.: Detail of schematic: Splitting of the GATE signal into GATE1, GATE2 and merging of the outputs from Digital 1/2 to a single output line DATA OUT to the encoder and delaying data by 1 clock cycle.

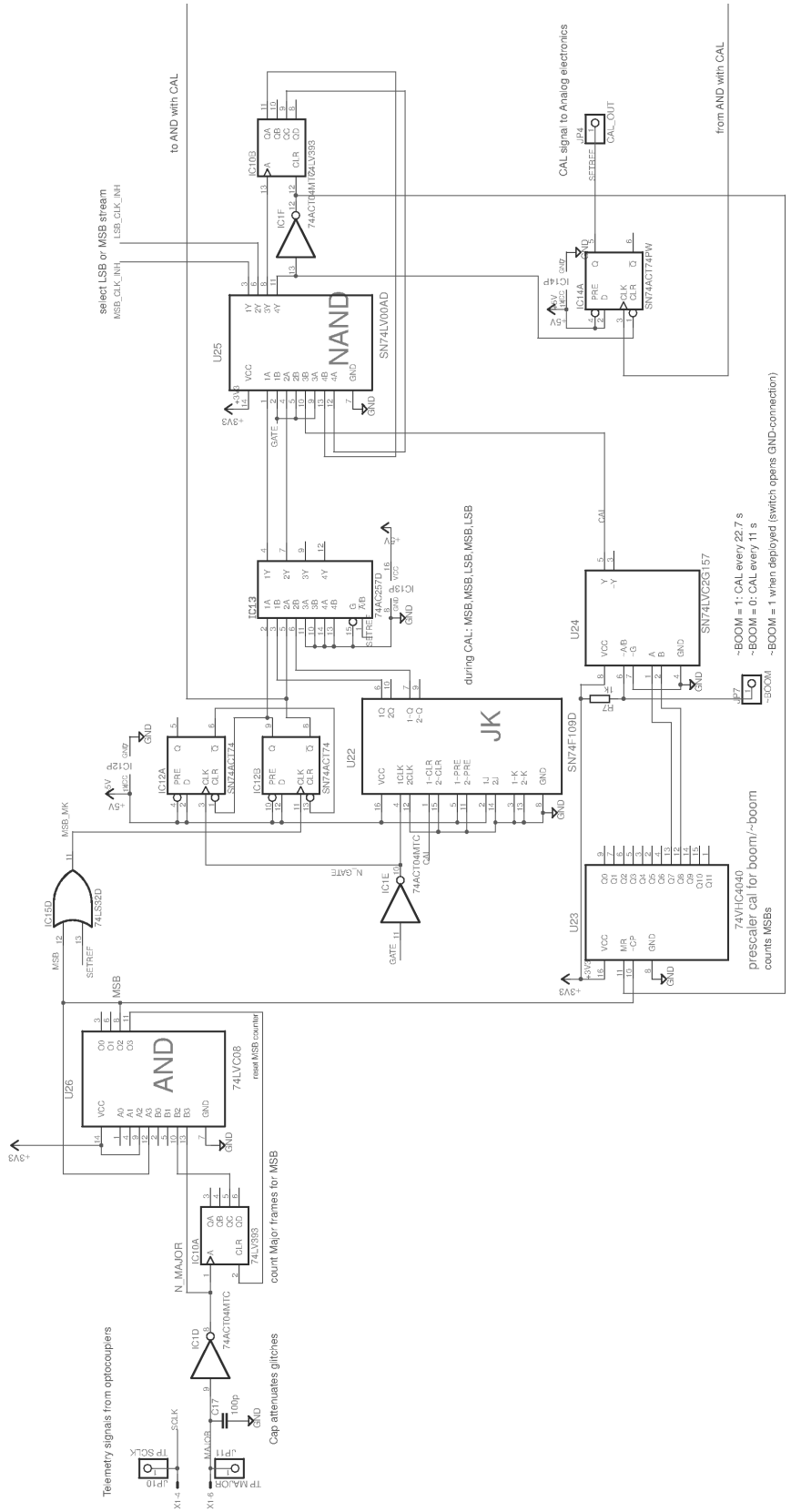

Figure 5.4.: Detail of schematic: Every fourth Major Frame (IC10A) sets the MSB_MK flag. The next output stream will be MSB. U23 determines the time between Calibration (CAL) impulses by counting MSBs. The multiplexer U24 processes the signal status of the boom deployment switch.

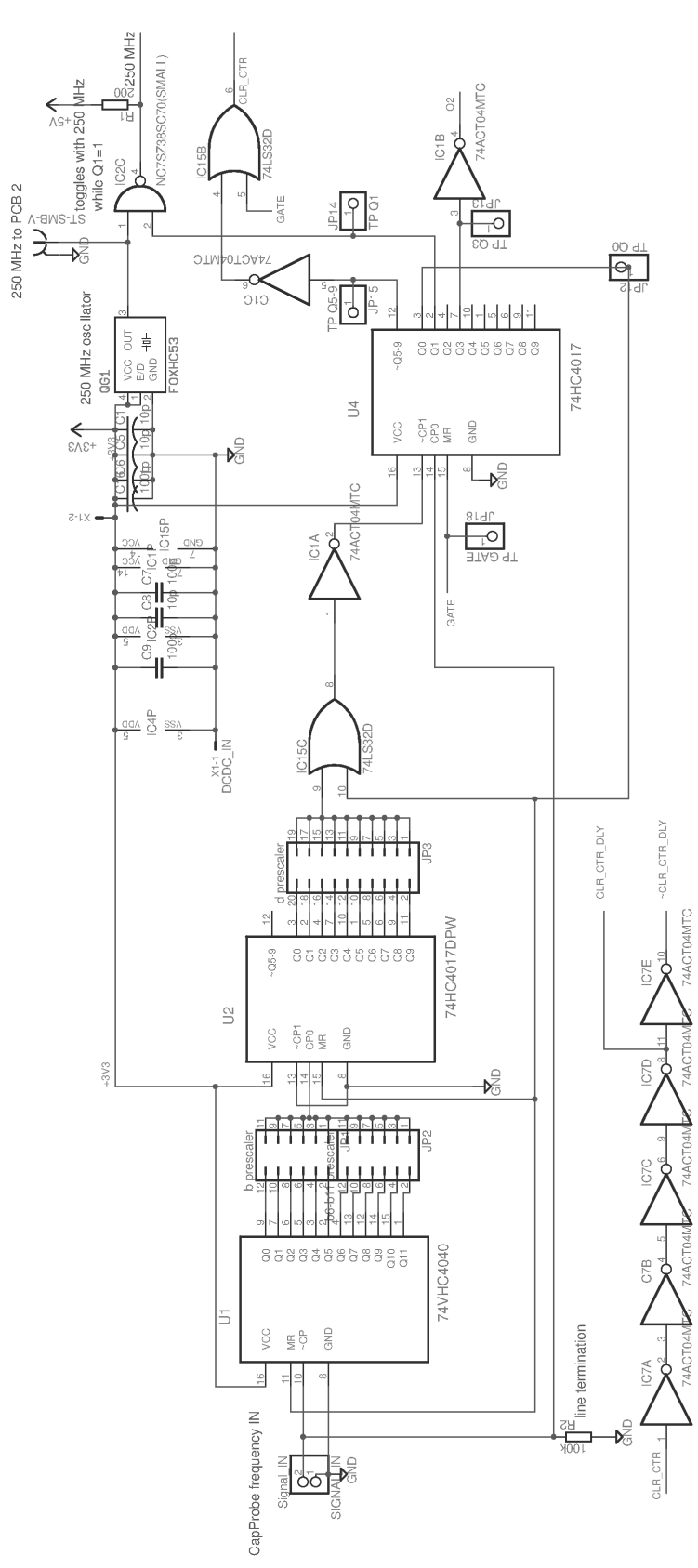

Figure 5.5.: Detail of schematic: The input period from the CapProbe is stretched by a prescaling factor adjustable with JP2 and JP3 (see Ch. 5.4) and then gated with a 250 MHz clock, generating a 250 MHz counter clock while the scaled input is high. U4 controls the counter electronics in dependence of the input signal.

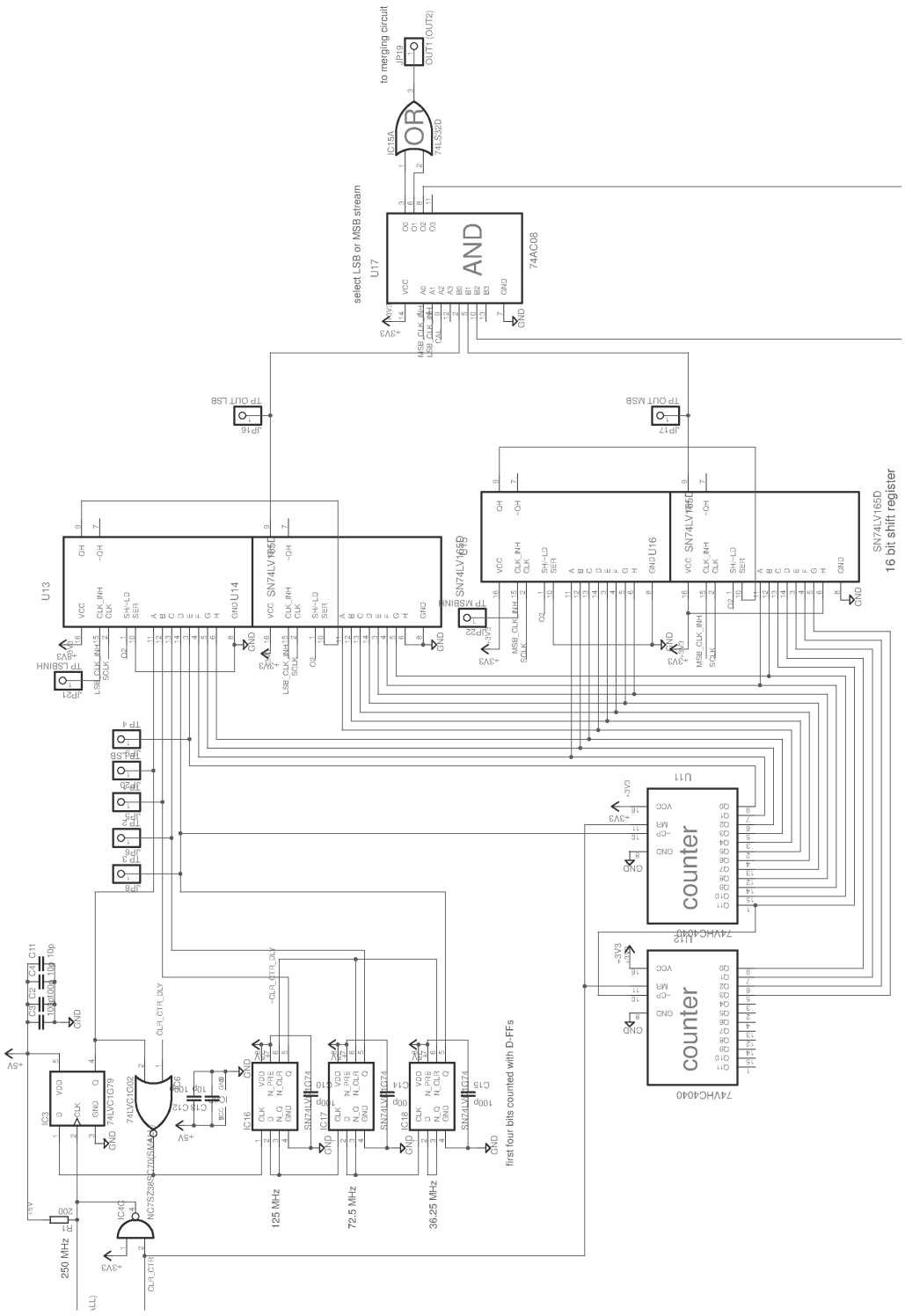

Figure 5.6.: Detail of schematic: The four least significant bits are created by using D-flip-flops IC3, IC16 to IC18. The output of the last flip-flop clocks the subsequent 12 bit counters U11 and U12. The counter value is loaded to four parallel in-serial out shift registers.

5.3.2. Oscilloscope screenshots

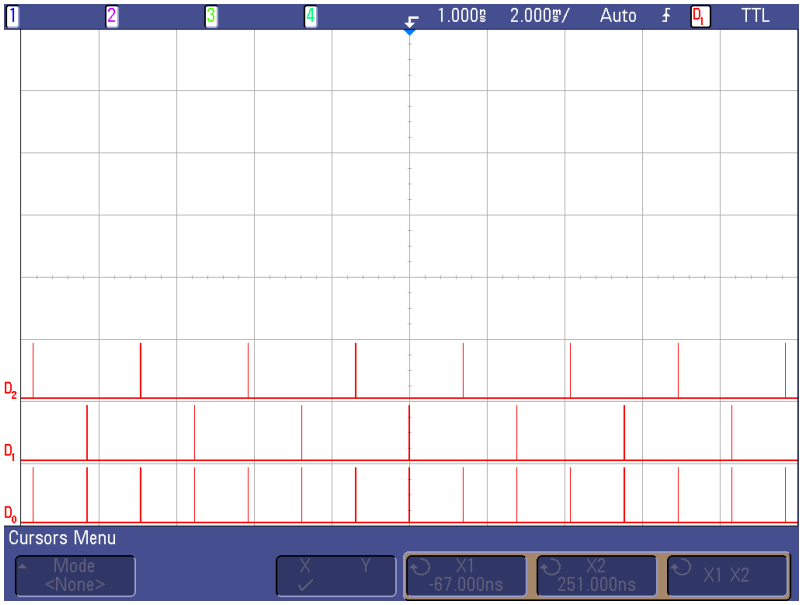

Figure 5.7.: The GATE-signal from the service module is received with 722 Hz and is split into two alternating signals GATE1 and GATE2 with 361 Hz each.
D2=GATE2, D1=GATE1, D0=GATE

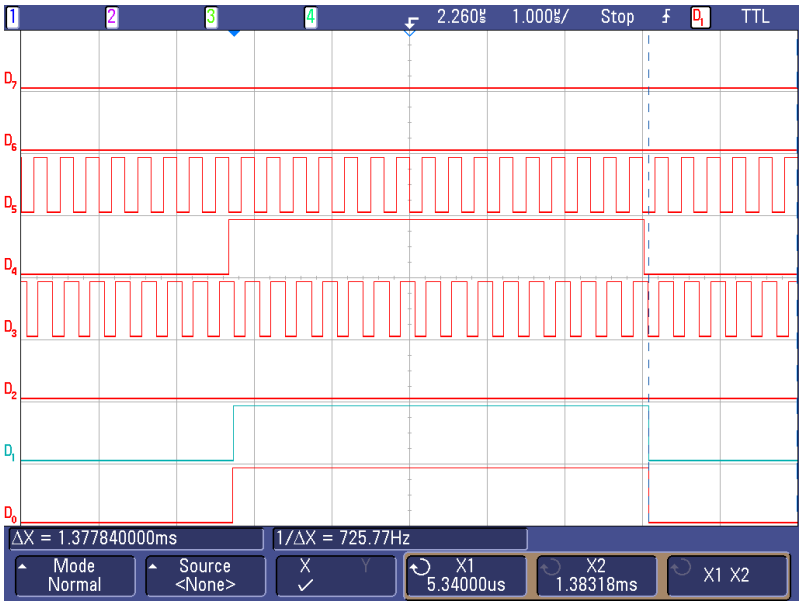

Figure 5.8.: A GATE signal is 16 clock cycles long. It starts with the falling edge of SCLK.
D5=original SCLK, D4=original GATE, D3=SCLK_opto = SCLK delayed by optocoupler, D1=GATE1, D0=GATE_opto

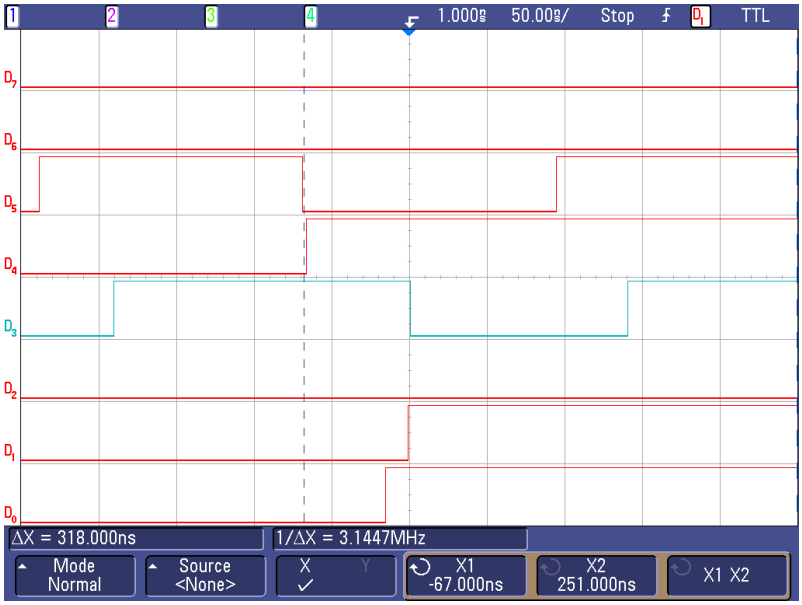

Figure 5.9.: All signals from the service module are delayed by the propagation delay of the interface optocouplers. $t_{pLH} \simeq 50$ ns but $t_{pHL} \simeq 70$ ns, hence GATE_opto rises before the falling edge of SCLK_opto. Fortunately GATE1 gets additionally delayed by the alternation, so that it starts correctly with the falling edge of SCLK_opto.
D5=original SCLK, D4=original GATE, D3=SCLK_opto=SCLK delayed by optocoupler, D1=GATE1, D0=GATE_opto

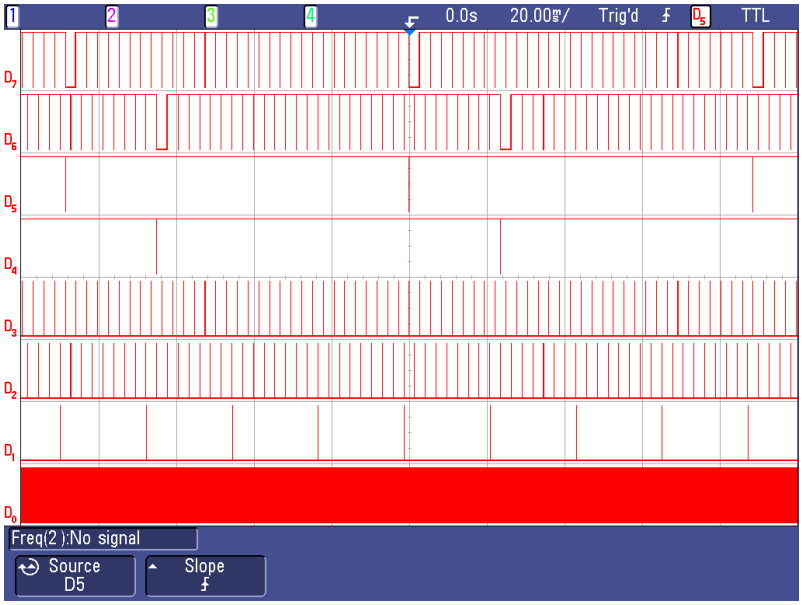

Figure 5.10.: The output data consists of a serial stream of the 16 least significant bits (LSB stream) and a stream of the 16 most significant bits (MSB stream). Since the MSB stream is not expected to change frequently, it is only output at the start of every fourth MAJOR frame, which is equal to every 32^{nd} LSB stream.
D7=OUT2, D6=OUT1, D5=MSB2, D4=MSB1, D3=GATE2, D2=GATE1, D1=MAJOR, D0=SCLK

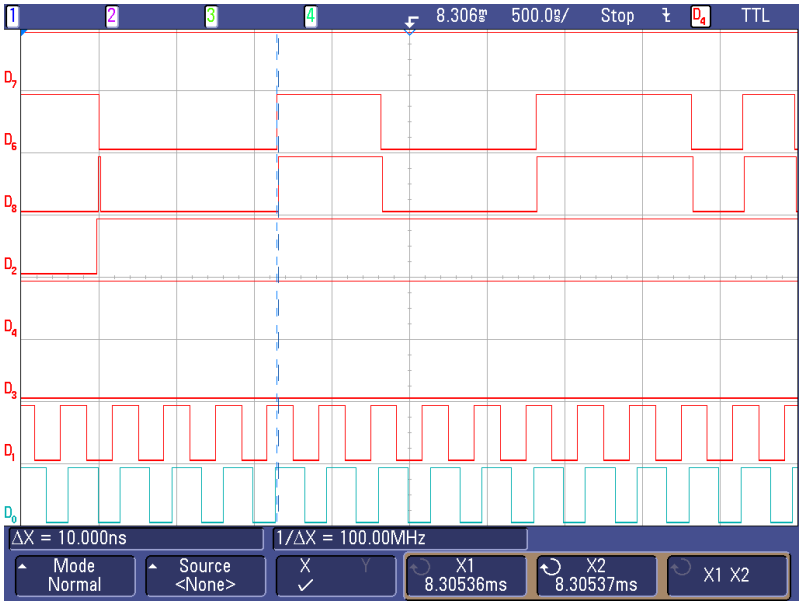

Figure 5.11.: The final output to the service module DATAOUT comes 9 ns after the output of the digital circuits OUT1 or OUT2. This delay is caused by the merging of OUT1 and OUT2 and by the line driver. D6=OUT1, D8=DATAOUT, D2=GATE1, D1=original SCLK, D0=SCLK_opto

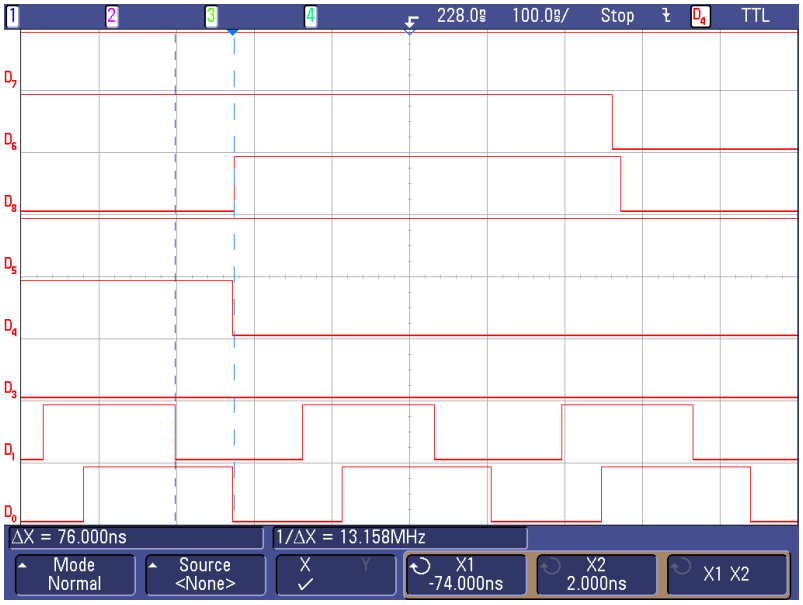

Figure 5.12.: As already mentioned the t_{pHL} of the optocoupler is about 70 ns. The final output data is valid short after the falling edge of SCLK_opto which is 76 ns after the original edge. D8=DATAOUT, D1=original SCLK, D0=SCLK_opto

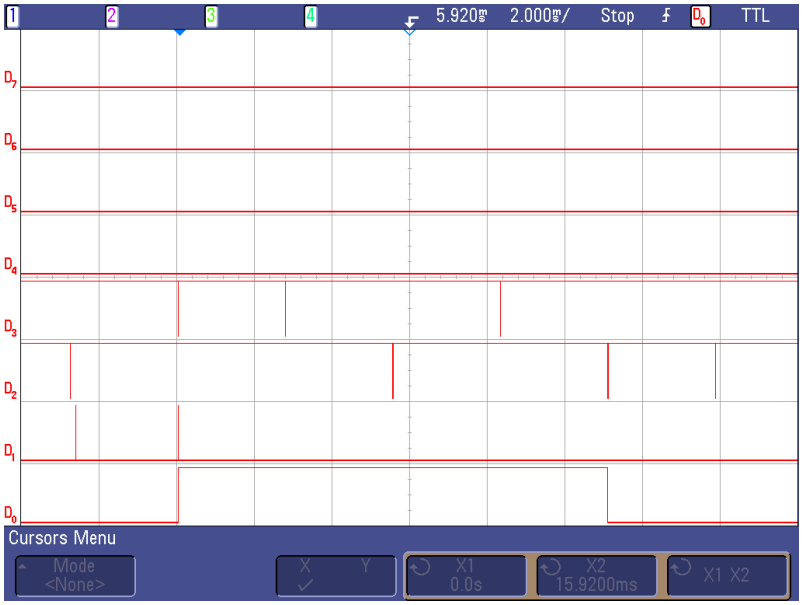

Figure 5.13.: The calibration signal CAL stays high for 11.08 ms. That is the time in which 4 GATE signals at 361 Hz are received. During calibration the usual procedure of 32LSB-1MSB-32LSB is interrupted and replaced with 2MSB-1LSB-1MSB-1LSB. It is likely that the data of the first MSB stream is not usable because of the acquisition time of the analog circuit.
D3=MSB_INH, D2=LSB_INH, D0=CAL

5.4. Setting the prescaler P_s

To achieve higher resolution the input signal frequency is scaled down by a factor P_s. In other words, the measurement time is increased by extending the signal period to nearly the time between two GATE signals T_{Gate}.

$$T_{Signal} \cdot P_s \leq T_{Gate} \tag{5.2}$$

The prescaler value P_s has to be set for the lowest expected signal frequency f_{min} (largest period T_{Signal}).

$$P_s \leq \frac{f_{min}}{f_{Gate}} \tag{5.3}$$

The expected minimum frequencies were evaluated through calibration of the Cap Probe circuit, see Ch. 4.4:

HF probe: $f_{min} = 7.55\,\text{MHz}$ LF probe: $f_{min} = 223.35\,\text{kHz}$

Thus, inserting to Eq. (5.3):

$$P_{s,HF} \leq 20\,914 \qquad P_{s,LF} \leq 618$$

In order to fully exploit the available resolution of 20 bit, the prescaler P_s should be chosen is high as possible to maximize the counting value N. There are two rows of jumpers, namely row JP1 (b) and JP3 (d) (see Fig. 5.14), with which the prescaler P_s can be set according to

$$P_s = 2^b(2d-1) \qquad \text{where b = 0 - 11, and d = 0 - 9} \tag{5.4}$$

Choosing of the available values, the ideal prescaler for HF and LF probe would be $P_{s,HF} = 20\,480$ and $P_{s,LF} = 576$. As safety margin the following values were chosen

$$P_{s,HF} = 18\,432 \qquad \text{(b = 11, d = 5)}$$
$$P_{s,LF} = 416 \qquad \text{(b = 5, d = 7)}$$

which are suitable for frequencies as low as 6.65 MHz and 150 kHz, respectively.

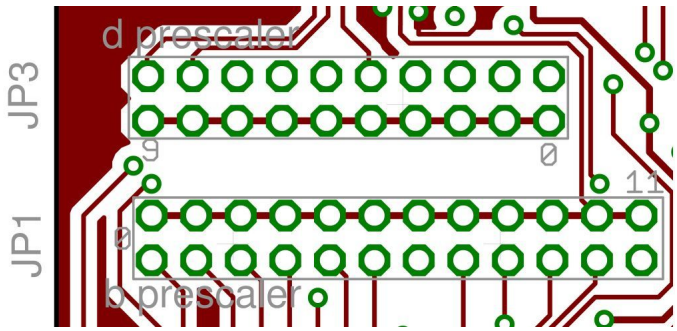

Figure 5.14.: Detail of PCB top layer illustrating the two rows of jumpers used to set the prescaler variables d and b. Upper row from the left: d = 9 to 0. Lower row from the left: b = 0 to 11.

5.4.1. Required number of output bits

Note that the prescaler setting and hence the minimum expected frequency influences the number of bits needed to represent the output frequency. According to Eq. (5.1) the maximum counter value for HF and LF probe is with the chosen prescaler values:

$$N_{max,HF} = \frac{f_c \cdot P_{s,HF}}{f_{min,HF}} = \frac{250\,\text{MHz} \cdot 18\,432}{7.55\,\text{MHz}} = 610\,331$$
$$N_{max,LF} = \frac{f_c \cdot P_{s,LF}}{f_{min,LF}} = \frac{250\,\text{MHz} \cdot 416}{223.35\,\text{kHz}} = 46\,563$$

Representing those numbers needs 20 bit and 16 bit, respectively. Accordingly, for the actual application a 20 bit data stream is enough. Since 30 data bits are available 10 bits are redundant.

5.5. Interpretation of the output data

Fig. 5.15 shows an example of a digital output for the LF Cap Probe according to Fig. 5.16 (MSB stream) and Fig. 5.17 (LSB stream). The bits 14 to 5 are redundant. The first bit of an MSB stream is always high (H) the one of an LSB stream always low (L). Interpreting bit 19 to 0 as 20 bit binary number yields a counter value of $N = 440\,313$. By rearranging Eq. (5.1) one can determine the measured Cap Probe frequency f:

$$f = \frac{f_c \cdot P_s}{N} \tag{5.5}$$

Inserting $f_c = 250\,\text{MHz}$, $P_{s,LF} = 416$ and the counted value $N = 440\,313$ into the above equation results in $f = 236\,195.6\,\text{Hz}$.

Bit	20	19	18	17	16	15	14	13	12	11	10	9	8	7	6	5	4	3	2	1	0
MSB stream	H	0	1	1	0	1	0	1	1	0	1	1	1	1	1	1					
LSB stream						L	0	1	1	0	1	1	1	1	1	1	1	1	0	0	1

Figure 5.15.: Example of a digital output for the LF Cap Probe according to Fig. 5.16 (MSB stream) and Fig. 5.17 (LSB stream)

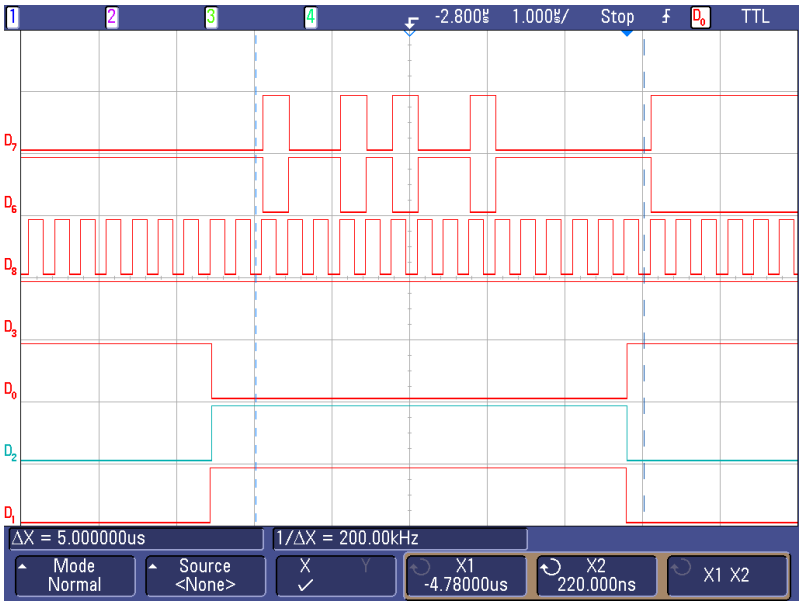

Figure 5.16.: Example of a digital output (differential): MSB stream. The first data is sampled about 1.5 clock cycles after GATE goes active = left cursor. 16 bits are sampled. The last sample is taken at the right cursor. The data is 1-0-1-1-0-1-0-1-1-0-1-1-1-1-1-1.
D7=N_ DATAOUT, D6=DATAOUT, D8=SCLK, D3=LSB_ INH, D0=MSB_ INH, D2=GATE2, D1=GATE

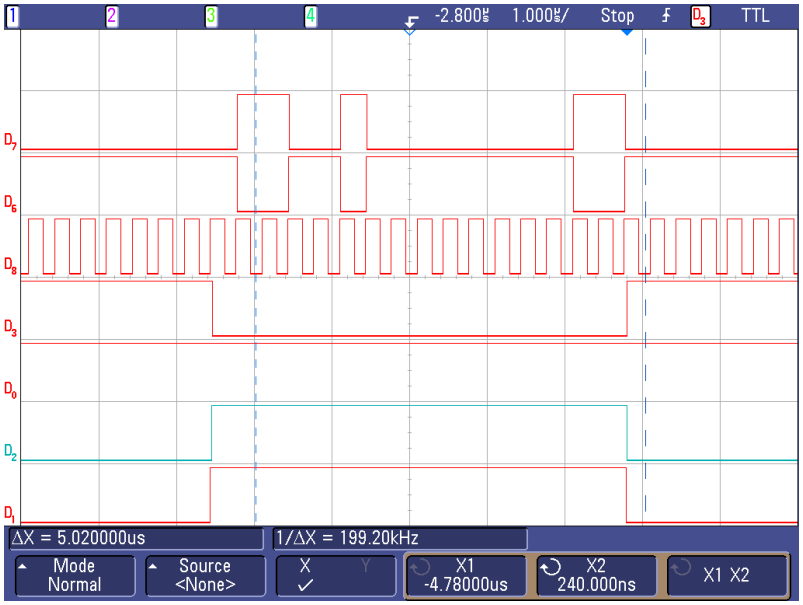

Figure 5.17.: Example of a digital output (differential): LSB stream. The first data is sampled at the left cursor. The last sample is taken at the right cursor. The data is 0-0-1-1-0-1-1-1-1-1-1-1-1-0-0-1. D7=N_ DATAOUT, D6=DATAOUT, D8=SCLK, D3=LSB_ INH, D0=MSB_ INH, D2=GATE2, D1=GATE

5.6. Why not use a microcontroller?

The counting frequency of the actual circuit is 250 MHz. The data output requires 20 bits but the circuit would be able to count up to 28 bits. Performing these requirements with a microcontroller would need a device with a system clock much higher than 250 MHz and an integrated counter unit of at least 32 bits (28 bits are not usual). Of course such controllers exist and their price is not worth noting. But they come in very tiny QFN or BGA packages.
The circuits resulting from this work were projected to be used on not more than six payloads, meaning a small number of pieces layouted manually and soldered by hand. The PCBs were printed at the Institute[1], leading to PCB design rules and layer restrictions which did not allow the use of the above packages. Of course, one could have printed and eventually assembled the PCBs outside the Institute but the arising prototyping costs and idle times were in no relation to the chosen implementation using discrete logic devices.

An alternative for future designs could be to implement the counter electronics, *i.e.* frequency input to shift registers, as done in the actual work, but to realize the processing of the PCM encoder signals using a low-level microprocessor.

[1] Institute of Electronics, TU Graz

6. Power supply

6.1. MaxiDusty grounding strategy

Each instrument has its own twisted pair for power distribution. The return lines are all connected to a single point of reference inside the common power distribution unit.
The MaxiDusty interface recommendations specify that every instrument must have its own DC/DC converter to convert +28 V to the required supply voltages. Furthermore the galvanic isolation in the converters avoids ground loops. Linear regulators should only be used *after* the DC/DC converter to keep the overall power consumption low.
The structure of the payload is used as the common point for all return currents. Connections between PCB ground and the payload structure are necessary due to the galvanic isolation in the DC/DC converter.

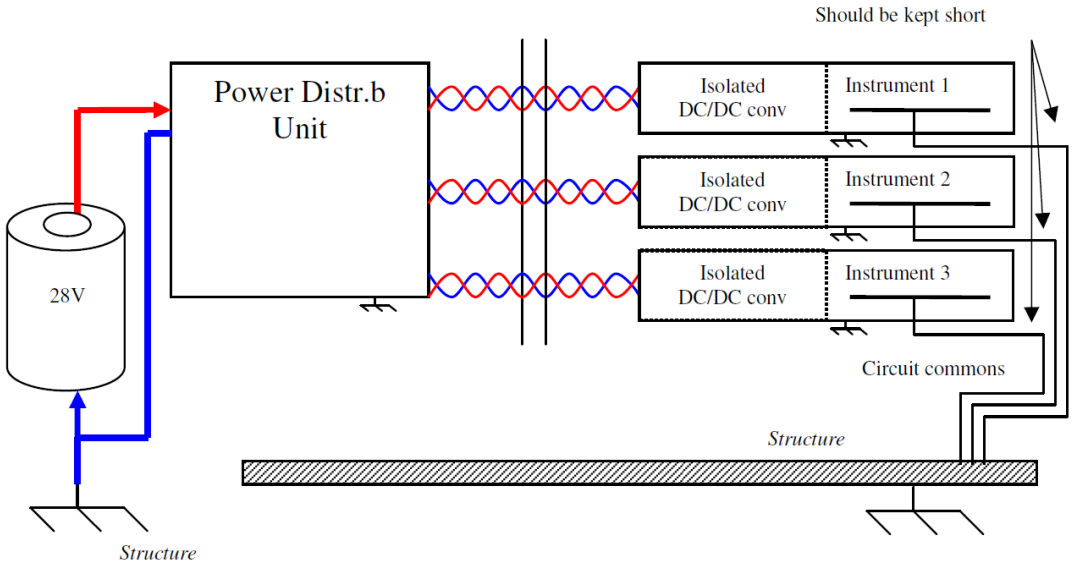

Figure 6.1.: Schematically description of the grounding strategy used in the Hotel payload . Each instrument is isolated from the common power distribution unit by its own DC/DC converter. The structure of the payload is used as the common point for all return currents [Andøya Rocket Range, 11 August 2009].

6.2. Power supply unit (DC/DC)

The electronics needs altogether four power levels, *i.e.* ±12 V for the analog electronics (and +12 V for the Faraday experiment), +5 V for the analog and parts of the digital electronics and finally +3.3 V for the rest of the digital electronics. The power supply unit (DC/DC for short) housed in the Main Box provides these voltages.
First the 28 V battery supply is converted to ±12 V with an DC/DC buck converter, ensuring galvanic isolation from the payload's power distribution unit. In order to reduce the overall power consumption a second DC/DC buck converter is used - rather than a linear regulator - to produce +5 V from the +12 V for the analog and digital supply. The third power domain +3.3 V is exclusively used by the digital electronics. It is produced from the +5 V by a linear regulator.

The differential input signals from the PCM encoder are pre-processed at the DC/DC PCB. The signals are converted to single ended by using optocouplers as specified by the payload engineer [Andøya Rocket Range, 11 August 2009] (see Ch. 5.2). Three jumpers offer the possibility to invert the control signals SCLK, GATE and MAJOR (just in case!).
All signals to the Digital PCBs are accessible through 6 pin connectors providing GND, +3.3 V, +5 V and the control signals. Note that the GATE splitting and the output merging circuits depicted in Fig. 5.3 are actually also located on the DC/DC PCB but not illustrated in this chapter for clearness.

The bypass capacitor selection and the PCB layout is according to the application notes and datasheets of the components (converters, regulator, optocouplers).

6.3. Power consumption

The overall power consumption was aimed to be as low as possible. Therefore a combination of buck converters and linear regulator was used as described above. However, the overall current consumption of the probe electronics finally turned out to be 163 mA at 28 V resulting in a total power consumption of about 4.6 W.
Since the Faraday experiment is powered by the same supply unit its consumption of 27 mA has to be added, resulting in an overall current consumption of 190 mA at 28 V (5.3 W).
The main contributors to the overall consumption are

- the high counting speed of 250 MHz of the Digital electronics, *i.e.* the oscillator and the high speed flip-flops,
- the high oscillating frequency of 9 MHz of the Cap Probe circuit, requiring a high speed analog buffer to feedback the signal to the coax shield
- the need to digitize the Cap Probe RF signal and to drive it over approx. 1 m coax cable to the Main Box, and

Tables 6.1 exemplifies some measured current consumptions at the 28 V domain. Unfortunately the idle current of the used Traco THN 15-2422WI converter is as high as 40 mA. Powering in addition one Analog Box requires about 70 mA, the two Digital electronics draw 90 mA. The data of Table 6.2 shows that the Ion Probe circuit consumes far less power than the Cap Probe circuit, despite the great number of components needed to realize the logarithmic amplifier.

	+28 V
DC/DC idle	40 mA
DC/DC + 1x Analog Box	70 mA
DC/DC + 2x Digital	90 mA
overall probe electronics	163 mA
Faraday experiment	27 mA
overall	190 mA

Table 6.1.: Current consumption at +28 V domain (approx.)

	+12 V	-12 V	+5 V
HV Ion Probe circuit	4 mA	3 mA	0 mA
Analog Box (HV + HF)	46 mA	27 mA	11 mA

Table 6.2.: Current consumption of the analog electronics at ±12 V and +5 V domains (approx.)

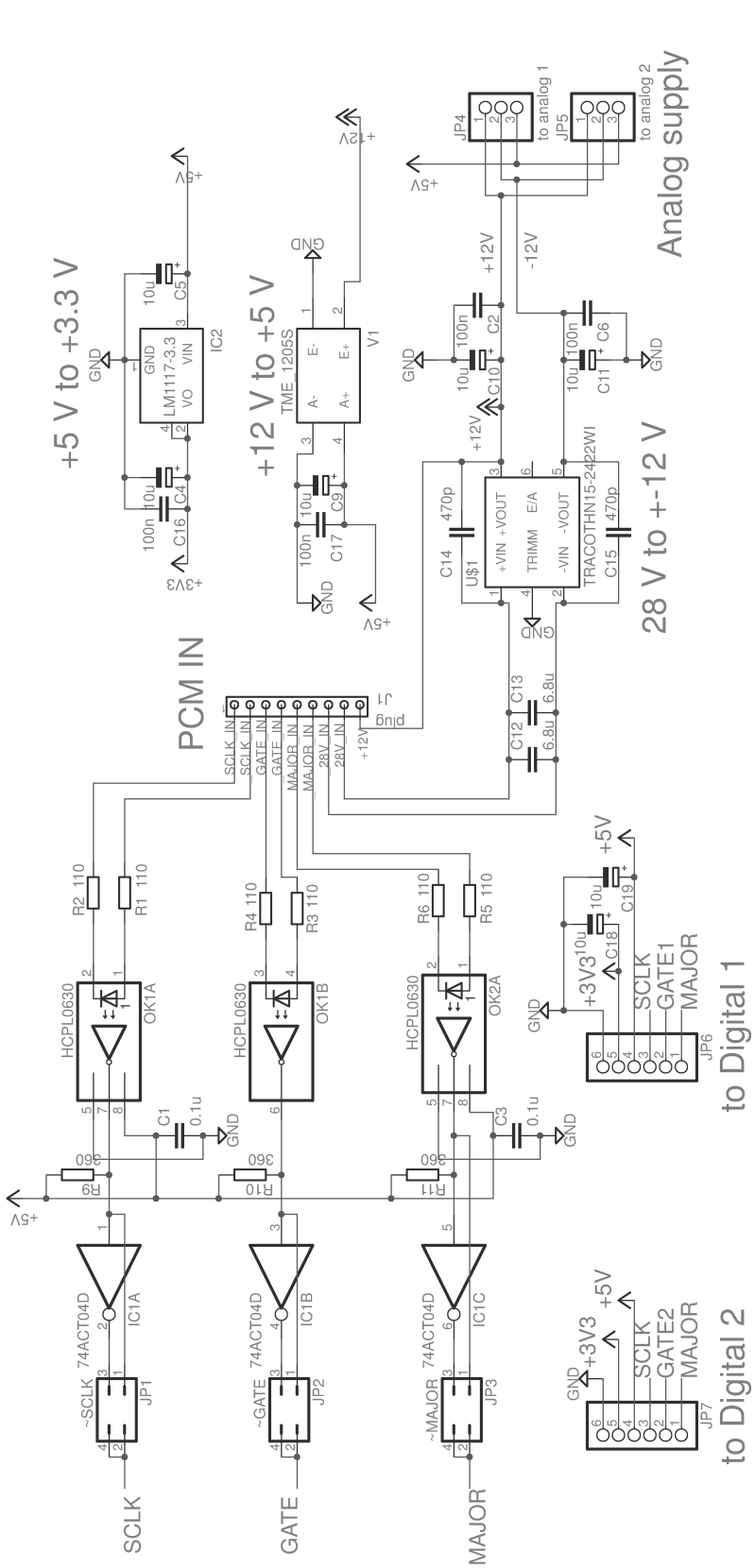

Figure 6.2.: Detail of schematic: DC/DC conversion and optocoupler interface. First the 28 V battery supply is converted to ±12 V with a DC/DC buck converter, ensuring galvanic isolation from the payload's power distribution unit. Another buck converter is used to produce +5 V for the analog and digital supply. The third power domain +3.3 V is produced from the +5 V by a linear regulator.

7. Mechanical arrangements

Each experiment consist of a number of components, *cf.* Fig. 7.1:
The probe itself is mounted on the boom. The boom is a stainless steel tube with an inner diameter large enough to accommodate the two cables connecting to the probe (Fig. 2.3). To each probe belongs one Analog Box housing the Ion Probe and the Cap Probe electronics, see Fig. 7.3. This box is located close to the boom mounting to minimize the cable lengths and therefore its influence on the measurement. It provides one chamber for each PCB mainly to prevent the Cap Probe's RF signal from interfering the extremely sensitive current measurement circuit.
The boom hinge is equipped with a microswitch. Its signal is passed through the Analog Box to the Main Box where it is processed by the Digital electronics.
The Main Box is located two decks below the Analog Boxes (Fig. 7.8). It provides the interface to the Analog Boxes and to the PCM encoder, altogether three connectors each the size of a 15 pin D-sub. The three PCBs (Fig. 7.4) form a stack which can easily be put in and out of the housing (Fig. 7.5). However, once assembled it is laborious to access the prescaler jumpers on the Digital boards. Since the Digital boards are identical it does not matter which Analog Box is connected to which Digital interface. But one has to set the prescaler on the Digital board according to the connected Cap Probe.

Generally, mechanical vibrations due to the rocket's launch need to be considered. Sensitive mechanical parts like big circuit components (1 GΩ-resistors), connectors and screws have to be glued before launch.

7.1. Connectivity

Fig. 7.7 illustrates the connections between the three boxes and inside the Main Box. Accordingly, Fig. 7.8 gives an estimation of the cable lengths between the boxes and the probes.
The Main Box is connected with a 15 pin D-sub plug to the PCM encoder. Pins 1 to 8 carry the four differential input signals from the encoder. Pins 9 to 14 output the measurement results. The outputs of the two Cap Probes are alternatingly transmitted to a single line (Pins 9, 10). Pin 15 provides the supply for the Faraday experiment. All inputs are routed to the DC/DC board (PCB 1) where they are pre-processed and then forwarded to the Digital PCBs. The Analog Boxes are connected with a special connector the size of a 15 pin D-sub which provides 2 coaxial and 5 regular pins on a single plug (termed 7W2 = 7 pins with 2 special pins). The 'Boom deployed' signal from the microswitch (not depicted in the figure) is bypassed to the digital electronics which generate the calibration (Cal) signal for the analog electronics in accordance to the boom status. The analog 'Ion out' voltage signal is

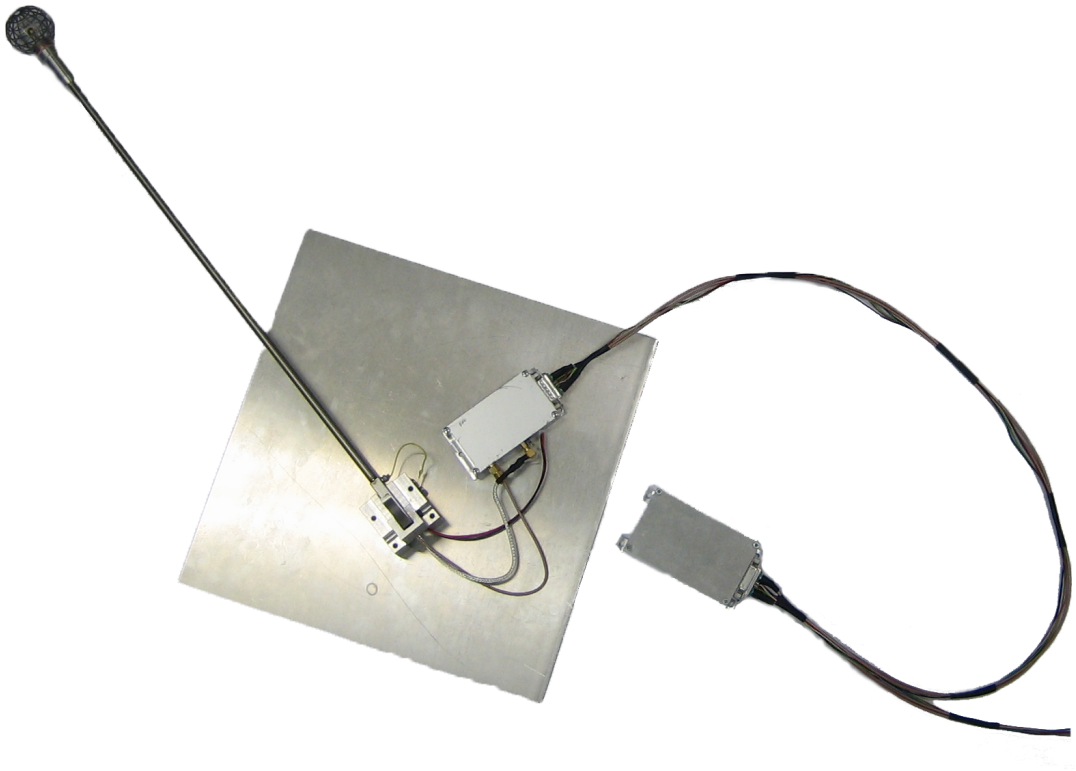

Figure 7.1.: Photo of half of the assembled system showing one of two Analog Boxes, booms and probes and the Main Box. The Analog Boxes are located near the booms, the Main Box can be 'far' away. The triax and coax cable connecting the probe run side-by-side inside the boom. (The Analog Boxes and the booms (*i.e.* the probes) have to be at the same potential. During tests this has to be manually secured, here with a metal plate.)

Figure 7.2.: Interface of an Analog Box. From the left: Cap Probe (SMA connector), Ion Probe (SMC connector + 2 pin header for outer triax shield), 2 pin connector for boom deployment microswitch, 7W2 connector to Main Box

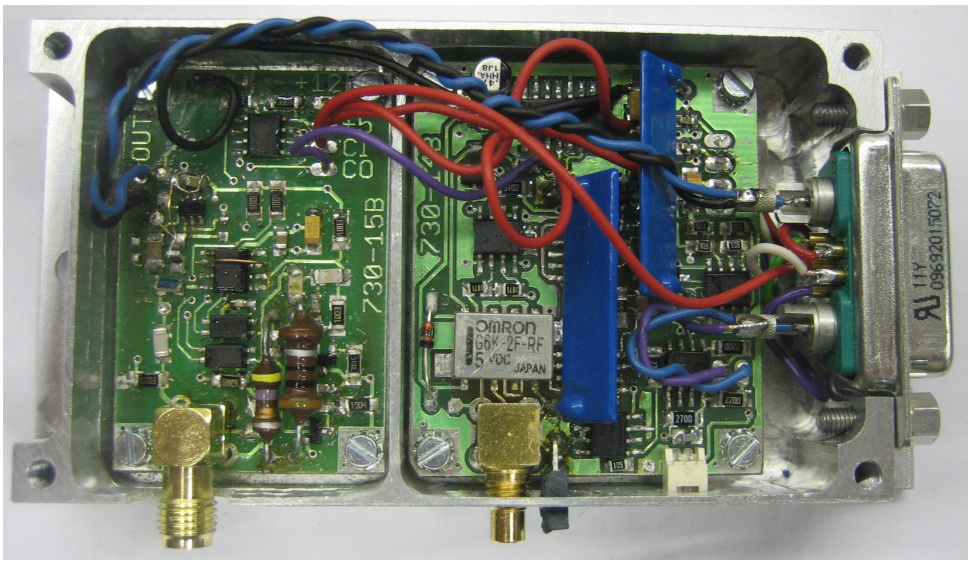

Figure 7.3.: Inside view of the Analog Box. left: Cap Probe electronics, right: Ion Probe electronics. Note the large 1 GΩ resistors (blue). A resistor with a larger value would be mechanically too large for the box.

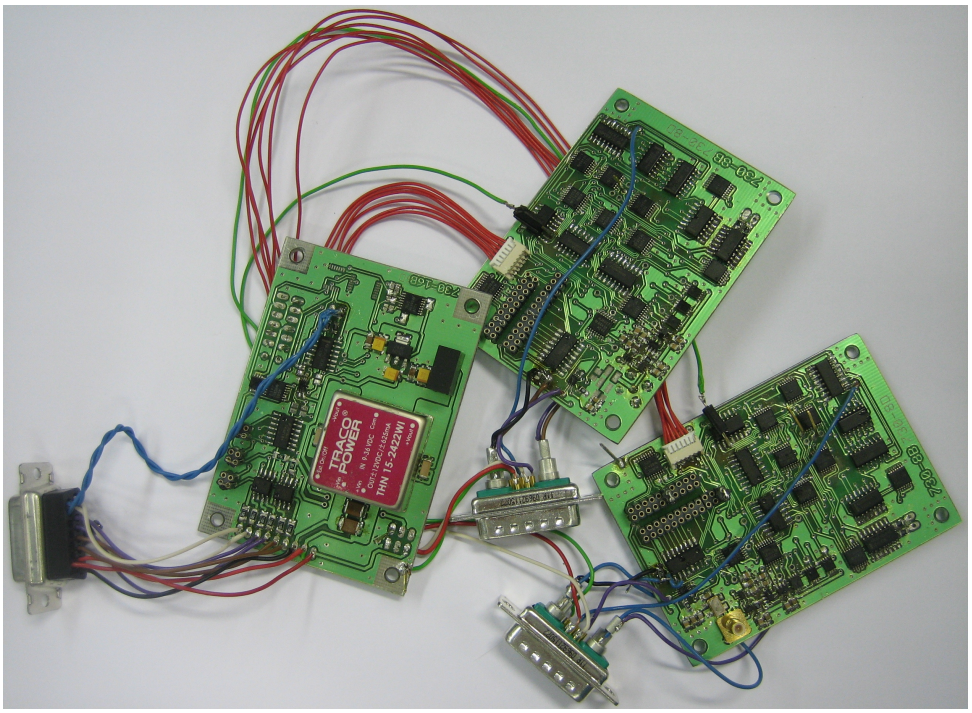

Figure 7.4.: The three PCBs of the Main Box: DC/DC and two Digital electronics. A 15 pin D-sub connector (left) is the interface to the PCM encoder. The Digital electronics are connected to the Analog Boxes with special 7W2 connectors, providing 2 coaxial pins besides 5 normal pins. Note the two rows of jumpers on each Digital PCB used to set the prescaler. Note also the golden SMB connector which provides the 250 MHz oscillator signal to the second Digital PCB.

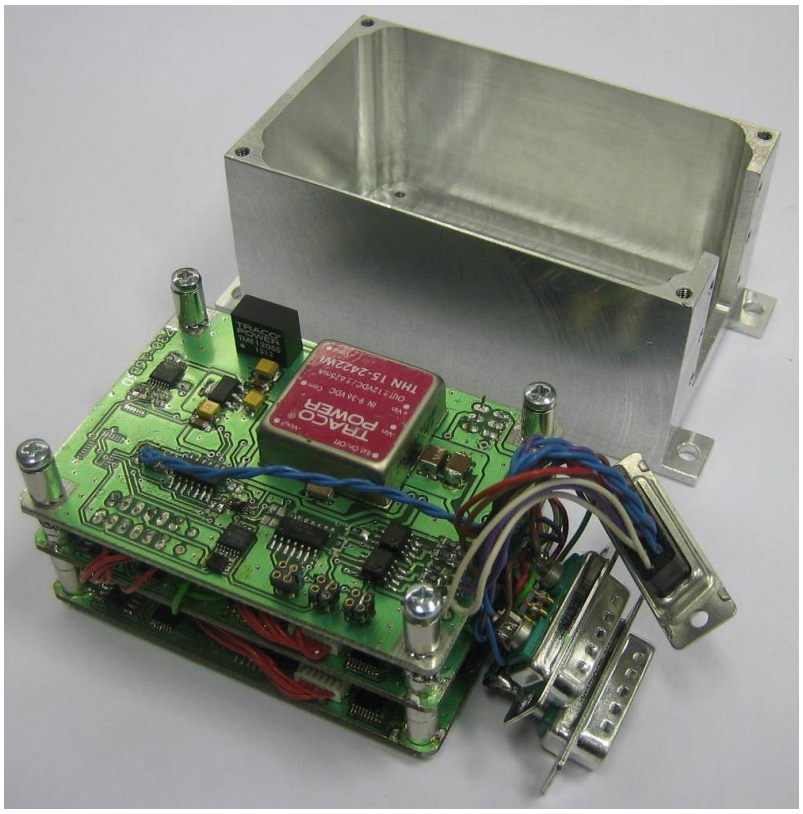

Figure 7.5.: The three PCBs of the Main Box assembled and ready to be put into the box. At the top the DC/DC board, below the two Digital PCBs. A vertical SMB connector passes the 250 MHz counter frequency from the lowest PCB to the one above. The screws are at ground potential providing a low impedance path between the boards.

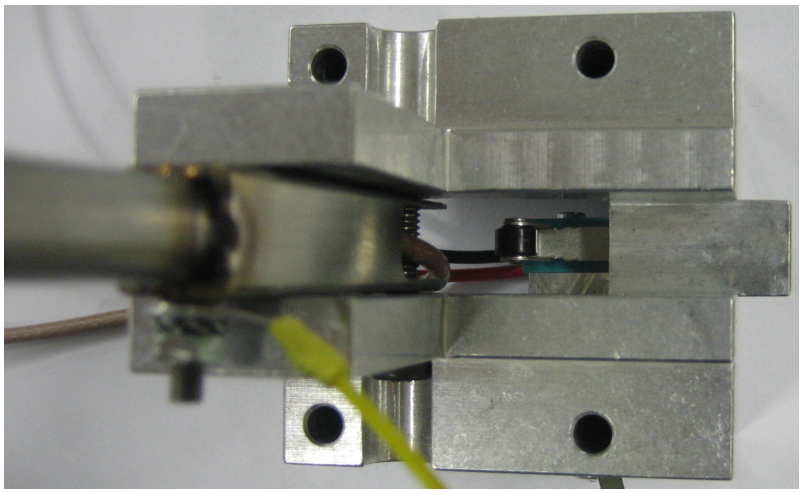

Figure 7.6.: Detail view showing the microswitch inside the boom mounting. When the boom deploys it drops onto the switch.

already provided by the Ion Probe electronics. Hence it is simply passed through the Main Box to the respective pins 11 to 14.
Since the shield of the Cap Probe coax, which is directly connected to the PCBs, is at ground potential a low impedance path between the boxes is ensured, reducing ground bounce.

Triaxial connectors are expensive but above all far too large compared to the box dimensions and common triaxial cables are too bulky to fit inside the boom. Hence the triaxial cable and connector for the Ion Probe electronics were self-made, see Fig. 7.9. For this purpose the shield of a coaxial cable was peeled off and slipped over a thinner coaxial cable. The connector is a combination of a coaxial SMC connector and an additional 2-pin header plug with which the outer shield is connected to ground potential.

As safety arrangement it is ensured that the connectors for the Cap Probe and the Ion Probe cannot be interchanged. The Cap Probe uses an SMA plug which has a diameter notable larger than this of the SMC plug of the Ion Probe. Both connectors use a threaded interface so to ensure a secure connection (see Fig. 7.2).

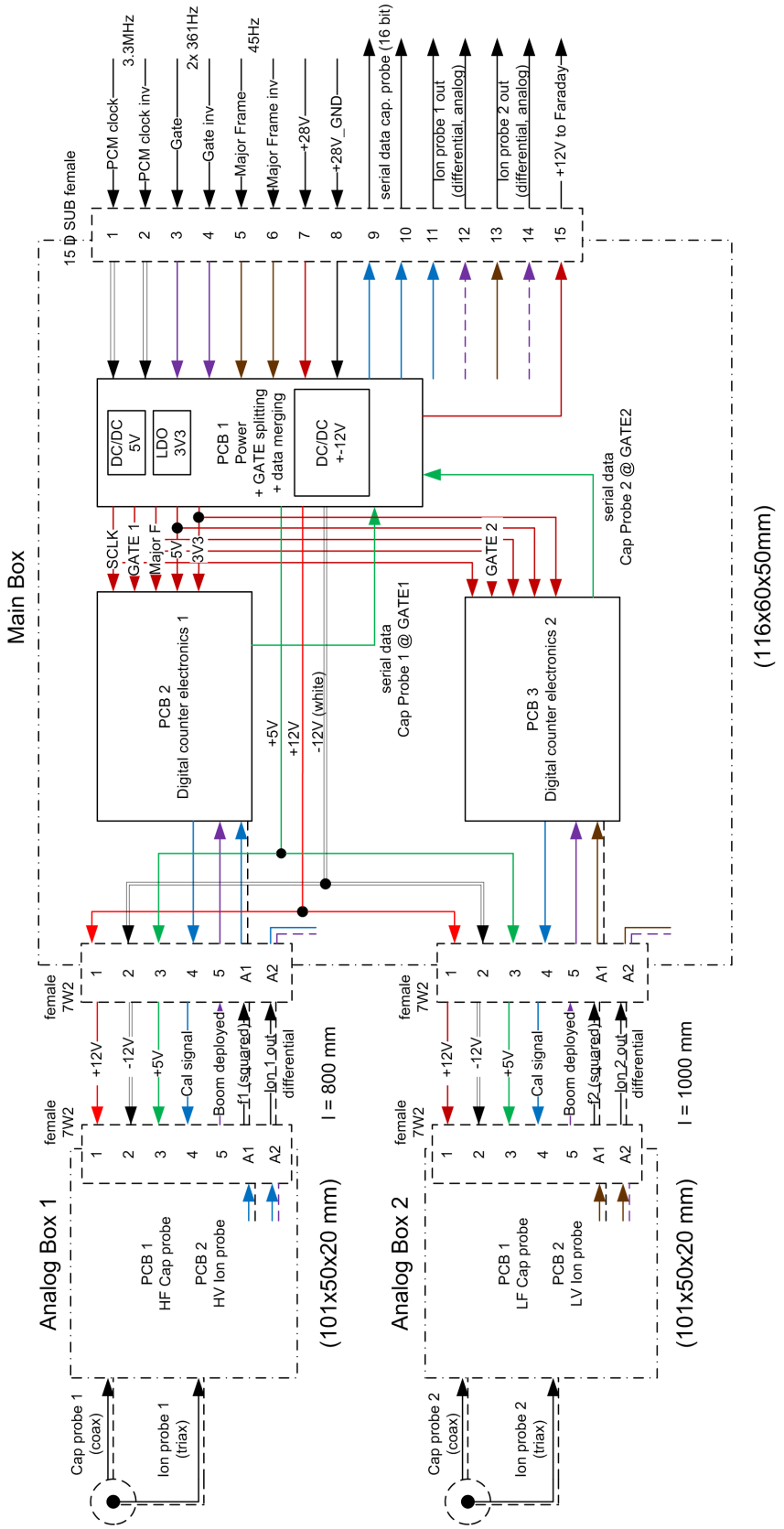

Figure 7.7.: Connection scheme illustrating the connections between the boxes and inside the Main Box. The figure also indicates the used cable colors.

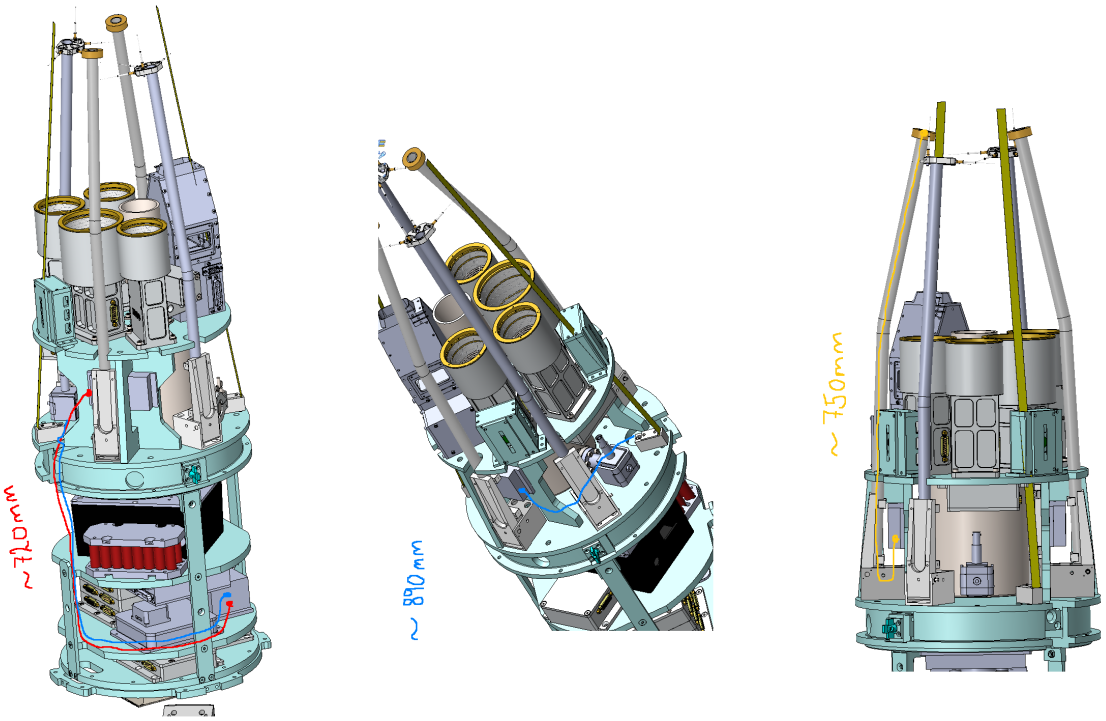

Figure 7.8.: Cable lengths estimated by Andøya Rocket Range. The figure also shows the locations of the three boxes. The coax and triax cables through the booms to the probes are about 750 mm long. One Analog Box is closer to the Main Box than the other. The cable harness are 720 mm and 890 mm, respectively.

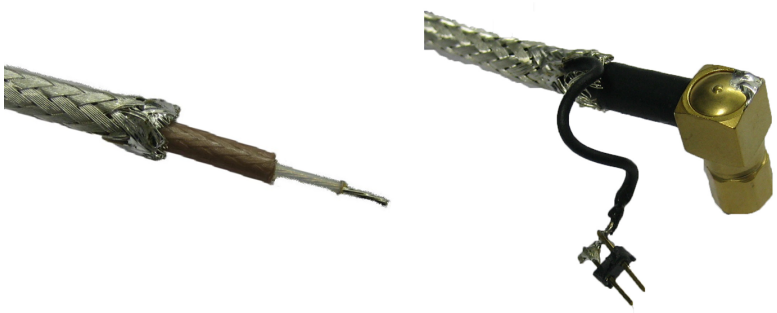

Figure 7.9.: Self-made triaxial cable and connector for the Ion Probe electronics.

8. Summary

The objective of this MSc Thesis was to produce an updated version of a combined ion and capacitance probe to be flown on the forthcoming MaxiDusty sounding rocket payload. The old circuits were modernized with the aim to make them smaller, faster and more accurate by using modern components and minimizing leakages and stray capacitances.
The signal outputs were adjusted to the interface specifications of MaxiDusty.

Actually, due to the increased complexity of the analog circuits they turned out to be not smaller than those used before. However the measurable ion current could be extended down to 1 pA, although the measurement of currents lower than 10 pA is extremely temperature dependent. The probe's bias voltage can now be precisely chosen in the range of about -2 V to -8.6 V by the use of voltage references rather than serial batteries.
The Cap Probe electronics enable to chose between operation frequencies as low as 200 kHz or as high as 9 MHz by only changing the inductance value.
The digital counter electronics provide a resolution of $1.44 \cdot 10^{-6}$ by using a 250 MHz counter frequency. This is significantly higher than before.

In order to make the results of this work comparable to those circuits used in the past and to potential future works Figs. 8.1 and 8.2 give equivalent circuits describing the behavior of the actual analog circuits.
According to the calibration values (see Figs. 4.9 and 4.8) the Cap Probe circuits behave like a parallel LC-resonator with the depicted values. A change in the Cap Probe's capacitance ΔC results in a measured frequency f of

$$f = \frac{1}{2\pi\sqrt{L \cdot (C + \Delta C)}} \tag{8.1}$$

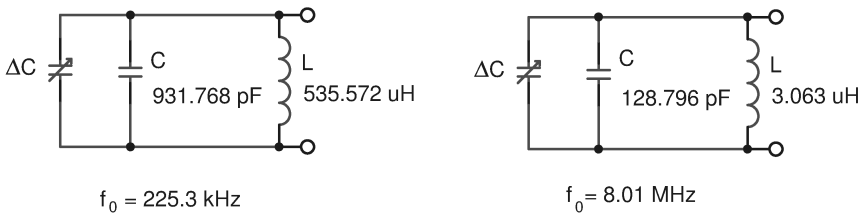

Figure 8.1.: Equivalent circuits of the Cap Probe electronics. C also includes the probes free space capacitance $C_0 = 2.5$ pF. f_0 is the operation frequency for $\Delta C = 0$. left = LF circuit, right = HF circuit

The frequency and capacitance resolution was determined as:

HF probe:	Δf=12.37 Hz	$\Delta C_{res} = 0.412 \cdot 10^{-3}$ pF	@ 361 samples/s
LF probe:	Δf=0.48 Hz	$\Delta C_{res} = 4.176 \cdot 10^{-3}$ pF	

Summarizing, the capacitance resolution of the HF probe is about ten times better than that of the LF probe!

For the purpose of comparison: The LF Cap Probe circuit (near 900 kHz) of [Friedrich, 1979] had a frequency resolution of $\Delta f = 32$ Hz at 1000 samples/s. Better comparable, because it used the same LF frequency is the LF Cap Probe circuit (about 240 kHz) of [Friedrich, Boh, et al., 1994] which had a capacitance resolution of $\Delta C = 8 \cdot 10^{-3}$ pF at 2000 samples/s. Both are excelled by the actual design.

The Ion Probe can be described as current source with an extremely high source resistance R. The cable's capacitance and the input capacitance to the measurement circuit together form with the source resistance a $\tau = RC$ time constant which limits the time response of the electronics. τ depends on the input current as does, *e.g.* the influence of the dielectric absorption of the coax cable. At this work a triaxial cable was used in order to eliminate the cable's influence. This attempt is undertaken for the first time, which makes the comparison with other works valuable.
τ can be extracted from Figs. 3.15 and 3.16. A usual approach is to regard the time until the signal has raised to 90% of its final value as 5τ. Since the internal resistance of the current source used for the calibration measurements is known, one can derive the equivalent values listed in Table 8.1.

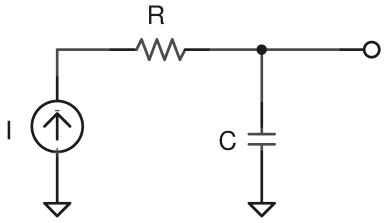

Figure 8.2.: Equivalent circuit of the Ion Probe electronics

current	R	5τ	C
1 pA	$10^{12}\,\Omega$	12 s	2.4 pF
10 pA	$10^{11}\,\Omega$	4 s	0.8 pF

Table 8.1.: Equivalent RC values in dependence of the input current

During the work a few ideas arose of how to further improve the electronics:

Cap Probe
: The output frequency could be prescaled directly instead of scaling after the digital electronics' input. Thereby the signal frequency to be transmitted could be drastically reduced. This would relax the requirements on the line driver.

Ion Probe
: A higher supply voltage would increase the common-mode input range and the output voltage range of the OPAs. Thereby the available range for the probe's bias voltage could be widened.
The ability to measure currents in the pA-range creates many problems, especially the usable measurement time during the in-flight calibrations is drastically reduced.

It needs to be considered if the measurement of such low currents is really necessary. A temperature sensor adjacent to the Ion Probe electronics might help to properly correct the ion current.

Digital

An alternative for future designs could be to implement the counter electronics as done in the actual work, but to realize the processing of the PCM encoder signals using a low-level microprocessor.

The actual realization of the counter electronics reached the limits of discrete CMOS components (*i.e.* the common families LVC, HC, AC and the like). If the counter frequency should be further increased without using a microcontroller or an FPGA one could use the differential low voltage ECL logic family which can handle frequencies in the GHz range.

Bibliography

Andøya Rocket Range (11 August 2009). *Instrument/PCM encoder interface recommendations and data handling*.

Beuth, K. and W. Schmusch (2013). *Elektronik 3. Grundschaltungen*. 17th ed. Würzburg: Vogel Business Media. ISBN: 9783834332868.

Böhmer, E. (2004). *Elemente der angewandten Elektronik*. 14th ed. Wiesbaden: Vieweg. ISBN: 3528010908.

Clapp, J.K. (1948). *An Inductance-Capacitance Oscillator of Unusual Frequency Stability*. *Proceedings of the I.R.E.* Vol. **36**. DOI: 10.1109/JRPROC.1948.233920. URL: www.ieeexplore.ieee.org.

Folkestad, K. (1970). *Ionospheric Studies by in Situ Measurements in Sounding Rockets*. NDRE Report **59**. PhD Thesis. Norwegian Defense Research Establishment.

Friedrich, M. (1979). *A fast, high resolution capacitance probe*. INW 7911. Department of Communication and Wave Propagation. Graz University of Technology.

Friedrich, M. (2012). *Free electrons - the spice of the mesosphere*. Norge 50 år i verdensrommet. PowerPoint presentation. Andenes: Graz University of Technology.

Friedrich, M. (2013). *New Players in the Mesophere. Assessing the Role of Meteoric Dust and Atomic Oxygen*. Application to the Austrian Research Fund. Graz University of Technology.

Friedrich, M. (2014). *The Lower Ionosphere Handbook*. in preparation. Graz University of Technology.

Friedrich, M., W. Boh, and H. Gosch (1994). *Equatorial ionospheric measurements. Part 1, Instrumentation*. INW 9402. Department of Communication and Wave Propagation. Graz University of Technology.

Friedrich, M. and K.M. Torkar (1995). *Equatorial ionospheric measurements. Part III, Preliminary Data*. INW 9501. Department of Communication and Wave Propagation. Graz University of Technology.

Friedrich, M., K.M. Torkar, R.A. Goldberg, J.D. Mitchell, C.L. Croskey, and G. Lehmacher (1997). *Comparison of Plasma Probes in the Lower Ionosphere*. *ESA-SP* **397**, pp. 381–386.

Friedrich, M., K.M. Torkar, S. Robertson, and Shannon Dickson (2013). *Bonus Results from Ion Probes*. *ESA-SP* **721**, pp. 75–80.

Grohe, P. (2011). *Design femtoampere circuits with low leakage, Part 1-3*. Texas Instruments. URL: http://www.edn.com/design/analog/4368681/Design-femtoampere-circuits-with-low-leakage-part-one.

Havnes, O. (2012). *MaxiDusty payload*. PowerPoint presentation. Andenes: Andøya Rocket Range.

Jacobsen, T.A. (1972). *High latitude ionospheric studies by rocket measurements with emphasis on RF-capacitance probes*. MSc Thesis. Intern rapport E-**204**. Norwegian Defense Research Establishment.

Keithley Instruments, Inc. (2004). *Low Level Measurements Handbook. Precision DC Current, Voltage and Resistance Measurements*. sixth edition. URL: http://www.keithley.com/knowledgecenter/knowledgecenter_pdf/LowLevMsHandbk.pdf.

Küpfmüller, K. (1968). *Einführung in die theoretische Elektrotechnik*. Springer.

Murata Manufacturing Co., Ltd. (2010). *Application Manual for Power Supply Noise Suppresion and Decoupling for Digital ICs. C39E*. Application Manual. Version July 2010. Murata Manufactoring Co., Ltd. URL: www.murata.com.

Neubig, B. and W. Briese (1997). *The Crystal Cookbook*. Feldkirchen: Franzis-Verlag. ISBN: 3-7723-5853-5. URL: www.axtal.com/info/buch.html.

Robertson, S., Shannon Dickson, M. Horányi, Z. Sternovsky, M. Friedrich, D. Janches, Linda Megner, and B. Williams (2014). *Detection of meteoric smoke particles in the mesosphere by a rocket-borne mass spectrometer*. *J. Atmos. Solar-Terr. Phys.* in press.

Tarstrup, J. and W. J. Heikkila (1972). *The Impedance Characteristic of a Spherical Probe in an Isotropic Plasma*. *Radio Sci.* **7(4)**, pp. 493–502. DOI: 10.1029/RS007i004p00493.

Texas Instruments Inc. (2013a). *AN-30 Log Convertes. SNOA641B*. Application Report. Version May 2013. Texas Instruments Inc. URL: www.ti.com.

Texas Instruments Inc. (2013b). *AN-311 Theory and Applications of Logarithmic Amplifiers. SNOA575B*. Application Report. Version April 2013. Texas Instruments Inc. URL: www.ti.com.

Tietze, U., C. Schenk, and E. Gamm (2012). *Halbleiter-Schaltungstechnik. 14. Auflage*. Springer. ISBN: 978-3-642-31025-6.

Ulrich, S. and M. Friedrich (1976). *An electrostatic Ion probe and the method to process its data*. INW 7605. Department of Communication and Wave Propagation. Graz University of Technology.

Zinke, O. and H. Brunswig (1999). "Oszillatoren (Schwingungserzeugung)." In: *Hochfrequenztechnik*. Ed. by A. Vlcek, H.L. Hartnagel, and K. Mayer. Springer-Lehrbuch. Springer Berlin Heidelberg. ISBN: 978-3-642-63678-3. DOI: 10.1007/978-3-642-58640-8_4. URL: http://dx.doi.org/10.1007/978-3-642-58640-8_4.

Appendix

Appendix A.

Ion Probe electronics

I_{in} in A	$V_{ideal,LogAmp}$ in V	$V_{out,LogAmp}$ in V @ 25 °C	35 °C	45 °C	50 °C	60 °C
1e-007	-1.05	-1.06	-1.07	-1.07	-1.04	-1.025
1e-008	-0.07768	-0.125	-0.13	-0.13	-0.115	-0.1
1e-009	0.8948	0.775	0.775	0.775	0.785	0.795
1e-010	1.867	1.82	1.805	1.8	1.795	1.78
1e-011	2.84	2.725	2.65	2.595	2.55	2.43
5e-012	3.132	3.09	2.91	2.805	2.72	2.555
4e-012	3.227	3.17	2.97	2.855	2.77	2.58
3e-012	3.348	3.29	3.04	2.9	2.805	2.605
2e-012	3.519	3.47	3.12	2.96	2.855	2.635
1e-012	3.812	3.7	3.23	3.04	2.91	2.67

Table A.1.: HV Ion Probe: measurement results with bias current compensation (LogAmp output voltages), illustrated in Fig. 3.8

I_{in} in A	V_{ideal} in V	V_{out} in V @ 25 °C	35 °C	45 °C	50 °C	60 °C
1e-007	4.95	4.96	4.97	4.97	4.94	4.925
1e-008	3.978	4.025	4.03	4.03	4.015	4
1e-009	3.005	3.125	3.125	3.125	3.115	3.105
1e-010	2.033	2.08	2.095	2.1	2.105	2.12
1e-011	1.06	1.175	1.25	1.305	1.35	1.47
5e-012	0.7676	0.81	0.99	1.095	1.18	1.345
4e-012	0.6734	0.73	0.93	1.045	1.13	1.32
3e-012	0.5519	0.61	0.86	1	1.095	1.295
2e-012	0.3806	0.43	0.78	0.94	1.045	1.265
1e-012	0.08789	0.2	0.67	0.86	0.99	1.23

Table A.2.: HV Ion Probe: measurement results with bias current compensation (final output voltages to PCM encoder), illustrated in Fig. 3.8

I_{in} in A	$V_{ideal,LogAmp}$ in V	$V_{out,LogAmp}$ in V @ 25 °C	35 °C	45 °C	55 °C	60 °C
1e-007	-1.05	-1	-1	-0.98	-0.975	-0.96
1e-008	-0.07768	-0.07	-0.06	-0.055	-0.05	-0.05
1e-009	0.8948	0.83	0.83	0.84	0.845	0.85
1e-010	1.867	1.89	1.88	1.89	1.89	1.91
1e-011	2.84	2.8	2.81	2.82	2.9	3.085
5e-012	3.132	3.11	3.12	3.16	3.34	5.82
4e-012	3.227	3.21	3.22	3.27	3.52	12
3e-012	3.348	3.32	3.35	3.42	3.84	12
2e-012	3.519	3.52	3.54	3.67	5.42	12
1e-012	3.812	3.88	3.92	4.57	12	12

Table A.3.: HV Ion Probe: measurement results without bias current compensation (LogAmp output voltages), illustrated in Fig. 3.9

I_{in} in A	$V_{ideal,LogAmp}$ in V	$V_{out,LogAmp}$ in V @ 25 °C	35 °C	45 °C	50 °C	60 °C
1e-007	-0.9941	-0.97	-0.97	-0.96	-0.95	-0.94
1e-008	-0.02166	-0.02	-0.02	-0.02	-0.01	-0.01
1e-009	0.9508	0.91	0.898	0.897	0.896	0.896
1e-010	1.923	1.903	1.881	1.872	1.864	1.853
1e-011	2.896	2.827	2.789	2.735	2.694	2.635
5e-012	3.188	3.084	3.021	2.945	2.88	2.793
4e-012	3.283	3.161	3.098	3.002	2.933	2.835
3e-012	3.404	3.255	3.18	3.07	2.993	2.881
2e-012	3.575	3.43	3.328	3.18	3.085	2.949
1e-012	3.868	3.615	3.468	3.329	3.174	3.009

Table A.4.: LV Ion Probe: measurement results with bias current compensation (LogAmp output voltages), illustrated in Fig. 3.10

I_{in} in A	V_{ideal} in V	V_{out} in V @ 25 °C	35 °C	45 °C	50 °C	60 °C
1e-007	4.894	4.87	4.87	4.86	4.85	4.84
1e-008	3.922	3.92	3.92	3.92	3.91	3.91
1e-009	2.949	2.99	3.002	3.003	3.004	3.004
1e-010	1.977	1.997	2.019	2.028	2.036	2.047
1e-011	1.004	1.073	1.111	1.165	1.206	1.265
5e-012	0.7116	0.816	0.879	0.955	1.02	1.107
4e-012	0.6173	0.739	0.802	0.898	0.967	1.065
3e-012	0.4958	0.645	0.72	0.83	0.907	1.019
2e-012	0.3246	0.47	0.572	0.72	0.815	0.951
1e-012	0.03187	0.285	0.432	0.571	0.726	0.891

Table A.5.: LV Ion Probe: measurement results with bias current compensation (final output voltages to PCM encoder), illustrated in Fig. 3.10

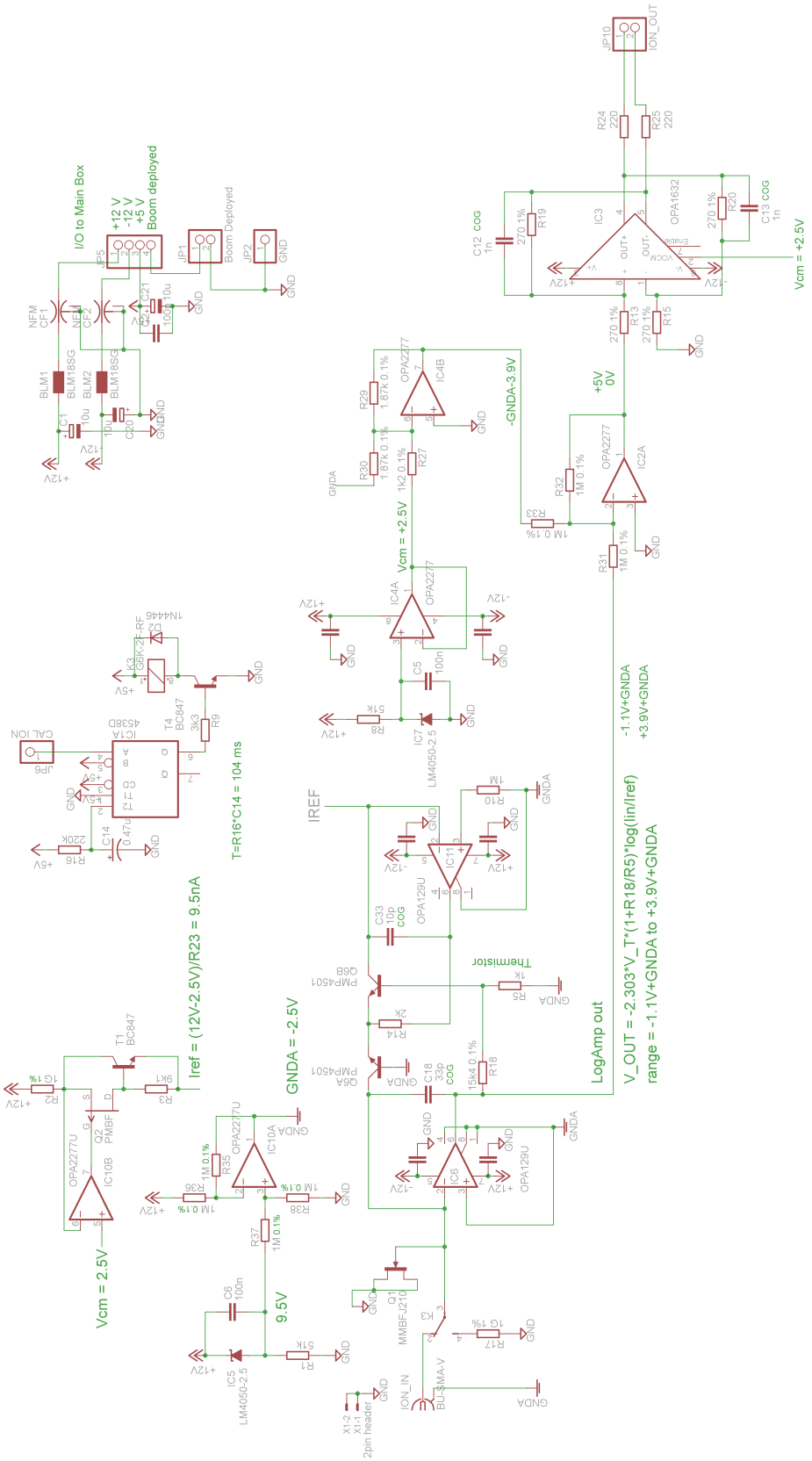

Figure A.1.: Schematic of LV Ion Probe electronics

I_{cal} in A	$V_{ideal,LogAmp}$ in V	$V_{out,LogAmp}$ in V	V_{ideal} in V	V_{out} in V
8.32e-007	-1.945	-1.885	5.845	5.744
8.32e-008	-0.9724	-0.985	4.872	4.861
8.32e-009	-0	-0.02	3.9	3.902
8.32e-010	0.9724	0.94	2.928	2.959
8.32e-011	1.945	1.855	1.955	2.057
8.32e-012	2.917	2.84	0.9827	1.067

Table A.6.: HV Ion Probe: calibration results with decade resistor, illustrated in Fig. 3.12

I_{cal} in A	$V_{ideal,LogAmp}$ in V	$V_{out,LogAmp}$ in V	V_{ideal} in V	V_{out} in V
2.48e-007	-1.378	-1.29	5.278	5.182
2.48e-008	-0.4052	-0.38	4.305	4.285
2.48e-009	0.5672	0.59	3.333	3.328
2.48e-010	1.54	1.513	2.36	2.373
2.48e-011	2.512	2.44	1.388	1.453
2.48e-012	3.485	3.56	0.4155	0.38

Table A.7.: LV Ion Probe: calibration results with decade resistor, illustrated in Fig. 3.13

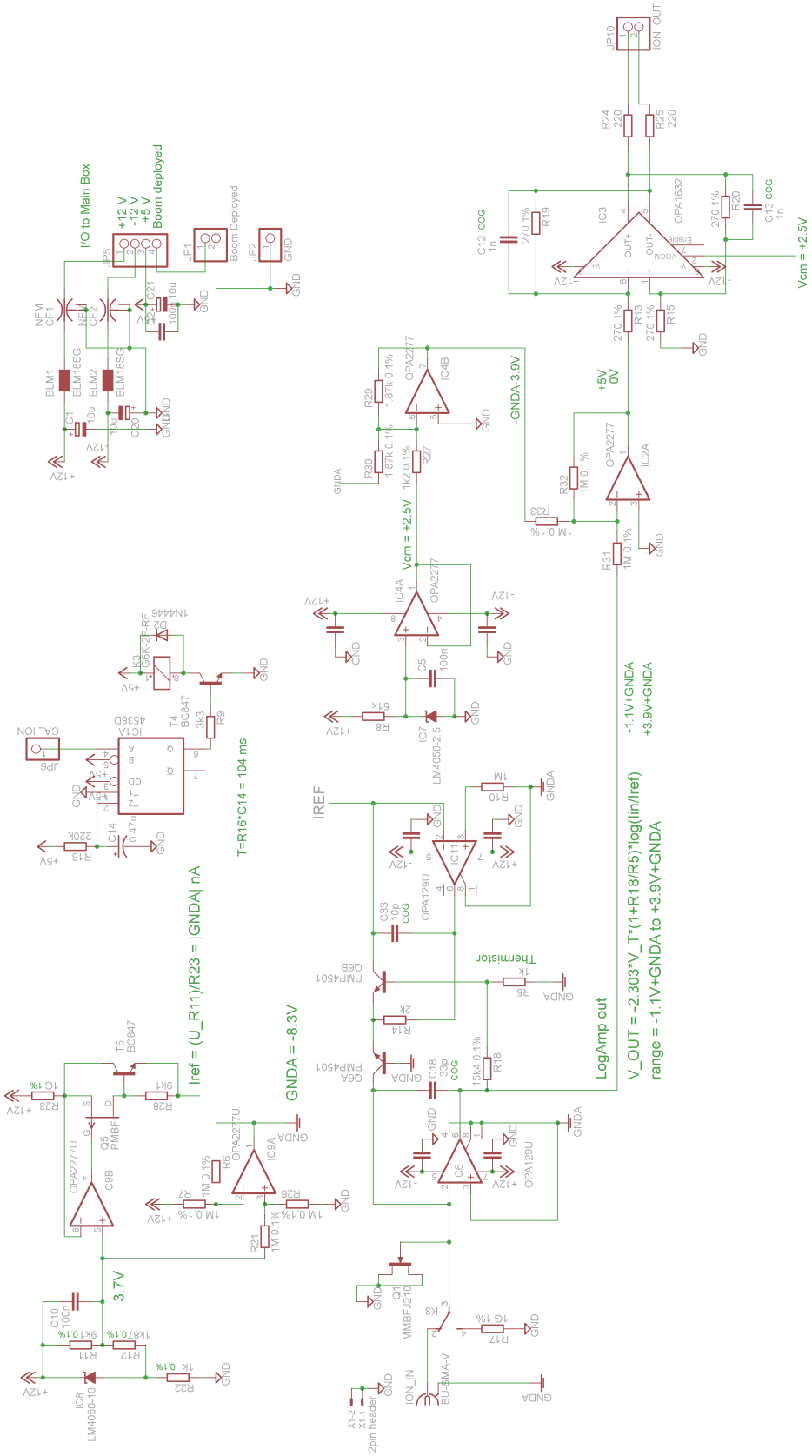

Figure A.2.: Schematic of HV Ion Probe electronics

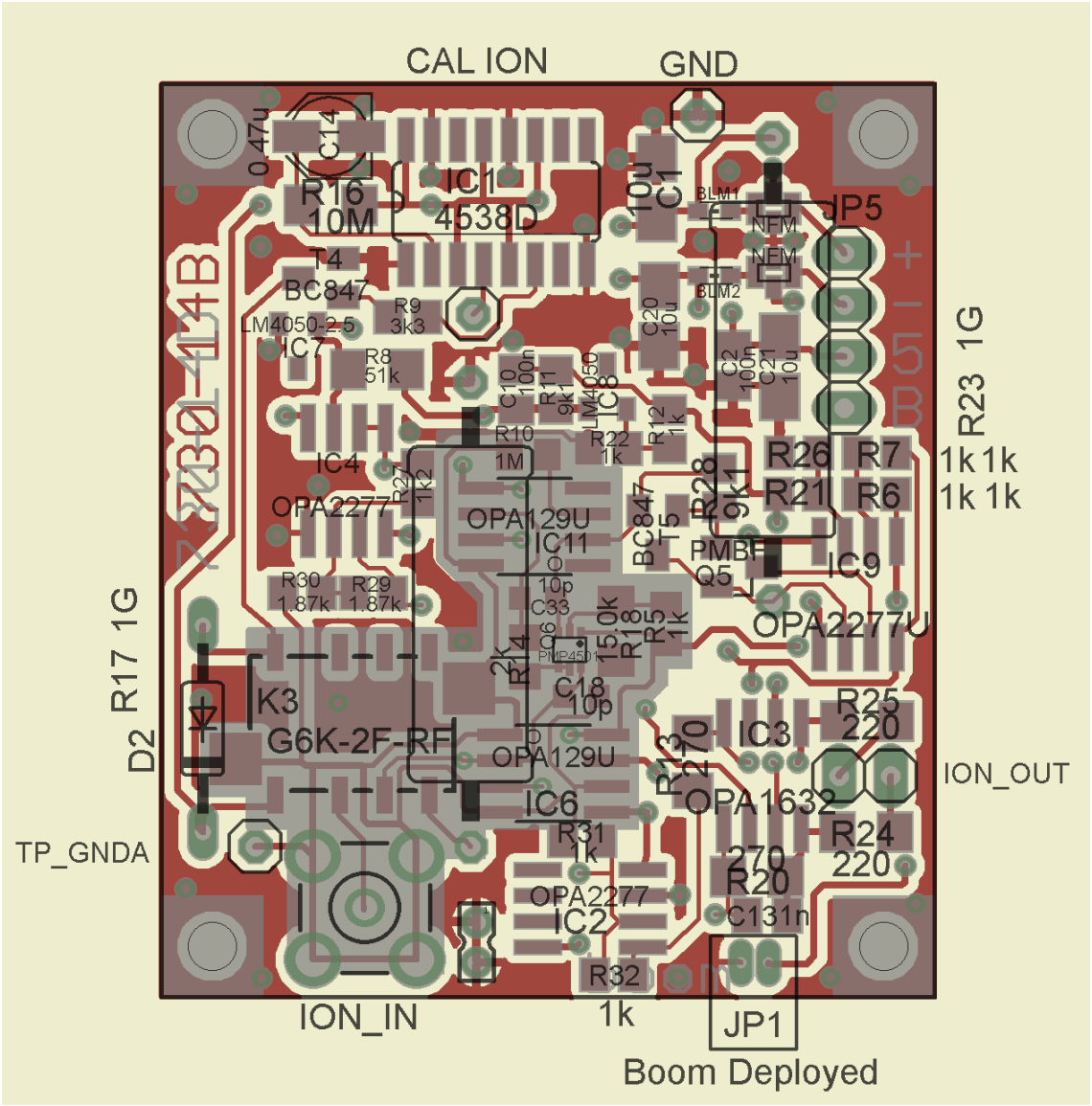

Figure A.3.: PCB Top layer. Note the removed solder mask around the input node.

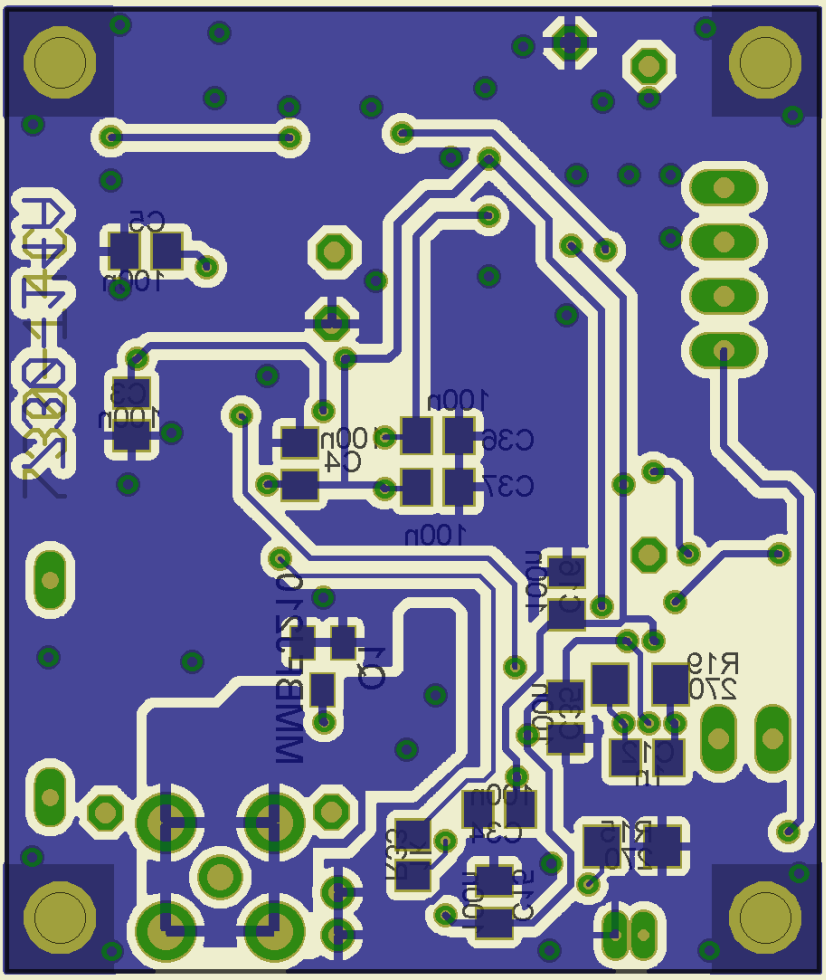

Figure A.4.: PCB Bottom layer. The plane below the input node is at GNDA potential.

Table A.8.: Bill of Materials: HV Ion Probe. Does not include standard resistors (1206, 1%) and standard capacitors (0805/1206, X7R).

Name	Device	Description	Package	pcs./PCB	Order Code		€ / pc.	Sum €
CF1, CF2	NFM18PC104R1C3D	3terminal cap 0.1uF	0603	2	RS	106-044	0,26	0,52
BLM1, BLM2	BLM18SB121	ferrit bead	0603	2	RS	724-1447	0,07	0,15
C1, C20, C21	10u	Tantalum Cap	1206	3	RS	719-0680	2,42	7,26
C12, C13	1n	COG/NPO	0805	2	RS	773-8443	0,30	0,59
C18	33p	COG/NPO	0603	1	RS	698-3958	0,48	0,48
C33	10p	COG/NPO	0603	1	RS	264-4494	0,02	0,02
IC1	MC14538BD	Monoflop	SOIC16	1	RS	518-9489	0,51	0,51
C14	0.47uF Elko	EEEHA1HR47R		1	Farnell	1973357	0,73	0,73
T4, T5	BC847	NPN Transistor	SOT23	2	RS	690-0091	0,11	0,22
K3	G6K-2F-RF	HF Relais	G6K-RF	1	Mouser	653-G6K-2F-RF-DC5	18,18	18,18
D2	BAS45A	Diode	DO35-10	1	RS	508-270	0,19	0,19
IC2, IC4, IC9	OPA2277U	High precision dual OPA	SOIC8	3	RS	661-0723	7,64	22,92
IC7	LM4050AEM3-2.5	voltage reference 2,5V	SOT23	1	RS	534-3071	2,30	2,30
IC8	LM4040AIM3-10.0	voltage reference 10V	SOT23	1	RS	533-8451	1,50	1,50
Q5	PMBFJ174	p-channel JFET	SOT23	1	RS	626-3263	0,36	0,36
R17, R23	1GOhm Resistor	+-1%, -100ppm/K	26,5mm	2	RS	296-0667	9,78	19,56
ION_IN	SMC	socket right angle		1	Farnell	1169656	6,53	6,53
IC6, IC11	OPA129	ultra low input bias current OPA	SOIC8	2	RS	661-0669	6,20	12,40
Q6	PMP4501V	matched NPN pair	SOT666	1	RS	725-8638	0,52	0,52
R5	TFPT0805L1001FV	PTC-Thermistor 1k	0805	1	RS	684-1043	1,38	1,38
IC3	OPA1632	Fully-Diff. Line Driver	SOIC8	1	RS	619-9875	4,41	4,41
X1	2mm Header	right angle	2mm grid	1	RS	767-9583	2,07	2,07
at X1	2mm Plug		2mm grid	1	RS	765-6231	0,97	0,97
JP1	FCI - 10114831	1.25mm 2pole right angle	1.25mm grid	1	Farnell	2100773	0,15	0,15
at JP1	FCI - 10114826	1.25mm Housing	1.25mm grid	1	Farnell	2100709	0,11	0,11
	ABS1626503	Microswitch for Boom		1	RS	698-9918	n.a.	
R18	15k4 0.1%		0805	1	RS	215-3746	1,42	1,42
Q1	MMBFJ210	n-channel JFET						
R29, R30	1k87 0.1%		0805	2	RS	215-2715	1,96	3,92
R27	1k2 0.1%		0805	1	RS	662-0455	0,93	0,93
R6,R7,R21,R26,R31-R33	1M 0.1%		0805	7	RS	565-853	0,64	4,51
							total	**114,82**

Table A.9.: Bill of Materials: LV Ion Probe. Does not include standard resistors (1206, 1%) and standard capacitors (0805/1206, X7R).

Name	Device	Description	Package	pcs./PCB	Order Code		€ / pc.	Sum €
CF1, CF2	NFM18PC104R1C3D	3terminal cap 0.1uF	0603	2	RS	106-044	0,26	0,52
BLM1, BLM2	BLM18SB121	ferrit bead	0603	2	RS	724-1447	0,07	0,15
C1, C20, C21	10u	Tatalum Cap	1206	3	RS	719-0680	2,42	7,26
C12, C13	1n	COG/NPO	0805	2	RS	773-8443	0,30	0,59
C18	33p	COG/NPO	0603	1	RS	698-3958	0,48	0,48
C33	10p	COG/NPO	0603	1	RS	264-4494	0,02	0,02
IC1	MC14538BD	Monoflop	SOIC16	1	RS	518-9489	0,51	0,51
C14	0.47uF Elko	EEEHA1HR47R		1	Farnell	1973357	0,73	0,73
T1, T5	BC847	NPN Transistor	SOT23	2	RS	690-0091	0,11	0,22
K3	G6K-2F-RF	HF Relais	G6K-RF	1	Mouser	653-G6K-2F-RF-DC5	18,18	18,18
D2	BAS45A	Diode	DO35-10	1	RS	508-270	0,19	0,19
IC2, IC4, IC10	OPA2277U	High precision dual OPA	SOIC8	3	RS	661-0723	7,64	22,92
IC5, IC7	LM4050AEM3-2.5	voltage reference 2,5V	SOT23	2	RS	534-3071	2,30	4,60
Q2	PMBFJ174	p-channel JFET	SOT23	1	RS	626-3263	0,36	0,36
R17, R2	1GOhm Resistor	+-1%, -100ppm/K	26,5mm	2	RS	296-0667	9,78	19,56
ION_IN	SMC	socket right angle		1	Farnell	1169656	6,53	6,53
IC6, IC11	OPA129	ultra low input bias current OPA	SOIC8	2	RS	661-0669	6,20	12,40
Q6	PMP4501V	matched NPN pair (statt LM394)	SOT666	1	RS	725-8638	0,52	0,52
R5	TFPT0805L1001FV	PTC-Thermistor 1k	0805	1	RS	684-1043	1,38	1,38
IC3	OPA1632	Fully-Diff. Line Driver	SOIC8	1	RS	619-9875	4,41	4,41
X1	2mm Header right angle		2mm grid	1	RS	767-9583	2,07	2,07
at X1	2mm Plug		2mm grid	1	RS	765-6231	0,97	0,97
JP1	FCI - 10114831	1.25mm 2pole right angle	1.25mm grid	1	Farnell	2100773	0,15	0,15
at JP1	FCI - 10114826	1.25mm Housing	1.25mm grid	1	Farnell	2100709	0,11	0,11
	ABS1626503	Microswitch for Boom		1	RS	698-9918	n.a.	
R18	15k4 0.1%		0805	1	RS	215-3746	1,42	1,42
Q1	MMBFJ210	n-channel JFET						
R29, R30	1k87 0.1%		0805	2	RS	215-2715	1,96	3,92
R27	1k2 0.1%		0805	1	RS	662-0455	0,93	0,93
R31-R33,R35-R38	1M 0.1%		0805	7	RS	565-853	0,64	4,51
							total	**115,62**

Appendix B.

Cap Probe electronics

clearance $d - r_0$ in mm	C in pF	ΔC in pF	f in kHz	f^{-2} in kHz^{-2}
2	5.52435	3.02435	224.913	19.7684
3	5.08543	2.58543	224.986	19.7555
4	4.78747	2.28747	225.03	19.7478
5	4.56548	2.06548	225.062	19.7422
10	3.93906	1.43906	225.134	19.7296
15	3.62568	1.12568	225.17	19.7233
20	3.43041	0.93041	225.191	19.7196
25	3.29519	0.79519	225.207	19.7168
30	3.19539	0.69539	225.215	19.7154
50	2.96534	0.46534	225.238	19.7114
70	2.85081	0.35081	225.254	19.7086
100	2.75682	0.25682	225.257	19.708
150	2.67817	0.17817	225.261	19.7073

Table B.1.: LF Cap Probe: calibration data, illustrated in Fig. 4.9

clearance $d - r_0$ in mm	C in pF	ΔC in pF	f in MHz	f^{-2} in MHz^{-2}
2	5.52435	3.02435	7.9175	0.0159523
3	5.08543	2.58543	7.9336	0.0158876
4	4.78747	2.28747	7.9442	0.0158453
5	4.56548	2.06548	7.9516	0.0158158
10	3.93906	1.43906	7.9715	0.0157369
15	3.62568	1.12568	7.9809	0.0156999
20	3.43041	0.93041	7.9866	0.0156775
25	3.29519	0.79519	7.9904	0.0156626
30	3.19539	0.69539	7.9931	0.015652
50	2.96534	0.46534	7.9976	0.0156344
70	2.85081	0.35081	8.0009	0.0156215
100	2.75682	0.25682	8.0029	0.0156137
150	2.67817	0.17817	8.0048	0.0156063

Table B.2.: HF Cap Probe: calibration data, illustrated in Fig. 4.8

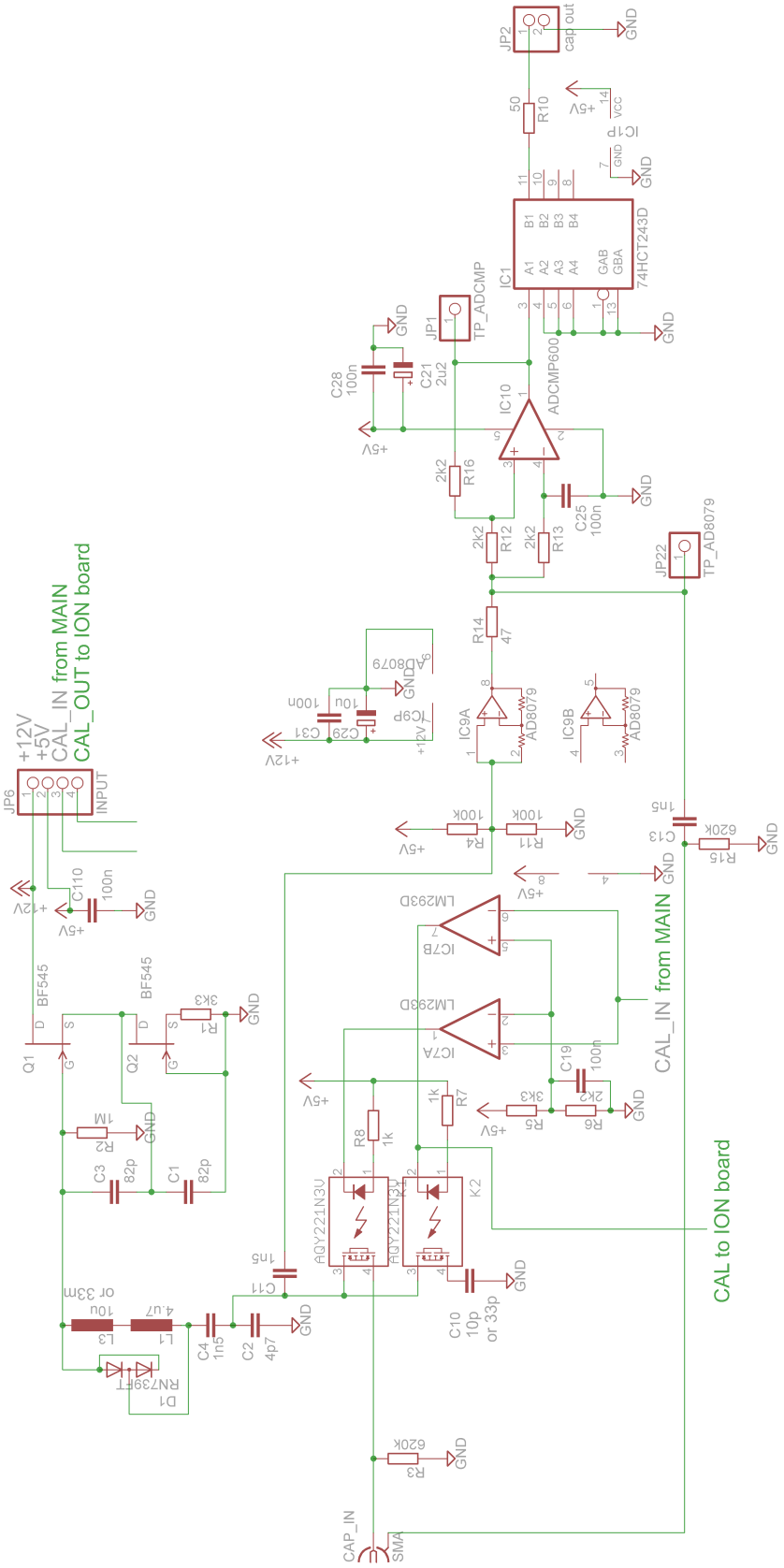

Figure B.1.: Schematic of Cap Probe electronics

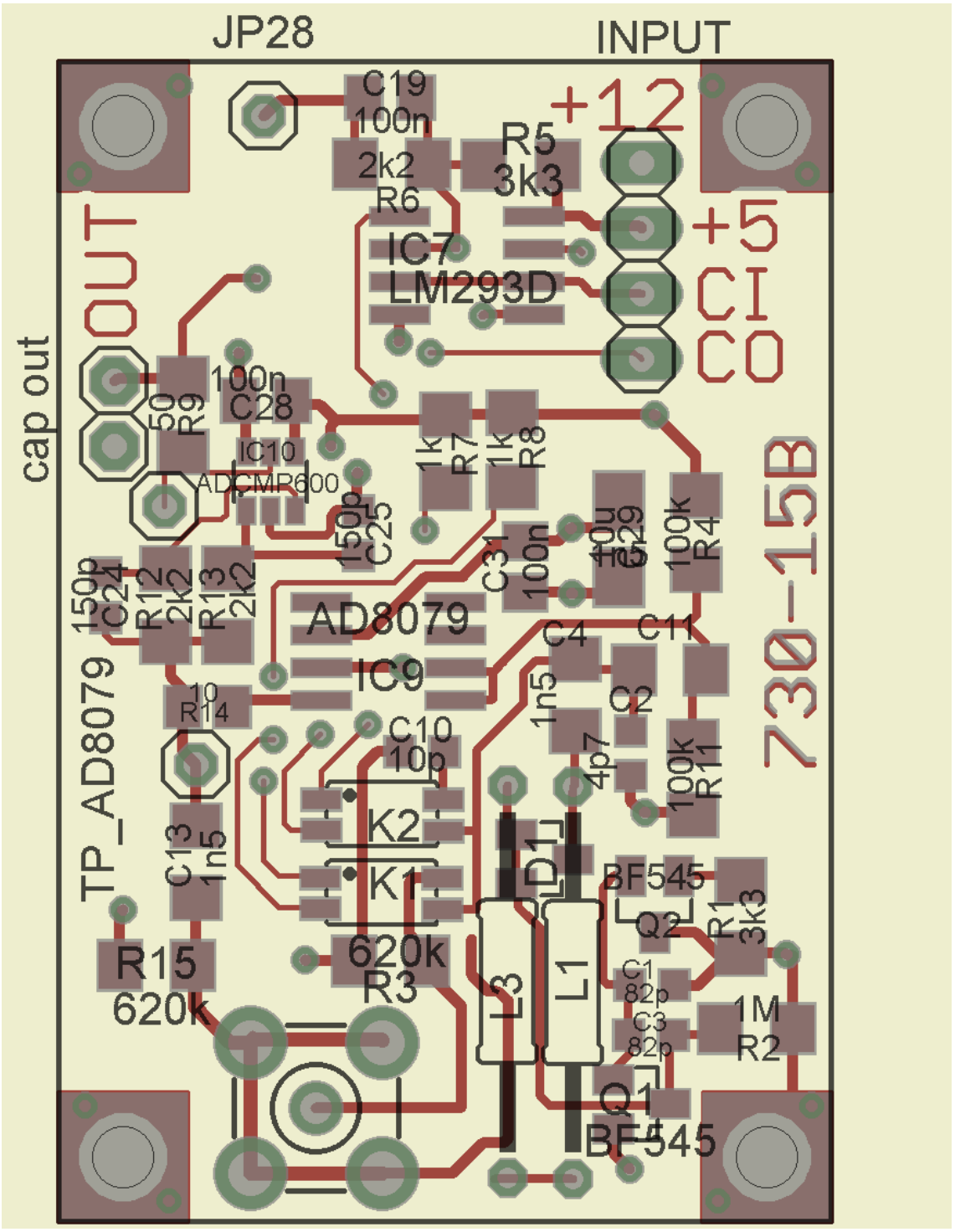

Figure B.2.: PCB Top layer. The series of L1 and L3 results in L2.

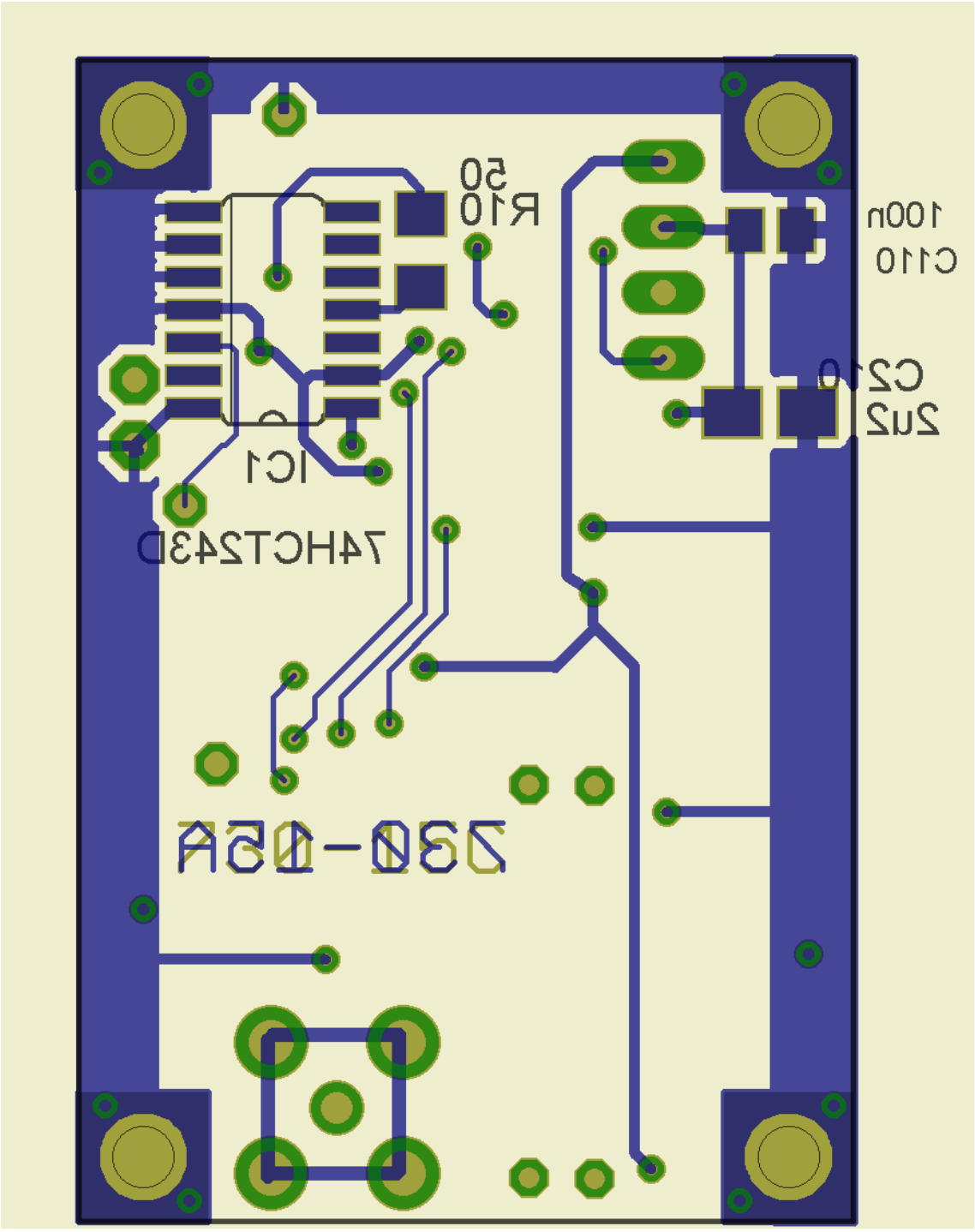

Figure B.3.: PCB Bottom layer. No ground plane in order to reduce stray capacitance.

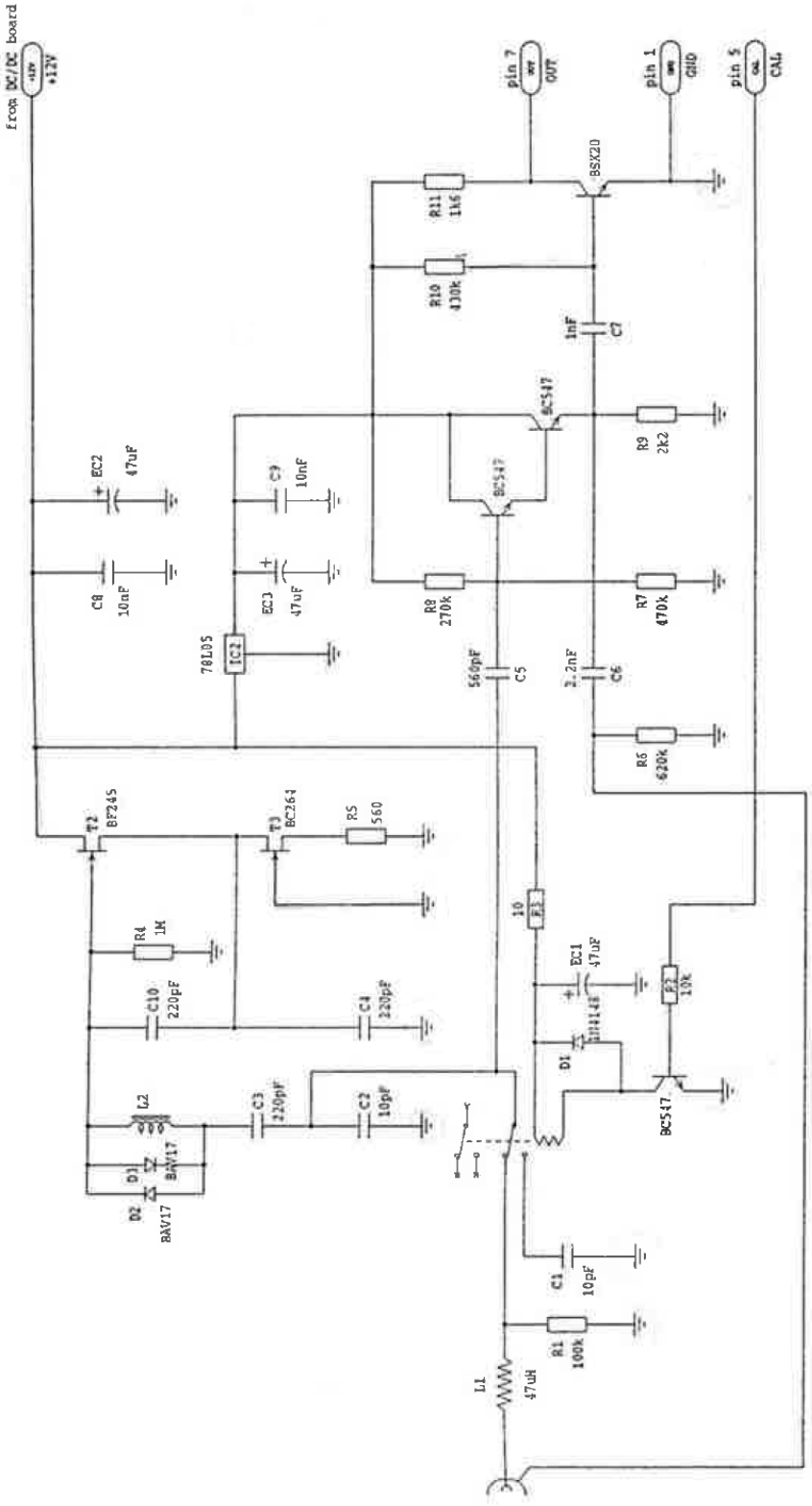

Figure B.4.: Cap Probe electronics from [Friedrich, Boh, et al., 1994]

Name	Device	Description	Package	pcs./PCB	Order Code		€ / pc.	Sum €
C1,C3	82p	COG/NPO	0805	2	RS	788-0465	0,62	1,23
C4, C11, C13	1n5	COG/NPO	1206	3	RS	393-7494	0,43	1,28
C2	4p7	COG/NPO	0805	1	RS	788-0402	0,44	0,44
C10	10p	COG/NPO	0805	1	RS	264-4494	0,02	0,02
Q1, Q2	BF545B	n-channel JFET	SOT23	2	RS	626-2333	0,50	0,99
L1	4u7	ferrite core inductor	4mm grid	1/0	Farnell	1644259	0,11	0,11
L3 (HF)	10u	ferrite core inductor	4mm grid	1/0	Farnell	515565	0,84	0,84
L3 (LF)	13R336C	33mH radial lead inductor	5mm grid	0/1	Farnell	2062712	0,71	0,71
D1	RN739F	PIN Diode	SOT323	1	RS	700-2621	0,28	0,28
K1, K2	AQY221N3V	low capacitance photomos relais	SSOP	2	RS	699-6607	9,58	19,16
CAP_IN	SMA	socket right angle		1	RS	783-9647	1,21	1,21
IC7	LM293AD	Komparator	SOIC8	1	Farnell	8389225	0,31	0,31
IC9	AD8079ARZ	260MHz Buffer	SOIC8	1	Farnell	1838858	10,33	10,33
IC10	ADCMP600	high speed comparator	SOT23-5	1	RS	697-7543	4,41	4,41
IC1	74HCT243D	line transceiver	SOIC14	1	RS	663-0559	0,80	0,80
C29	10u	Tantalum Cap	1206	1	RS	719-0680	1,21	1,21
C21	2u2	Tantalum Cap	3216-18	1	RS	648-0660	0,19	0,19
							total	**43,54**

Table B.3.: Bill of Materials for LF or HF Cap Probe circuit. Does not include standard resistors (1206, 1%) and standard capacitors (0805/1206, X7R).

Appendix C.

Digital counter electronics

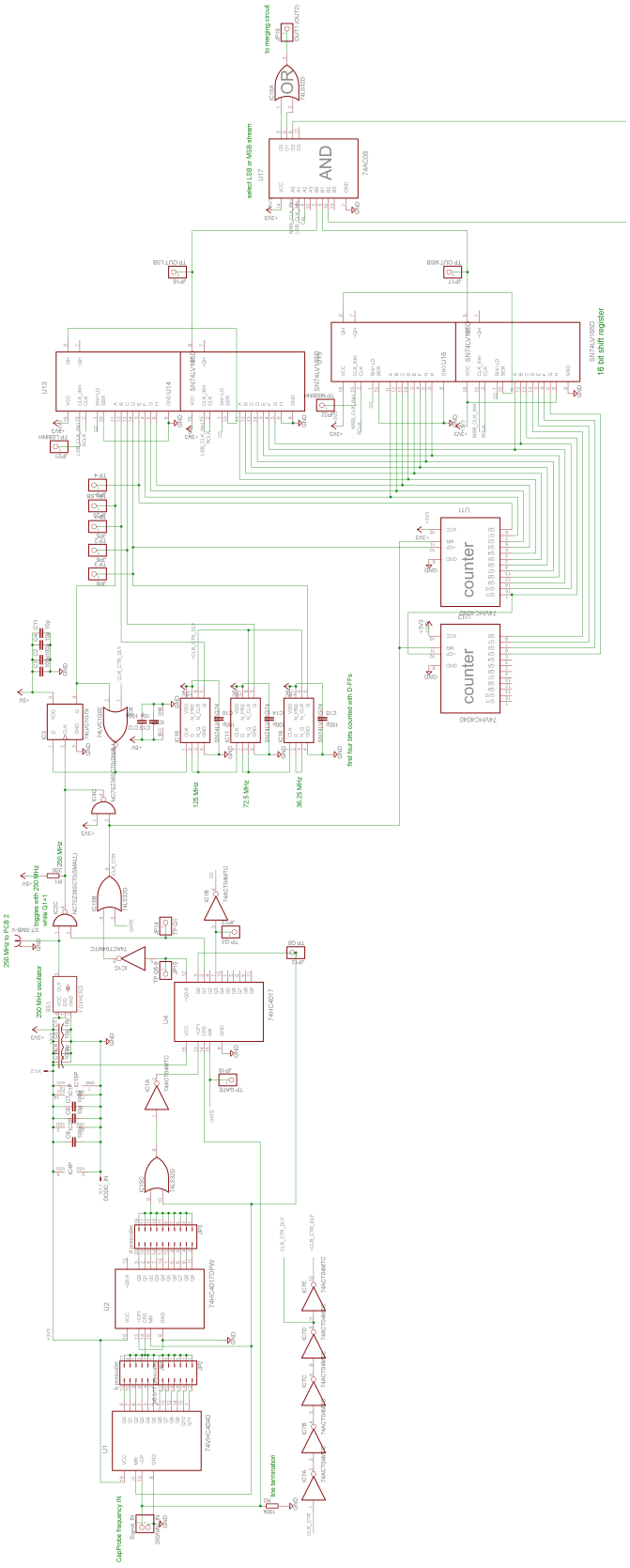

Figure C.1.: Schematic of Digital counter electronics: prescaler and counter

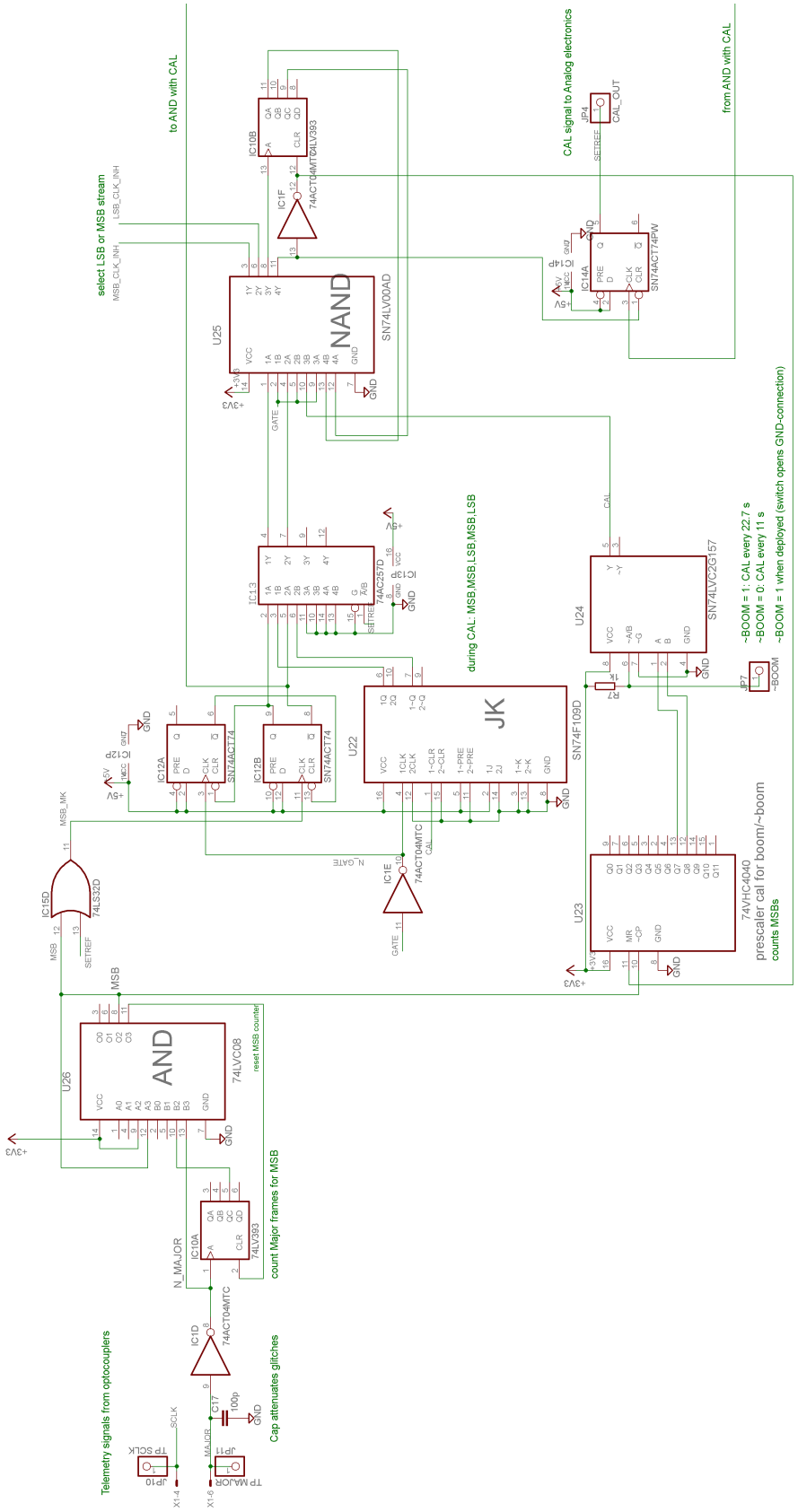

Figure C.2.: Schematic of Digital counter electronics: control signal processing

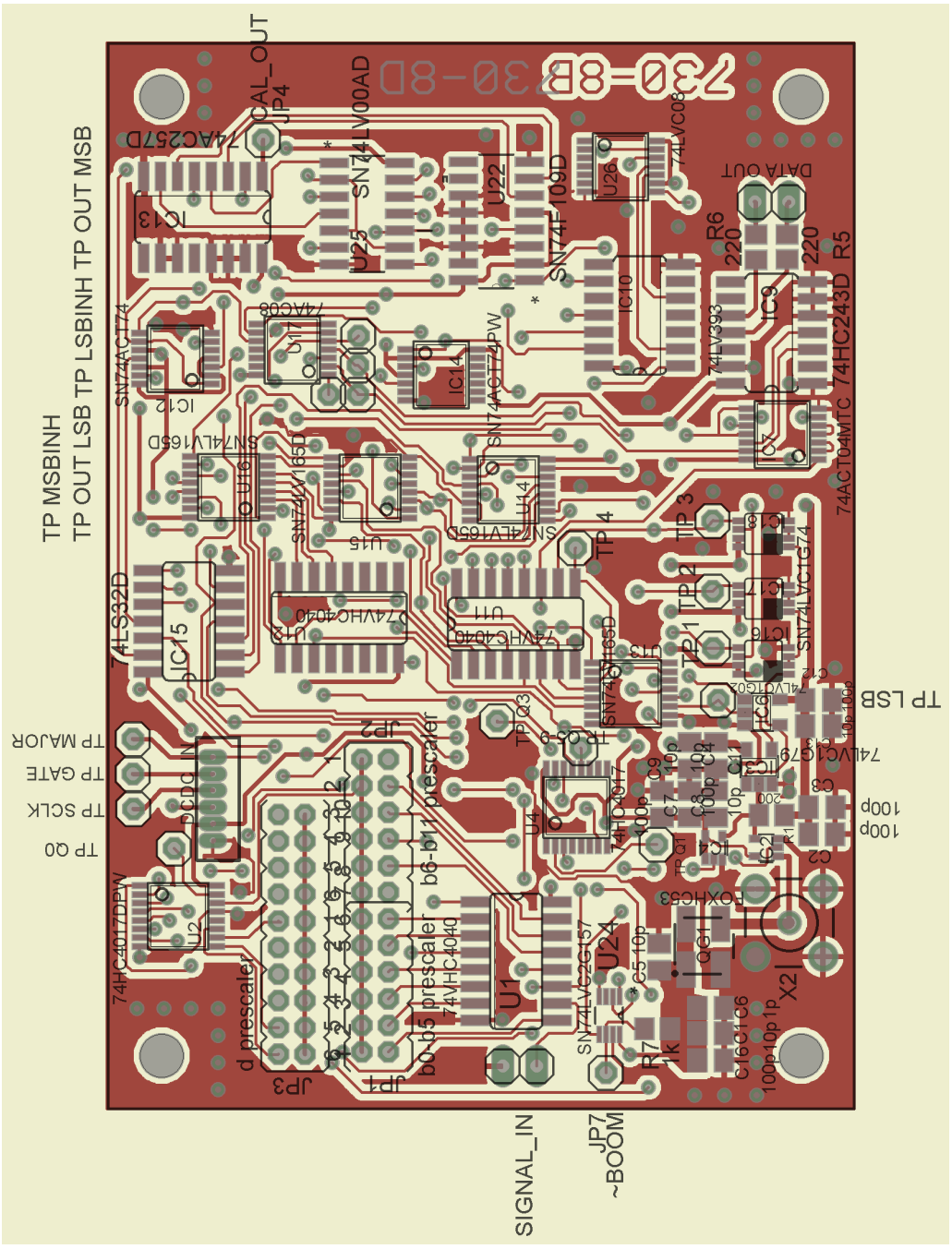

Figure C.3.: PCB Top layer

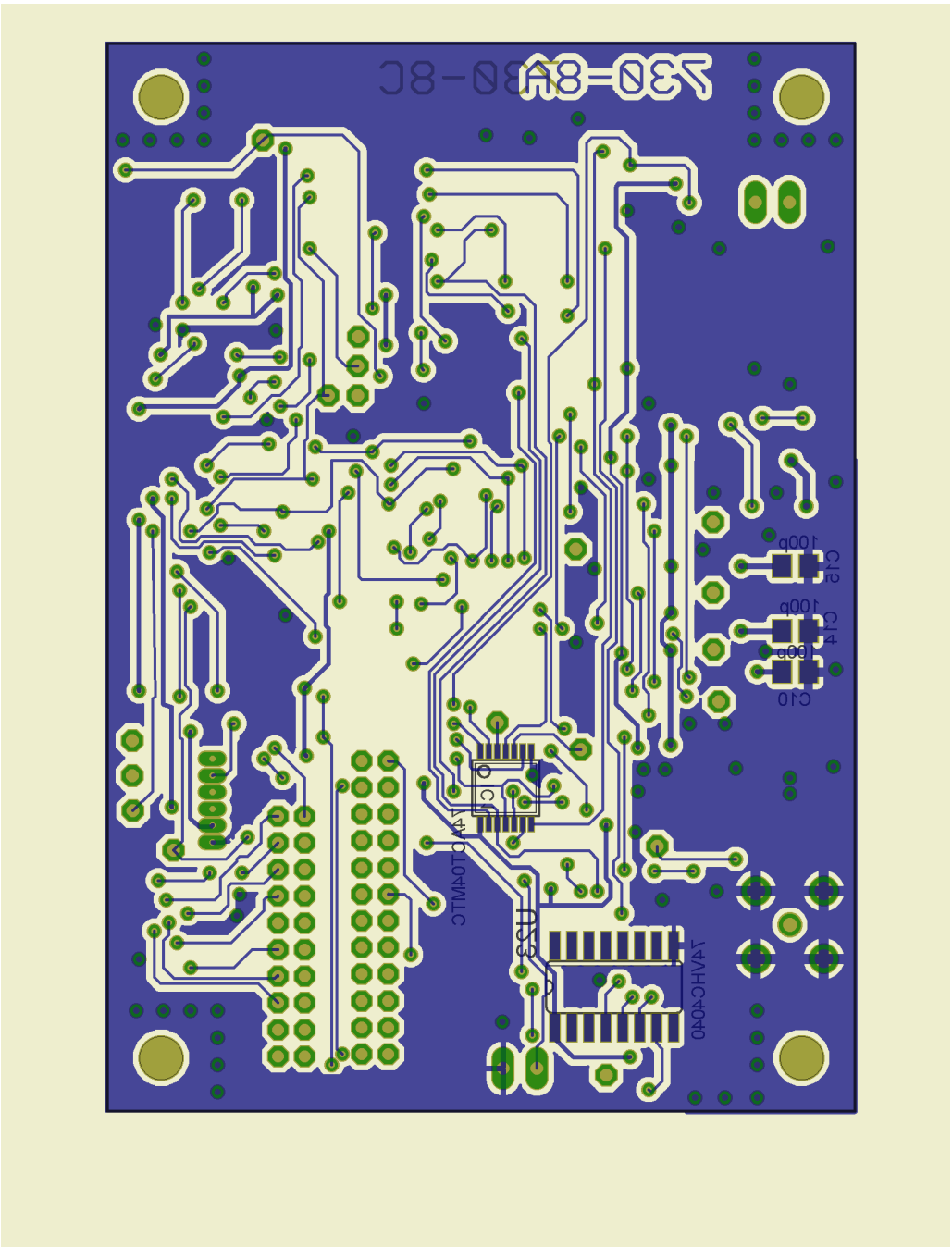

Figure C.4.: PCB Bottom layer

Name	Device	Description	Package	pcs./PCB	Order Code		€ / pc.	Sum €
IC1, IC7	74ACT04	hex Inverter	TSSOP	2	RS	663-1023	0,31	0,62
IC10	74LV393	dual 4bit counter	SOIC	1	RS	663-2757	0,53	0,53
IC12, IC14	SN74ACT74PW	dual D-FF	TSSOP	2	RS	662-7632	0,19	0,38
U1, U11, U12, U23	74VHC4040M	12Bit binary counter	SOIC	4	Farnell	1607651	0,83	3,30
U13-16	74LV165	shift register	TSSOP	4	RS	663-2717	0,43	1,70
U17, U26	74LVC08	quad2input AND	TSSOP	2	RS	662-8588	0,12	0,24
U2, U4	CD74HC4017PW	decade counter	TSSOP	2	RS	662-7128	0,58	1,16
U22	74ACT109M	JK FF	SOIC	1	Farnell	1752828	0,54	0,54
U24	SN74LVC2G157DCUR	Multiplexer	VSSOP	1	Farnell	2114109	0,56	0,56
U25	74LV00	quad NAND	SOIC	1	Farnell	1287598	0,19	0,19
IC15	SN74LVC32ADBR	quad OR	SSOP	1	RS	662-8991	0,14	0,14
IC3	SN74LVC1G79DBVT	250MHz D FlipFlop	SOT23	1	RS	662-8796	0,56	0,56
IC16, IC17, IC18	SN74LVC1G74DCTR	200MHz D FlipFlop with Reset	SSOP-8	3	Farnell	2120448	0,44	1,32
IC6	SN74LVC1G02DBV	single NOR	SOT23	1	RS	662-8673	0,53	0,53
IC2, IC4	NC7SZ38P5X	Open Drain NAND	SOT23	2	Farnell	2144406	0,12	0,24
QG1	FXO-HC536R-250	250MHz HCMOS Oscillator		1	RS	672-1371	14,72	14,72
IC13	CD74AC257M	data selector for cal	SOIC	1	RS	662-9806	0,66	0,66
X1	6 pin micro connector	wire to board conn. PCB	1.25mm grid	1	RS	279-9291	0,54	0,54
to X1	6 pin micro connector	receptacle	1.25mm grid	1	RS	279-9178	0,29	0,29
to X1		crimped lead		1	RS	279-9544	0,72	0,72
X2	SMB	straight PCB socket		0/1	RS	193-8855	10,43	10,43
to X2	SMB	straight PCB plug		1/0	Farnell	1206013	2,17	2,17
							total	41,55

Table C.1.: Bill of Materials for *one* Digital Counter circuit. Does not include standard resistors (1206, 1%) and capacitors.

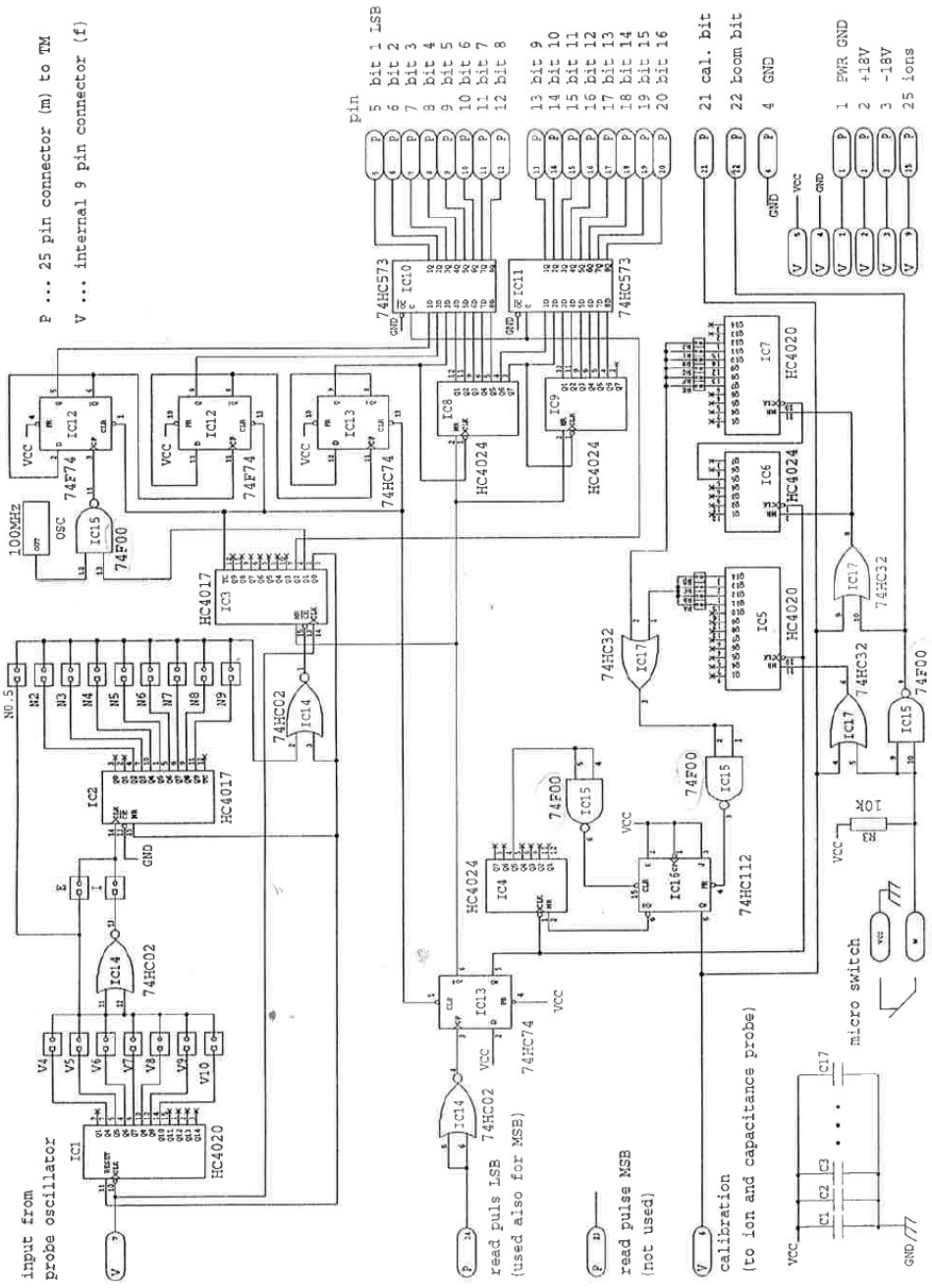

Figure C.5.: Digital counter electronics from [Friedrich, Boh, et al., 1994]

Appendix D.

DC/DC electronics

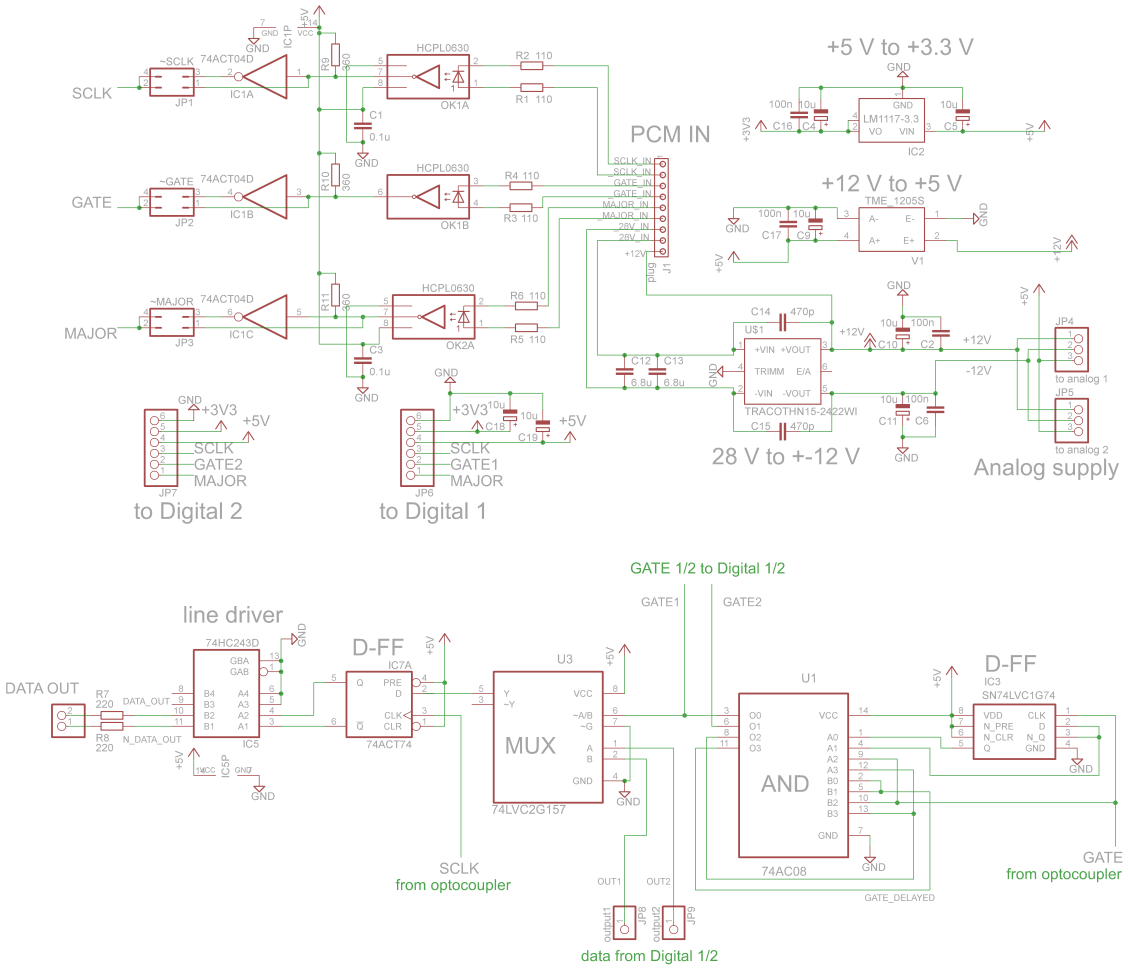

Figure D.1.: Complete schematic of DC/DC board

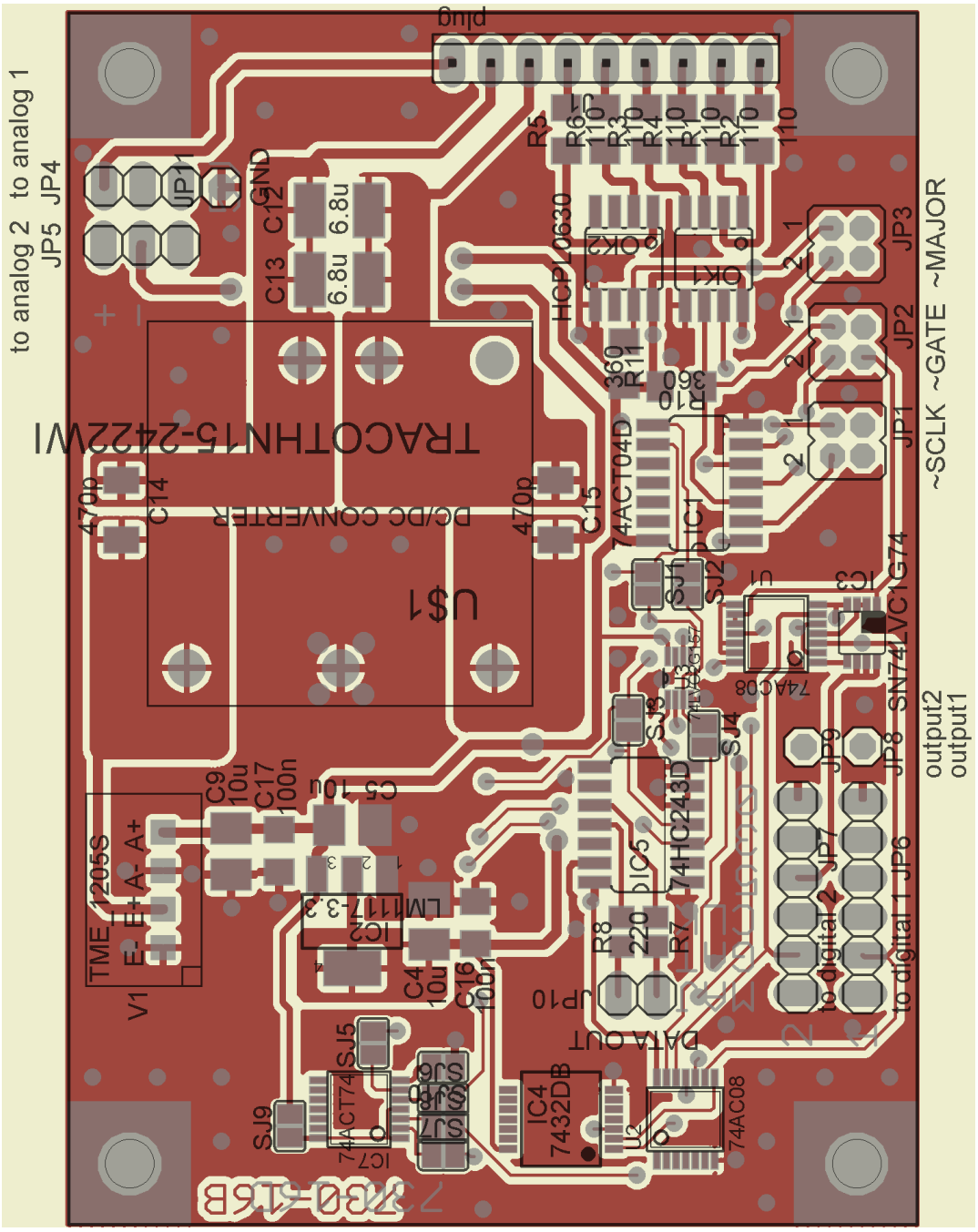

Figure D.2.: PCB Top layer

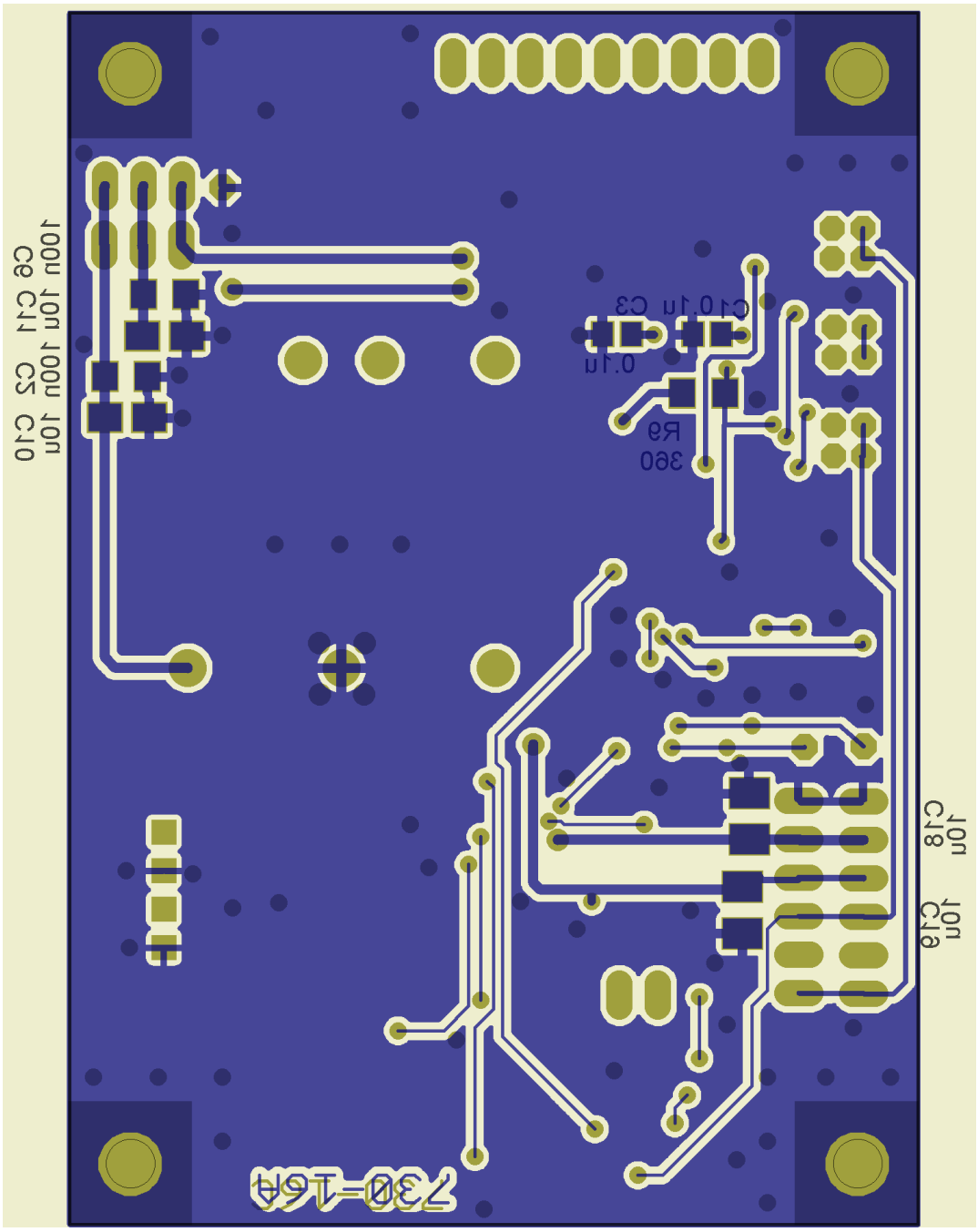

Figure D.3.: PCB Bottom layer

Name	Device	Description	Package	pcs./PCB	Order Code		€ / pc.	Sum €
US1	Traco THN15-2422WI	+-12V DC/DC +-625mA		1	Farnell	2080701	40,70	40,70
V1	TME 1205S	5V DC/DC 200mA		1	RS	189-6953	4,30	4,30
IC2	LM1117IMP	linear regulator 3V3	SOT223	1	Farnell	1469051	1,21	1,21
OK1, OK2	HCPL0630	dual optocoupler	SOIC8	2	RS	547-4046	3,90	7,80
IC1	74ACT04D	Hex Inverter	SOIC14	1	RS	663-1029	0,22	0,22
IC3	SN74LVC1G74DCTR	D-flip flop with Reset	SSOP-8	1	Farnell	2120448	0,44	0,44
IC5	74HCT243D	line transceiver	SOIC14	1	RS	663-0559	0,80	0,80
IC7	SN74ACT74PW	dual D-flip flop	TSSOP	1	RS	662-7632	0,19	0,19
U1	74AC08	quad2input AND	TSSOP	1	RS	662-7553	0,17	0,17
U3	SN74LVC2G157	Multiplexer	SSOP-8	1	RS	662-8941	0,42	0,42
C12, C13	6u8	50V MLCC	1812	2	Farnell	1843170	1,40	2,80
C14, C15	470p	2kV MLCC	1808	2	Farnell	1886065	n.a.	
C4,C5,C9-C11,C18,C19	10uF	Tantalum Cap	1206	7	RS	719-0680	1,21	8,47
C1-C3,C6,C16,C17	100n	X7R 0805	0805	6	RS	264-4416	0,03	0,20
JP1-JP3		jumper row 2mm		1	RS	701-9907	1,43	1,43
							total	**69,16**

Table D.1.: Bill of Materials for DC/DC board.

Name	Device	Description	pcs.	Order Code		€ / pc.	Sum €
Main/Analog	7W2 connector female	D-Sub Mixed Layout connector	4	RS	120-7583	3,03	12,12
Main/Analog	7W2 connector male	D-Sub Mixed Layout connector	4	RS	120-7582	2,38	9,52
Main/Analog	7W2 connector female	female coaxial contact	8	Farnell	1200481	5,77	46,16
Main/Analog	7W2 connector male	male coaxial contact	8	Farnell	1200482	5,36	42,88
Main/Encoder	15 pin D-Sub connector	housing female	1	Farnell	1345254	1,38	1,38
Main/Encoder	15 pin D-Sub connector	housing male	1	Farnell	1345151	1,04	0,11
Main/Encoder	15 pin D-Sub pin	crimp pin contact male	15	Farnell	1098472	0,19	0,84
Main/Encoder	15 pin D-Sub pin	crimp pin contact female	15	Farnell	1098424	0,16	0,71
screwlock	M3 screwlock female	for connector mounting	10	Farnell	4218061	0,92	9,24
Coax (+Triax)	MRG316.0125	RG316/U coaxial cable	8 m	Farnell	142332	91,26 (25m)	29,20
SMC Ion Probe	RG316/SMC connector	SMC right angle plug, solder pin	2	Farnell	1169654	9,00	18,00
SMA Cap Probe	RG316/SMA connector	SMA straight plug, solder pin	2	Farnell	1056357	4,11	8,22
Analog 1, 2	Analog Box		2				
Main	Main Box		1				
						total	**178,39**

Table D.2.: Bill of Materials for the connection between the boxes. Does not include box screwing and distance pieces.

Appendix E.

Drawings of Main Box and Analog Box

Main Box

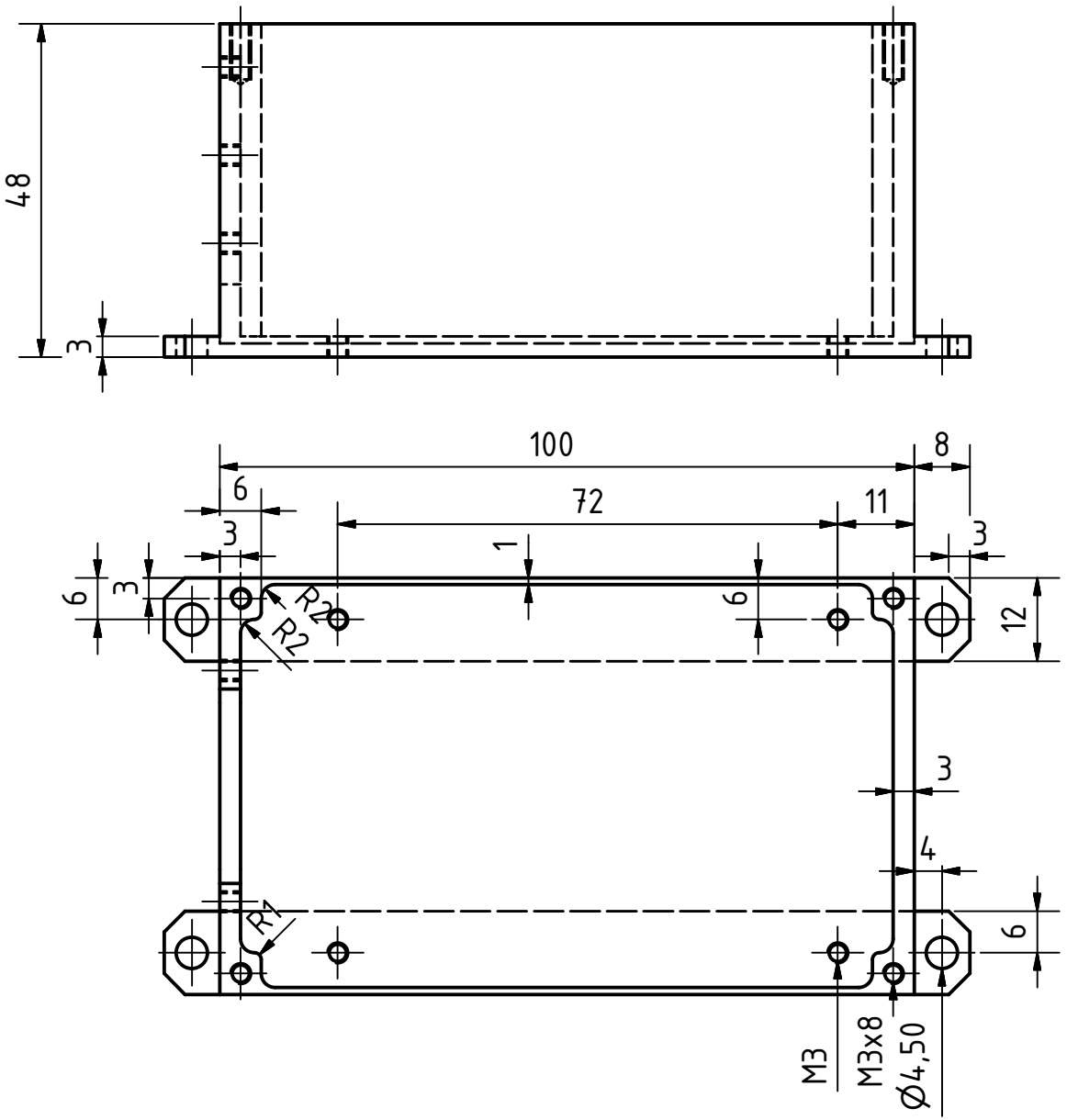
48
3
100
8
6
72
11
3
1
3
6
3
R2
R2
6
12
3
4
R7
6
M3
M3x8
Ø4,50

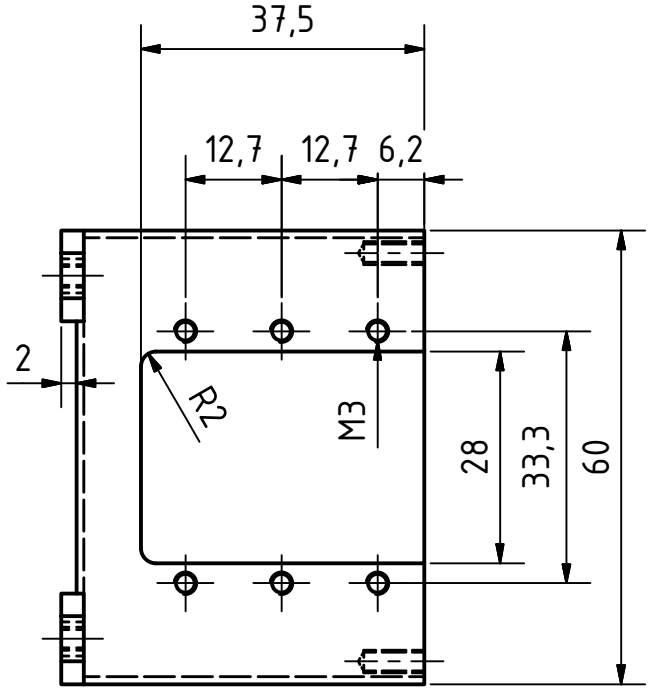
37,5
12,7
12,7
6,2
2
R2
M3
28
33,3
60

A-A (1 : 1)

to encoder

to Analog 2

to Analog 1

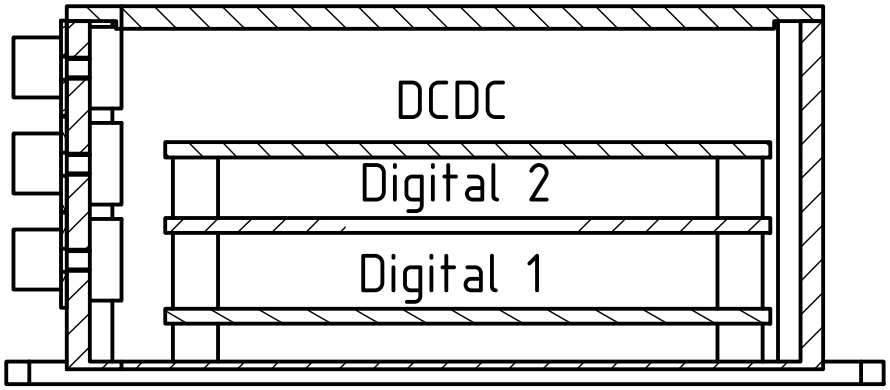

Main Box assembly

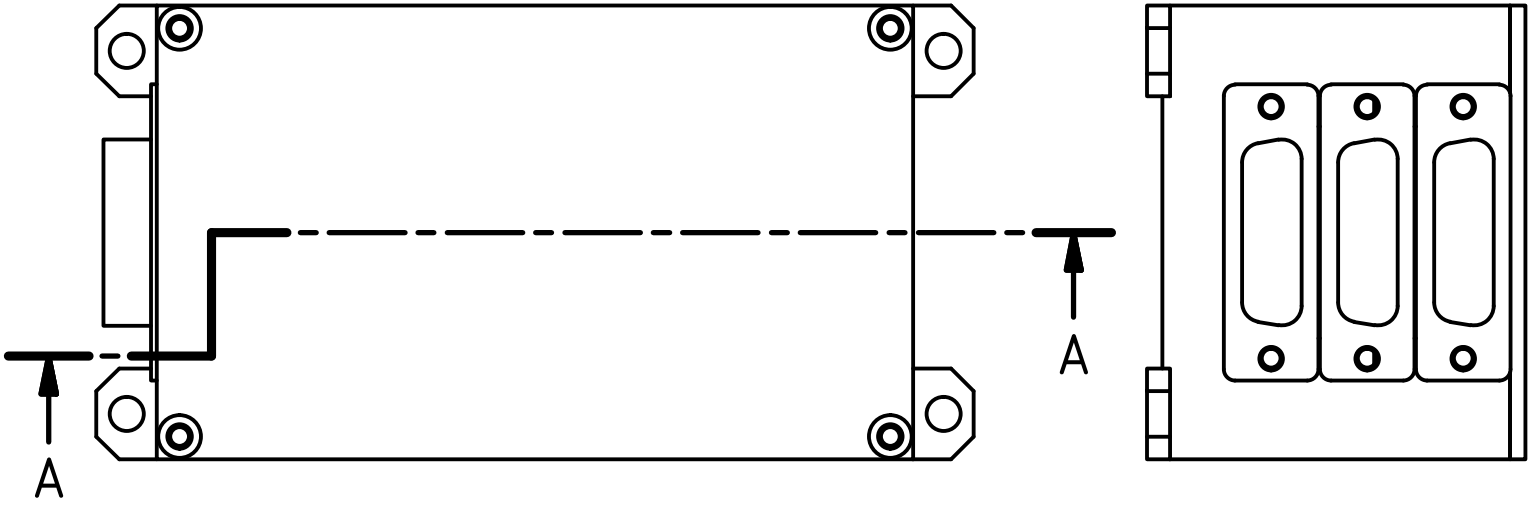

Analog Box

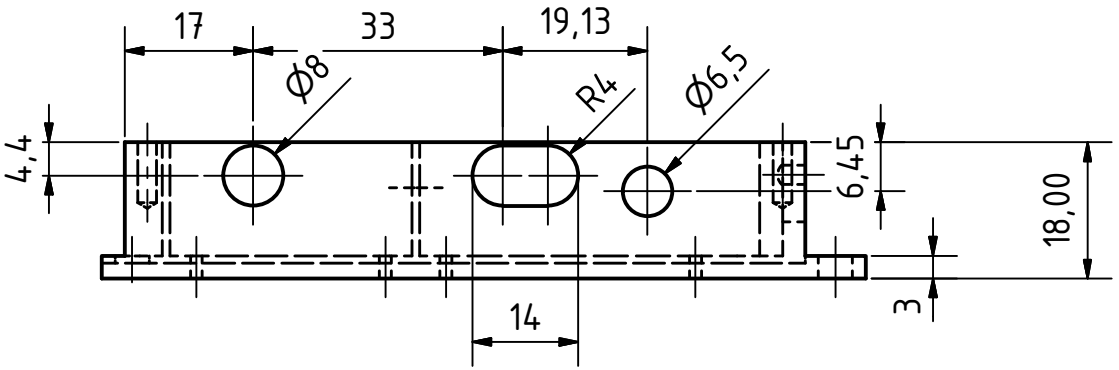

A-A (1 : 1)

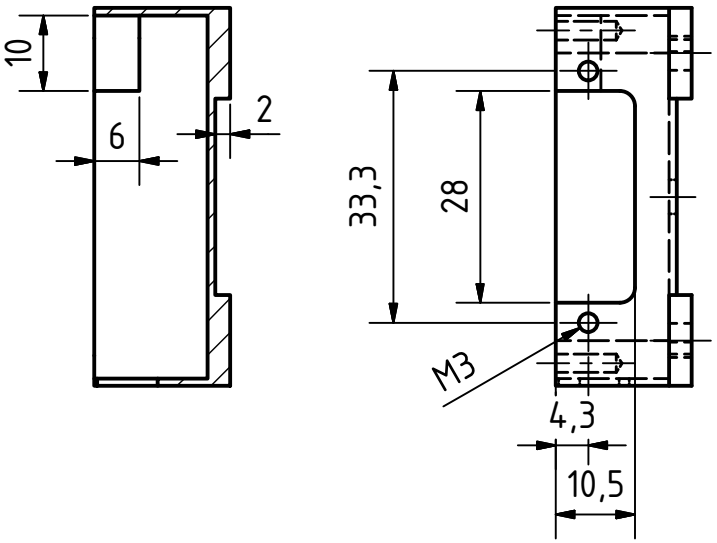

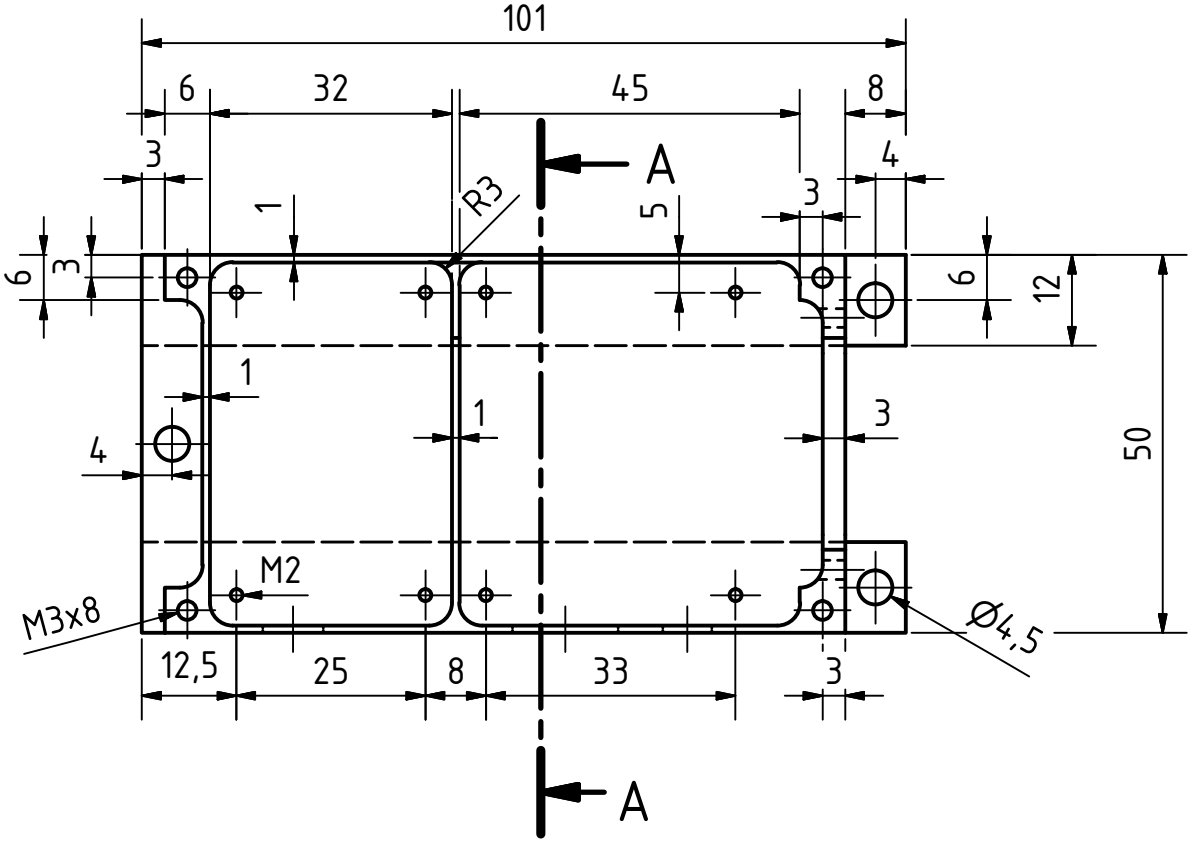

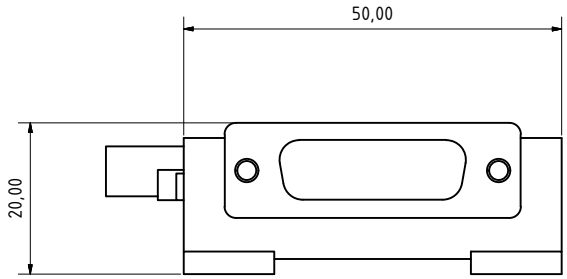

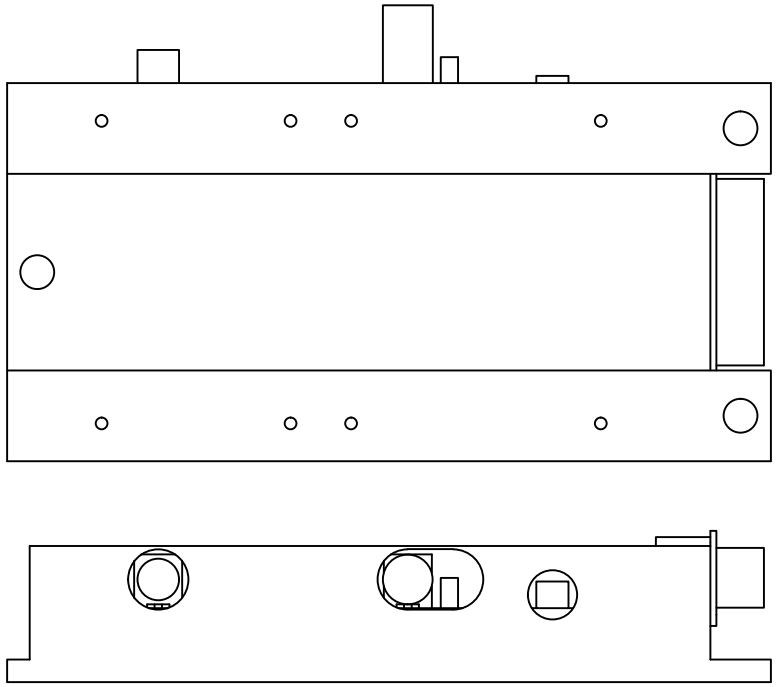

to Main Box

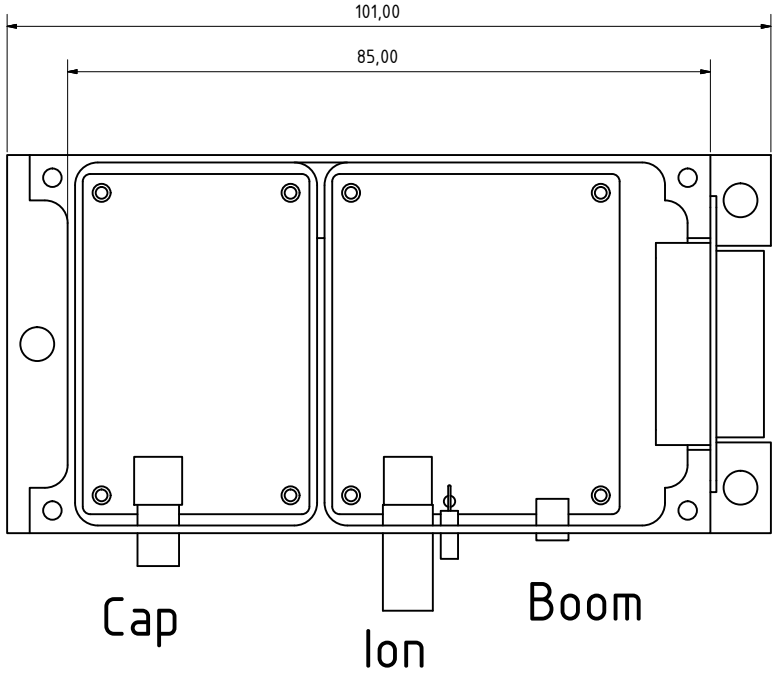

Analog Box assembly (without cover)